Electron spin and charge switching in a coupled quantum-dot–quantum ring system

B. Szafran,[1,2] F. M. Peeters,[1] and S. Bednarek[2]
[1]*Departement Natuurkunde, Universiteit Antwerpen (Campus Drie Eiken), B-2610 Antwerpen, Belgium*
[2]*Faculty of Physics and Nuclear Techniques, AGH University of Science and Technology, al. Mickiewicza 30, 30-059 Kraków, Poland*
(Received 12 March 2004; revised manuscript received 20 May 2004; published 17 September 2004)

Few-electron systems confined in a quantum dot laterally coupled to a surrounding quantum ring in the presence of an external magnetic field are studied by exact diagonalization. The distribution of electrons between the dot and the ring is influenced by the relative strength of the dot and ring confinement, and the magnetic field which induces transitions of electrons between the two parts of the system. These transitions are accompanied by changes in the periodicity of the Aharonov-Bohm oscillations of the ground-state angular momentum. The singlet-triplet splitting for a two electron system with one electron confined in the dot and the other in the ring exhibits piecewise linear dependence on the external field due to the Aharonov-Bohm effect for the ring-confined electron, in contrast to smooth oscillatory dependence of the exchange energy for laterally coupled dots in the side-by-side geometry.

DOI: 10.1103/PhysRevB.70.125310 PACS number(s): 73.21.La

I. INTRODUCTION

Coupling[1–14] between semiconductor quantum dots[15] results in the formation of so-called artificial molecules. Since most of the quantum dots have flat geometry, the coupling is realized either by vertical stacking[1–5] or by fabrication of dots coupled laterally on the same plane[6–14] Theoretical[6–11] considerations and experimental[12–14] realizations of laterally coupled dots are based on the idea of dots placed side by side. This paper is devoted to few-electron states in an essentially different geometry of lateral coupling, namely, to a quantum dot surrounded by a quantum ring[16] with a tunnel barrier separating both parts of the system. The confinement potential considered in this paper can be obtained using an atomic force microscope to locally oxidize[17] the sample surface which results in the depletion of the two-dimensional electron gas (2DEG) underneath it. Alternatively one can apply split gates with a central cap gate surrounded by a thin collar gate on top of a planar *n*AlGaAs-GaAs heterostructure containing a 2DEG. A proper geometry of split gates for the fabrication of the confinement potential considered in this paper was applied in the study[18] of effects related to electron localization on local fluctuations of the confinement potential in the low electron density regime. The system studied in the present paper would require a sufficiently strong confinement which is less perturbed by fluctuations. The effect of local perturbations can be largely diminished by optimization[19] of the size of electrodes for the strength of the electrostatic confinement potential.

Phase effects appearing in electron transport through quantum dots were studied in the Aharonov-Bohm interferometer.[20,21] The potential geometry studied in this paper is a two-dimensional counterpart of quantum-dot quantum-well structures.[22,23] Impurity effect on the single-electron states in a three-dimensional quantum ring for strong in-plane confinement has been studied.[24] Related to the present work is the magnetic coupling of a superconducting disk surrounded by a superconducting ring.[25] In contrast to the work of Ref. 25, in the system considered here the coupling between the ring and the dot occurs through quantum mechanical tunnelling. The transfer of the charge between a quanum ring and inline- as well as side-coupled quantum dot and its effect on the persistent currents in mesoscopic samples was previously studed in the Anderson-impurity-type model.[26]

We study the effect of the magnetic field on the confined one-, two-, and three-electron systems using an exact diagonalization approach. In quantum dots and rings the magnetic field induces ground-state angular momentum transitions. However, the role of the electron-electron interaction for the transitions in these two structures is different. In quantum rings the interaction is of secondary[27,28] importance for the angular momentum transitions which are mainly determined by the Aharonov-Bohm effect. In spinless[27,29] few-electron systems the ground-state angular momentum is not influenced by the Coulomb interaction, and for electrons with spin the angular momentum of the ground state differs from the noninteracting case by at most $\hbar$.[28] On the other hand, in quantum dots the Coulomb interaction influences strongly the values of the magnetic field at which the angular momentum transitions appear. Moreover, in two- and three-electron systems these transitions are absent if there is no electron-electron interaction. In this paper we study the hybrid magnetic-field evolution of the electron spectra in the dot-in-the-ring geometry.

The magnetic-field along with the angular momentum transitions induces a redistribution of the electron charge in quantum dots.[29,30] Here, we will show that in the considered geometry the magnetic field can be used to transfer the electrons from the dot to the ring or vice versa. We will also address the problem of the magnetic-field-induced trapping of electrons in local potential cavities.[31]

The spins of a pair of electrons localized in laterally coupled dots have been proposed[6] as a possible realization of coupled qubits. A universal quantum gate requires the possibility of application of single-qubit as well as two-qubit rotations. For this purpose one should be able to address each of the electrons individually as well as to control the state of the pair, which requires the spatial separation of electrons and a tunable coupling between them. We studied the singlet-

triplet splitting energy for the two-electron system with one electron localized in the dot and the other in the ring. We show that the angular momentum transitions, appearing for the ring-confined electrons as a consequence of the Aharonov-Bohm effect, lead to a simple piecewise linear dependence of the exchange energy on the external magnetic field. Since the unitary evolution in quantum computation needs precise control of the underlying qubit interaction this simple dependence makes our system a good candidate for the realization of the magnetic field controllable pair of spin qubits. Recently, it has been established[32] that the spin relaxation time in quantum dots defined by electric gates in two-dimensional electron gas is much longer than the qubit readout time in spin-to-charge conversion technique.

This papers is organized as follows: In the next section the present approach is explained, the single electron spectrum is described in Sec. III, the results for two and three electrons are given in Secs. IV and V, respectively, and Sec. VI contains the summary and conclusions.

II. THEORY

We study two-dimensional N-electron systems confined in circular potentials using the effective mass Hamiltonian

$$H = \sum_{i=1}^{N} h_i + \sum_{i=1}^{N} \sum_{j=i+1}^{N} \frac{e^2}{4\pi\varepsilon\varepsilon_0 r_{ij}} + BS_z g^* \mu_B, \qquad (1)$$

where ε is the dielectric constant, g^* is the effective Landé factor, μ_B is the Bohr magneton, S_z is the z component of the total spin, B is the magnetic field, and h_i stands for the single-electron Hamiltonian, which written in the symmetric gauge $\mathbf{A}=(-By/2, Bx/2, 0)$ has the form

$$h = -\frac{\hbar^2}{2m^*}\nabla^2 + \frac{1}{8}m^*\omega_c^2\rho^2 + \frac{1}{2}\hbar\omega_c l_z + V(\rho), \qquad (2)$$

with m^* the electron effective mass, l_z the z-component angular momentum operator, $\omega_c = eB/m^*$ the cyclotron frequency, and $V(\rho)$ the confinement potential. We adopt material parameters for GaAs, i.e., $m^*/m_0 = 0.067$, $\epsilon = 12.9$, and $g^* = -0.44$. The last term of Eq. (1), i.e., the spin Zeeman splitting energy is independent of the distribution of electrons between the different parts of the system as well as of the Coulomb interaction energy. Moreover, the value of the g^* factor can be tuned by the admixtures of Al substituting Ga.[33] We have therefore decided to neglect the Zeeman effect in most of the results presented in this paper (unless explicitly stated otherwise).

We model a strictly two-dimensional cylindrically symmetric potential of a quantum dot placed within the quantum ring with the following confinement potential:

$$V(\rho) = \min[m^*\omega_i^2\rho^2/2 + V_0, m^*\omega_o^2(\rho - R)^2/2], \qquad (3)$$

where $\hbar\omega_i$ and $\hbar\omega_o$ are the confinement energies of the dot and the ring, respectively, and the radius of the ring R is determined by the sum of oscillator lengths for the dot and ring potential and the barrier thickness (b) according to formula $R = \sqrt{2\hbar/m\omega_i} + \sqrt{2\hbar/m\omega_o} + b$. This potential is parabolic within both the quantum dot and the quantum ring, V_0 is the depth of the dot confinement with respect to the bottom of the quantum ring potential. The confinement potential (3) is shown in Fig. 1 for $\hbar\omega_i = 5$ meV, $\hbar\omega_o = 10$ meV, $V_0 = -5$ meV, and $b = 30$ nm. A model potential parametrized similarly to Eq.(3) was used previously for the description[10,11] of side by side quantum dots. The cusp present in simple potentials of this type (cf. Fig. 1) is rather unphysical and cannot be realized in real structures, however this shortcoming is of secondary importance since the cusp appears in a region of space where the barrier potential is largest and the wave functions of the lowest energy levels are small. In the weak coupling limit (for large barrier thickness) approximate formulas for the dot- and ring-confined states as functions of the magnetic field can be given (see below).

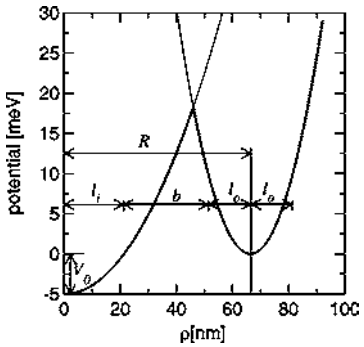

FIG. 1. Confinement potential [cf. Eq. (3) for $\hbar\omega_i = 5$ meV, $\hbar\omega_o = 10$ meV, $V_0 = -5$ meV, $b = 30$ nm, and the GaAs effective mass $m^*/m_0 = 0.067$. The dot oscillator length $l_i = \sqrt{2\hbar/m\omega_i}$ is equal to 21.33 nm and the oscillator length for the ring $l_o = 15.08$ nm which gives the ring radius $R = 66.4$ nm.

In the present paper the single-electron eigenfunctions for Hamiltonian (2) and definite angular momentum are obtained numerically on a radial mesh of points using the finite-difference approach. Eigenstates of the two- and three-electron Hamiltonian (1) are calculated using the standard configuration interaction method[34] with a basis composed of Slater determinants built with single-electron wave functions. The Coulomb matrix elements are evaluated by a two-dimensional[27] numerical integration. The few-electron states are described by the total spin S and angular momentum L quantum numbers. In this paper we discuss only the two- and three- electron states with nonpositive total angular momenta. We will therefore omit the minus sign for the angular momentum quantum number L.

III. SINGLE-ELECTRON STATES

The single-electron spectrum for $\hbar\omega_i = 6$ meV, $\hbar\omega_o = 11$ meV, $V_0 = 0$, and $b = 30$ nm is shown in Fig. 2(a). For this relatively large barrier thickness, the low part of the energy spectrum is essentially a sum of the spectra of an electron localized in the dot and in the ring. The solid lines in Fig. 2 correspond to states localized in the ring and dashed lines to s (lowest dashed line) and p states localized in the dot. The ring part of the spectrum exhibits Aharonov-Bohm oscillations. The angular momentum of the lowest-energy ring-localized states takes on the subsequent values $0, -1,$

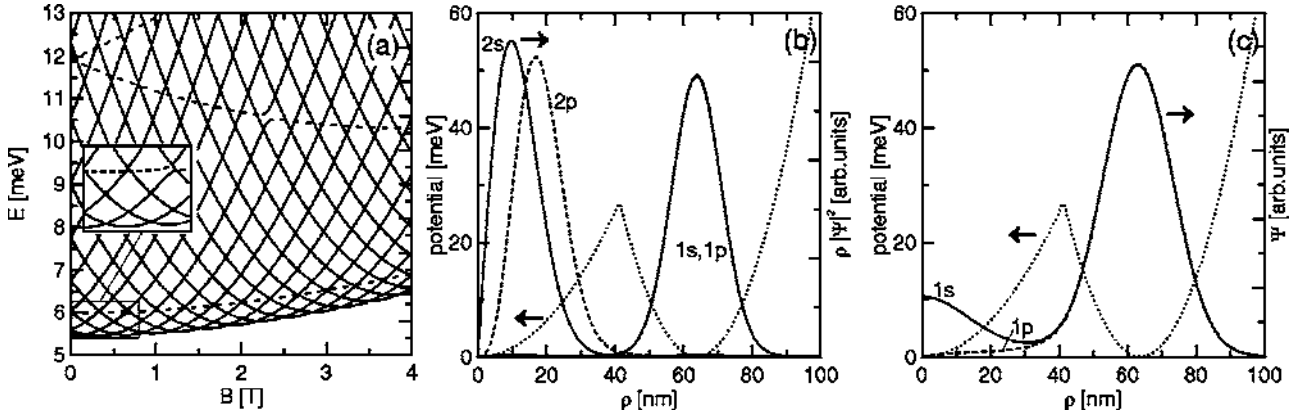

FIG. 2. Single-electron spectrum for $\hbar\omega_i=6$ meV, $\hbar\omega_o=11$ meV, $V_0=0$, and $b=30$ nm ($R=63.85$ nm). The solid lines correspond to states localized in the ring and the dashed lines to states localized in the dot. Lowest of the dashed lines corresponds to the *s* state and the two higher to *p* states. Inset shows the low-field and low-energy part of the spectrum-enlargement of the fragment surrounded by thin solid lines corresponding to anticrossing of 0 angular momentum dot- and ring-confined energy levels. Dotted lines in (b) and (c) shows the confinement potential (left scale) for the parameters applied in (a). Solid and dashed curves in (b) show the radial probability density $\rho|\psi|^2$ and in (c) the wave functions of the lowest states of *s* and *p* symmetry, respectively.

−2, etc. [in $\hbar$ units] when the magnetic field increases. The period of these oscillations is 0.337 T. This period corresponds to a flux quantum passing through a strictly one-dimensional ring of radius $R_{1D}=62.51$ nm which is in good agreement with the radius of the ring in the present model $R=63.85$ nm. The energy of the states localized in the dot change with the magnetic field more slowly than the energy of the ring-localized states. States with the same angular momentum change their order in anticrossings due to quantum mechanical tunnel coupling between the dot and the ring. Anticrossing for *s* states appears for *B* around 0.65 T [see inset of Fig. 2(a)]. A much wider anticrossing for *p* states is visible around 2.4 T.

Figure 2(b) shows the confinement potential for the parameters applied in Fig. 2(a) as well as the radial probability densities for the lowest *s*- and *p*-symmetry states. The radial densities for the ring-localized states do not depend on the angular momentum. However, Fig. 2(c) shows that the *s*-wave function penetrates the dot region in a much stronger way than the *p*-type wave function. It will have an important consequence for the singlet-triplet splitting of the two-electron states (see the next section). Note that the angular momentum has an opposite effect on the strength of the tunneling of the dot-localized states to the ring part of the potential. Barrier thickness is effectively smaller for the dot-localized states of higher angular momentum [cf. Fig. 2(b)].

The dependence of the energy of the lowest dot-localized state can be very well approximated by the expression for the lowest Fock-Darwin state, i.e., $E_{\mathrm{dot}}=V_0+\sqrt{(\hbar\omega_i)^2+(\hbar\omega_c/2)^2}$. Without the magnetic field the lowest energy ring-localized level is approximately equal to $\hbar\omega_o/2$, i.e., to the energy of the single-dimensional harmonic oscillator in the radial direction. In the external field the envelope of the lowest-energy ring-localized level can be quite well approximated by $E_{\mathrm{ring}}=\sqrt{(\hbar\omega_o/2)^2+(\hbar\omega_c/2)^2}$. These two formulas can be used in order to roughly determine whether the ground state of a single electron is localized in the dot or in the ring. For equal depth of the ring and the dot ($V_0=0$) the magnetic field does not change the order of the lowest-energy dot- and ring-confined states. However, for $V_0=0$ and $\omega_o\approx 2\omega_i$ the magnetic field can induce oscillations of the ground state localization from the dot to the ring, which results from the local deviations of the lowest ring-confined energy level from the smooth envelope [cf. Fig. 2(a)]. On the other hand, the magnetic field favors localization in the deep but small (thin) quantum dot (ring). This effect is illustrated in the following figure.

Figure 3 shows the energy spectrum for a $\hbar\omega_i$ which is increased with respect to Fig. 2 from 6 to 20 meV and the bottom lowered by $V_0=-14$ meV. For $B=0$ the low-energy part of the spectrum is the same as in the case shown in Fig. 2(a). However, the energy of the dot-localized state grows more slowly than the envelope of the ring-localized states. In consequence, the dot-localized state becomes the ground state for $B=3.3$ T. When the radius of the Landau orbit becomes smaller than the size of the local potential cavity, the electron can enter inside the dot without an extra increase of the kinetic energy due to the localization. Similar effects of trapping of electrons in local potential cavities at high magnetic fields are probably at the origin of the bunching of the charging lines observed in single-electron capacitance spec-

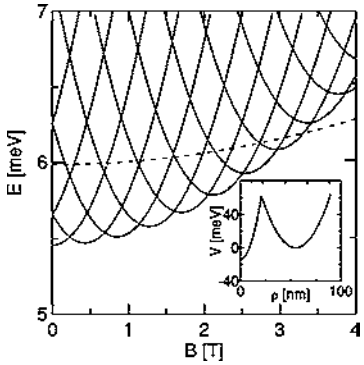

FIG. 3. Single-electron spectrum for $\hbar\omega_i=20$ meV, $\hbar\omega_o=11$ meV, $V_0=-14$ meV, and $d=30$ nm (potential is plotted in the inset). The solid lines correspond to states localized in the ring and the dashed line to the lowest-energy state localized in the dot.

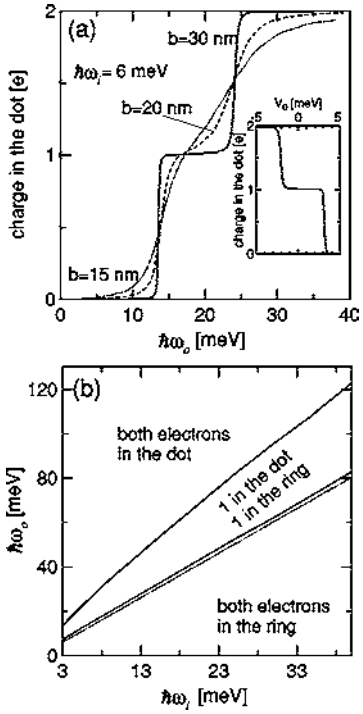

FIG. 4. Charge accumulated in the dot as a function of $\hbar\omega_o$ for different values of the barrier thickness and $V_0=0$. Inset in (a) shows the charge accumulated in the dot as function of V_0 for $b=30$ nm, $\hbar\omega_i=6$ meV, and $\hbar\omega_o=20$ meV. (b) Phase diagram for the distribution of two electrons for $B=0$, $V_0=0$, and $b=30$ nm. Solid lines in (b) divide regions of different electron localization in the two-electron system. Above the dotted line the ground state of a single electron is localized within the dot.

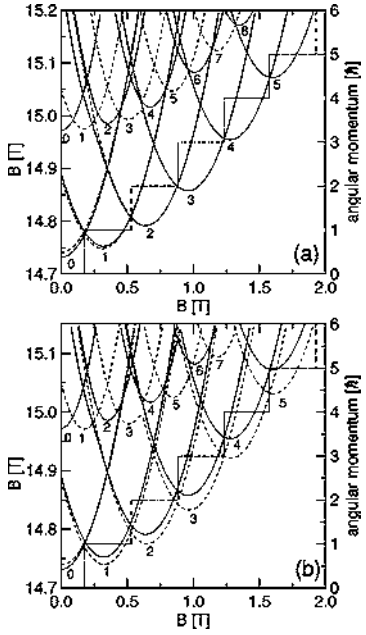

FIG. 5. Two-electron energy spectrum (left scale) for $b=30$ nm, $V_0=0$, $\hbar\omega_i=6$ meV, and $\hbar\omega_o=14$ meV (spin Zeeman effect neglected). Singlets (triplets) plotted with solid (dashed) lines. Numbers close to extrema of the lines denote the absolute values of the angular momentum in $\hbar$ units. The dotted line shows the absolute value of the angular momentum of the ground state of a *single* electron confined in the ring (right scale). (b) Same as (a) but with spin Zeeman effect included. Only the lowest energy level of the split spin triplet is plotted.

troscopy of large quantum dots.[31] The opposite effect, i.e., the change of the ground-state localization from the dot to the ring under influence of the external magnetic field is also possible if the ring is thin but with a bottom deeper than the dot.

IV. TWO ELECTRON SYSTEM

For $B=0$ the ground state of the electron pair corresponds to zero total spin and angular momentum independently of the electron distribution between the two parts of the confinement potential. The electron distribution in the system can be illustrated by the charge accumulated within the dot. This quantity is calculated as the integral of the radial probability density from the origin to the cusp of the confinement potential (cf. Fig. 1). Figure 4(a) shows the dependence of the charge accumulated within the dot as a function of the ring oscillator energy for different barrier thickness, the dot confinement energy $\hbar\omega_i=6$ meV and equal depth of the dot and ring ($V_0=0$). For $b=30$ nm the dependence of the charge accumulated in the dot on the ring confinement energy is almost stepwise and it becomes smoothened for thinner barriers for which the separation of electrons between the two parts of the system is less distinct. The transition of electrons between the ring and the dot can also be provoked by changing the relative depth of the confinement potentials for fixed oscillator energies. This is illustrated in the inset to Fig. 4(a) which shows the charge accumulated within the dot as a function of V_0 for the potential parameters $\hbar\omega_i=6$ meV, $\hbar\omega_o=20$ meV, $b=30$ nm, i.e., corresponding to the central plateau of the solid curve in the main part of Fig. 4(a).

Figure 4(b) shows the phase diagram for the spatial distribution of electrons in the two-electron system in the absence of the magnetic field for barrier thickness $b=30$ nm. Borders of regions corresponding to different electron distributions are marked with solid lines. Above the dotted line the ground state of a single electron is localized in the dot and below it–in the ring. The dotted line can be very well approximated by $\omega_o=2\omega_i$, which is in agreement with the approximate formulas for the lowest-energy dot- and ring-localized states given in the preceding section. In the noninteracting case this line would divide the regions in which both of the electrons are localized in the dot or in the well. In the presence of interaction a third region in which one of the electrons is localized in the dot and the other in the ring appears. This region of electron distribution starts slightly above the dotted line. This results from the fact that the Coulomb interaction, smallest for both electrons localized in the ring, stabilizes the ring-confined ground state for larger $\hbar\omega_o$ than in the noninteracting case. The central region of the phase diagram for which one electron resides in the dot and the other in the ring is particularly interesting from the point of view of potential spin quantum gate applications.[6]

Let us now look at the magnetic field dependence of the two-electron energy spectrum for the potential parameters

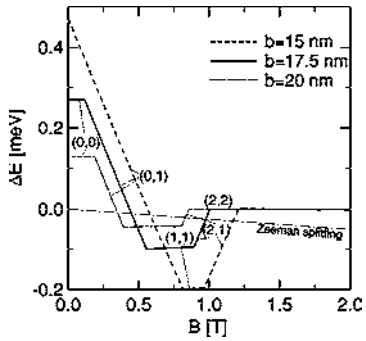

FIG. 6. Exchange energy, i.e., the energy difference of the lowest triplet and the lowest singlet energy levels for two electrons and $V_0=0$, $\hbar\omega_i=6$ meV, and $\hbar\omega_o=18$ meV for different values of the barrier width and spin Zeeman splitting is neglected. The dash-dotted line shows the Zeeman splitting between states with $S_z=0$ and $\hbar$.

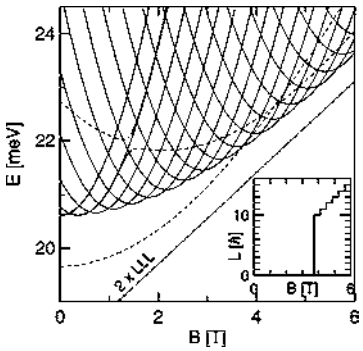

FIG. 7. Energy spectrum of two electrons for $b=30$ nm, $\hbar\omega_i=6$ meV, and $\hbar\omega_o=26$ meV (spin Zeeman effect neglected). The energy levels of states in which both (one) electrons are localized in the dot are plotted with dashed (solid) lines. The inset shows the ground state angular momentum. The dotted line corresponds to twice the lowest Landau level energy.

corresponding to one electron in the dot and the other in the ring, i.e., for $V_0=0$, $b=30$ nm, $\hbar\omega_i=6$ meV, and $\hbar\omega_o=14$ meV presented in Fig. 5(a). For this potential the one-electron ground state is localized in the dot. The angular momentum of the lowest excited ring-confined one-electron state is plotted with a dotted line (right scale). Comparison of this line with the ground-state energy crossings in the two-electron spectrum shows that the angular momentum transitions in the two-electron system are due to the Aharonov-Bohm effect for the electron confined within the ring. All the angular momentum of the system is therefore carried by the ring-confined electron while the electron confined in the dot remains in the *s* state. Singlet-triplet splitting of the ground state [cf. the distance between the dashed and solid lines in Fig. 5(a)] disappears at larger angular momentum. This effect can be understood if we look back at Fig. 2(c) showing that the dot penetration of the ring-localized single-electron states decrease with their angular momentum. In Fig. 5(a) above 14.9 meV the energy band corresponding to both electrons confined within the ring appears. Since in this band both ring-confined electrons are subject to the Aharonov-Bohm effect the angular momentum of the lowest state in the band grows roughly twice[28] as fast as in the ground state. The energy levels of even L correspond to spin singlets and of odd L to triplets. Around 0.6 T we observe an anticrossing of $L=3$ triplets corresponding to one and two electrons in the ring. The Zeeman effect [cf. Fig. 5(b)] for large B lifts the ground-state degeneracy with respect to the spin.

The energy difference between the lowest spin singlet and triplet states, i.e., the exchange energy[6]—an important quantity for the coupled spin qubit operations is also a very adequate measure of the strength of the tunnel coupling between the dot and the ring confined wave functions. Figure 6 shows the exchange energy (Zeeman energy neglected) for different values of the barrier thickness for $V_0=0$, $\hbar\omega_i=6$ meV, and $\hbar\omega_o=18$ meV, i.e., for the central point of the plateau corresponding to one of the electrons localized in the dot [cf. Fig. 4(a)]. The exchange energy is nearly independent of magnetic field when the lowest singlet and the lowest triplet possess the same angular momentum and it distinctly decreases (grows) with the magnetic field when the L of the lowest triplet is larger (smaller) than L of the lowest singlet. When the angular momentum of both singlet and triplet states exceed 2, the exchange energy vanishes. The exchange energy is a piecewise linear function of the magnetic field in contrast to smooth oscillatory dependence of the exchange interaction on the magnetic field for side-by-side dots (cf. Fig. 4 of Ref. 11). In side-by-side dots the magnetic field induces a continuous decrease of the overlap of the wave functions of electrons confined in different dots. For the dot in the ring geometry this decrease is discontinuous due to the Aharonov-Bohm effect for the ring confined electron. Since the Aharonov-Bohm magnetic period is inversely proportional to the square of the ring radius one can largely reduce the range of the magnetic field in which the exchange energy is nonzero by a mere increase of R.

The magnetic field can change the distribution of the electrons between the coupled cavities. Consider the case of $b=30$ nm, $V_0=0$, $\hbar\omega_i=6$ meV and $\hbar\omega_o=26$ meV. For these parameters in the absence of the magnetic field both electrons are localized within the dot [cf. Fig. 4(b)], but the state corresponding to one electron in the ring is close in energy. Figure 7 shows the magnetic field dependence of the two-electron energy spectrum for this potential. Energies of states corresponding to both electrons localized in the dot are plotted with dashed lines. The lower of these two energy levels is a spin singlet of *s* symmetry. The upper dashed line corresponds to a spin triplet of *p* symmetry, i.e., to the two-electron maximum density droplet.[35] Spin singlet of *p*-symmetry with both electrons localized in the dot lies higher in energy beyond the range presented in this figure. The energy levels plotted with solid lines correspond to one electron localized in the dot (in the lowest *s* state) and the other in the ring. For $B=1.44$ T an avoided crossings appears for the $L=1$ spin triplets. For $B=3.74$ T the energy level of the dot localized state crosses the energy level of the state with $L=10$ corresponding to one electron in the dot and the other in the ring. Note that below $B=3.74$ T in the ground-state the electrons are in the singlet state while above this field singlet and triplet states are nearly degenerate. Decoupling of spins, in the sense of vanishing exchange energy appears abruptly after crossing $B=3.74$ T. For $B=4.35$ T, a

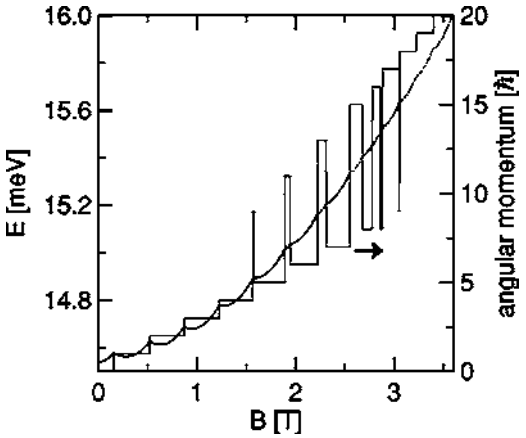

FIG. 8. Two-electron ground-state energy (left scale) for $b=30$ nm, $V_0=0$, $\hbar\omega_i=6$ meV, and $\hbar\omega_o=13.65$ meV (spin Zeeman effect neglected). Energy of states corresponding to one electron in the dot and the other in the ring plotted with solid line. Energy of states in which both the electrons are localized in the ring are plotted by the dotted curve. The thin solid step-like line gives the total angular momentum which is referred to the right axis.

crossing of dot-localized singlet and triplet states appears. The dotted line shows twice the lowest Landau energy level. For $B>4$ T the envelope of the energy levels with one electron in the dot and the other in the ring as well as the dot localized maximum density droplet run approximately parallel to the lowest Landau level (dotted line). Figure 7 shows that the magnetic field can change the electron occupation of the dot and the ring. Generally, for $V_0=0$ such an effect is not observed for a single electron. The appearance of this effect for two electrons is due to lowering of the Coulomb interaction energy when one of the electrons is transferred from the dot to the ring. Recently,[36] it was shown that in the infinite magnetic field limit the ground-state electron distribution can be identified with the lowest energy configuration of classical[37] point charges. For $V_0=0$ the lowest-energy classical configuration corresponds to both electrons localized in the ring. One should therefore expect that at higher magnetic fields the second electron should also be transferred to the ring. However, the magnetic fields at which this effect could appear are beyond the reach of our numerical calculations.

For $V_0=0$, $b=30$ nm, $\hbar\omega_i=6$ meV, and $\hbar\omega_o=13.65$ meV [the left end of the central plateau in the Fig. 4(b)] for $B=0$ one of the electrons is localized in the dot and the other in the ring, but the state with two electrons localized in the ring is not much higher in energy. Figure 8 shows the ground-state energy and the ground-state angular momentum as functions of the magnetic field for this set of parameters. The state with one electron in the dot remains the ground state up to 1.6 T. Between $B=1.6$ T and $B=3.1$ T the state with two electrons in the ring is almost degenerate with the state with one ring-confined electron and as a consequence the localization of the ground state changes several times as the magnetic field is increased. Ground-state ring-localization becomes established above 3.1 T. The period of the angular momentum transitions becomes halved with respect to the low magnetic fields, for which the ring is occupied by a single electron.

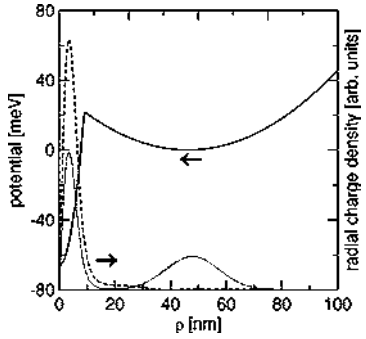

FIG. 9. Solid line (left scale): the external potential $\hbar\omega_i=50$ meV and $\hbar\omega_o=6$ meV, $b=20$ nm, $V_0=-66$ meV. The ground state for $B=0$ corresponds to the $L=0$ singlet with one electron in the dot and the other in the ring. Radial density of this state plotted with dotted line (right scale). The first excited s singlet state corresponds to both electrons in the dot (dashed line).

The magnetic field can induce opposite transitions of the electrons from the ring to the dot if the dot is small but deep. Consider the following set of parameters $\hbar\omega_i=50$ meV, $\hbar\omega_o=6$ meV, $b=20$ nm, and $V_0=-66$ meV. Figure 9 shows the confinement potential and the radial probability density for the lowest two-electron singlet states with total angular momentum equal 0. For zero magnetic field in the ground-state one electron is localized in the ring and the other one in the dot. In the first excited s singlet state both electrons reside within the dot. Note that in this case the ground state is more extended than the excited state as a consequence of the electron-electron interaction preventing the second electron from entering the dot. The magnetic field energy dependence is displayed in Fig. 10. The magnetic field has only a small influence on the energy of the singlet with both electrons localized in the dot. Around $B=2$ T, singlets corresponding to different electron distribution change their energy order with a pronounced anticrossing. For $B=5.725$ T the dot-localized singlet becomes the ground state. In this structure the Aharonov-Bohm oscillations are interrupted by the magnetic field which removes the second electron from the ring. As a consequence a giant singlet-triplet energy difference appears for $B>5.725$ T. This transition appears in spite of the Coulomb interaction energy which is increased when the second electron is trapped in the central cavity.

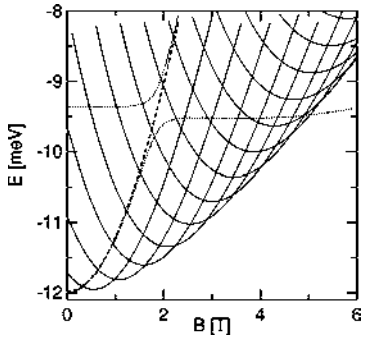

FIG. 10. Two-electron energy spectrum for the potential parameters of Fig. 9. Dotted lines show the energy levels of s singlets. The dashed line corresponds to the s triplet.

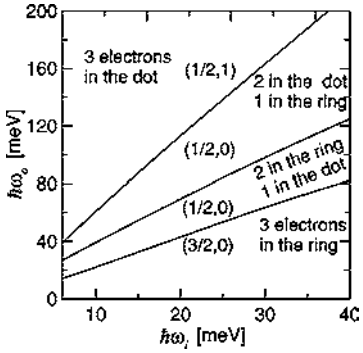

FIG. 11. Phase diagram for the electron distribution in the ($\hbar\omega_i$, $\hbar\omega_o$) plane for $V_0=0$ and $b=30$ nm in the absence of the magnetic field. Solid lines separate regions of different electron distributions. Numbers denote the ground-state total spin and total angular momentum quantum number (S,L).

V. THREE ELECTRONS

Distribution of electrons in the three electron system without the magnetic field for $V_0=0$ and $b=30$ nm is plotted in Fig. 11. Regions of different electron distribution are separated by the solid lines. For large dot confinement energy, i.e., $\omega_i \gg \omega_o$ all the electrons reside in the ring and the ground state corresponds to total spin $S=3/2$ and zero[28]angular momentum. In the single-particle picture this state corresponds to electrons having parallel spin and occupying states with angular momentum $l=-1,0$, and 1 (in $\hbar$ units). For increasing ring confinement the electrons enter the dot one by one. In states with two electrons of opposite spins occupying the dot or the ring (cf. two central regions in Fig. 11 the ground state corresponds to $S=1/2$ and $L=0$. When the ring confinement energy is much larger (five times or more) than the dot confinement all the electrons occupy the lowest dot-confined energy levels forming the state of spin $S=1/2$ and angular momentum $L=1$.

In the preceding section we showed that for equal depth of the ring and the dot ($V_0=0$) the electron-electron interaction triggered the magnetic-field-induced transitions of electrons from the dot to the ring. We found that in the three-electron system the magnetic field can also induce the opposite transition from the ring to the dot. This is illustrated in Fig. 12 which shows the energy spectrum for $V_0=0$, $b=30$ nm, $\hbar\omega_i=6$ meV, and $\hbar\omega_o=37$ meV. Solid lines in Fig. 12 show the energy levels corresponding to two electrons of opposite spins in the dot and one electron confined in the ring. All these states have $S=1/2$. Dashed lines correspond to spin-polarized states with $S=3/2$ in which the two dot-confined electrons occupy the 1*s* and 1*p* states. Energy levels corresponding to three electrons localized in the dot are shown by dotted curves. Quantum numbers of the dot-confined states are given in the figure. Thick solid steplike line at the bottom of the figure shows the absolute value of the ground-state angular momentum which is referred to the right axis. At $B=0$, the energy of the state in which all three electrons are localized in the dot with $L=1$ is 1 meV higher in energy (cf. dotted line above 42 meV) above the ground state with two electrons in the dot and one in the ring. This energy level decreases initially with increasing magnetic

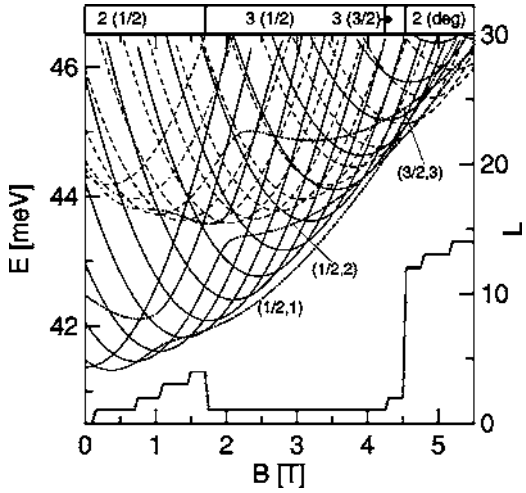

FIG. 12. Energy spectrum for $N=3$, $V_0=0$, $b=30$ nm, $\hbar\omega_i=6$ meV, and $\hbar\omega_o=37$ meV. The solid (dashed) lines show the lowest energy levels with the two dot-confined electrons with $S=1/2$ and opposite ($S=3/2$ and the same) spin and one electron in the ring. The states with the two dot-confined electrons of parallel spins are almost degenerate with respect to the spin orientation of the electron in the ring. The only exception is the state with $L=2$. The lower of the dash-dotted line shows this state for $S=1/2$ and the upper for $S=3/2$. Dotted lines correspond to all electrons confined in the dot. Quantum numbers (L,S) of these states are indicated in the figure. Only nonpositive angular momenta are shown. The thick solid line in the lower part of the figure shows the the ground-state angular momentum quantum number (right scale). The panel above the upper axis shows the number of electrons in the dot n_d and S for the ground state in format $n_d(S)$, "deg" stands for degeneracy of the $S=1/2$ and $3/2$ states.

field due to the interaction of the magnetic field with the magnetic momentum of the *p* electron. This decrease results in an anticrossing of the $L=1$ energy levels corresponding to two and three dot-confined electrons around $B=1$ T. Another consequence of this anticrossing is a visibly increased region of $L=1$ ground-state stability between 0.15 and 0.7 T. Subsequently for $B=1.7$ T, the state with three electrons in the dot and $L=1$ becomes the ground state. The transition of the third electron from the ring to the dot happens in spite of the electron-electron interaction which is not strong enough to prevent it.

For $B=0$, the energy of the lowest spin polarized state (cf. dashed lines) with $L=1$ is equal to about 44.25 meV. In this state the two electrons confined in the dot have the same spin and occupy 1*s* and 1*p* energy levels, while the ring-confined electron occupy the orbital with $l=0$. Note that level crossings appear at the same magnetic fields as in the lower branch with $S=1/2$ where two electrons are in the 1*s* orbital confined in the dot (cf. solid lines in the Fig. 13). The angular momentum quantum number of these states is equal to the ring confined electron plus 1 - the angular momentum of the dot-confined subsystem. For the adopted large barrier thickness $b=30$ nm the states of this band with $S=3/2$ are almost degenerate with $S=1/2$ states (omitted in the figure), i.e., the energy of the system is not influenced by the orientation of the spin of the ring-confined electron. The only exception appears for the $L=2$ state. The lower (upper)

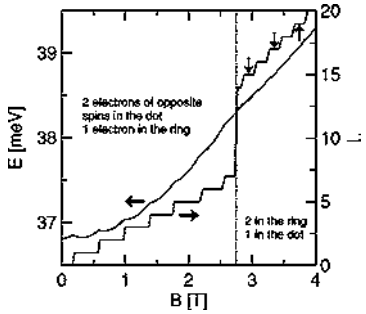

FIG. 13. Ground-state energy (left scale) and the absolute value of the ground-state angular momentum (right scale) for $N=3$, $V_0=0$, $b=30$ nm, $\hbar\omega_i=6$ meV, and $\hbar\omega_o=27$ meV. The dotted vertical line marks the magnetic field for which the electron distribution is changed. The vertical arrows on the L staircase correspond to triplet state of the ring subsystem.

dashed-dotted line shows the energy of the state with $L=2$ and $S=1/2$ $(3/2)$. The reason of the lifted degeneracy is the fact that the energy of the state with $L=2$ and $S=1/2$ is pushed downward by the anticrossing with the dot-confined state of the same quantum numbers, similarly as the above discussed $L=1$, $S=1/2$ energy level in the lower part of the spectrum.

The angular momentum of the ground state with three-electrons confined in the dot changes from 1 to 2 at $B=4.3$ T (cf. the crossing of the dotted lines). Above 4.5 T the ground state corresponds again to two electrons in the dot and one in the ring like for $B=0$ T, but now the dot-confined subsystem is spin-polarized (cf. the crossing of the dashed and dotted lines).

Figure 13 shows the ground-state energy for the same parameters as studied in Fig. 12 but with the ring confinement energy reduced from 37 to 27 meV. At $B=0$ the ground state still corresponds to two electrons in the dot and one in the ring, but the state with two ring-confined electrons is higher in energy by less than 1 meV. The envelope of the lowest energy level with one electron in the ring grows with the magnetic field faster than the envelope of the energy levels with two ring-confined electrons which results in the change of the ground-state electron distribution at $B=2.75$ T. The dotted line in Fig. 12 marks the change in the electron distribution. Left of this line the ground state has $S=1/2$, the two dot-confined electrons are in the spin singlet, and the spin of the ring confined electron is arbitrary. Right of this line the spin-configuration of the ring-confined subsystem oscillates from singlet (for even L) to triplet (for odd L) [cf. also the branch of ring confined electrons in Fig. 5(a)]. The magnetic fields for which the ring subsystem is in the triplet state have been marked by vertical arrows on the angular momentum staircase. The states with spin singlet of the ring subsystem correspond to $S=1/2$. Since the angular momenta of both ring-confined electrons exceed 6 the tunnel coupling between the dot and ring wave functions is negligible [cf. Fig. 8] and the spin of the dot confined electron does not influence the energy. Therefore, the states with triplet configuration of spins in the ring subsystem correspond to $S=1/2$ and $S=3/2$ degeneracy.

The envelope of the lowest $N=3$ energy levels with three electrons and two electrons in the ring run almost parallel to each other as a function of the external field. One should expect[36] that for equal depth of the ring and the dot at very large magnetic field the three-electron ground state corresponds to electrons forming an equilateral triangle in the ring, but in the studied magnetic field range we did not observe a distinct transition of the last electron from the dot to the ring.

VI. SUMMARY AND CONCLUSIONS

We have considered a quantum dot inside a quantum ring–a unique example of lateral coupling realized with conservation of circular symmetry of the confinement potential. A simple model for the potential was used. The model assumes parabolic confinement in both the dot and the ring so approximate formulas can be given for the lowest-energy single-electron dot- and ring-confined states. One-, two-, and three-electron systems were studied using the exact diagonalization approach. We have investigated the distribution of electrons between the dot and the ring. This distribution depends not only on the parameters of the confinement potential but it can also be altered by an external magnetic field, which therefore can be used as a driving force to transfer the electrons from the dot to the ring or *vice versa*. The passage of an electron from the dot to the ring should be detectable by a change of the Aharonov-Bohm magnetic period. The present model also allows for simulation of the magnetic field induced electron trapping in local potential cavities. We have studied the exchange energy in the two electron system with one electron confined in the dot and the other in the ring. Due to the angular momentum transitions resulting from the Aharonov-Bohm effect for the ring-confined electron, the singlet-triplet splitting exhibits a piecewise linear dependence on the external magnetic field. This should be a more elegant method for the control of the spin-spin coupling than the smooth oscillatory dependence predicted for side-by-side coupled dots.[11]

ACKNOWLEDGMENTS

This paper has been partly supported by the Polish Ministry of Scientific Research and Information Technology in the framework of the solicited Grant No. PBZ-MIN-008/P03/2003, the Flemish Science Foundation (FWO-Vl), the Concerted Action programme (IUAP), and the University of Antwerpen (VIS and GOA). One of us (B.S.) is supported by the Foundation for Polish Science (FNP).

[1] J. J. Palacios and P. Hawrylak, Phys. Rev. B **51**, 1769 (1995).
[2] B. Partoens and F. M. Peeters, Phys. Rev. Lett. **84**, 4433 (2000).
[3] M. Pi, A. Emperador, M. Barranco, F. Garcias, K. Muraki, S. Tarucha, and D. G. Austing, Phys. Rev. Lett. **87**, 066801 (2001).
[4] M. Bayer, P. Hawrylak, K. Hinzer, S. Fafard, M. Korkusinski, Z. R. Wasilewski, O. Stern, and A. Forchel, Science **291**, 451 (2001).
[5] S. Bednarek, T. Chwiej, J. Adamowski, and B. Szafran, Phys. Rev. B **67**, 205316 (2003).
[6] D. Loss and D. P. DiVincenzo, Phys. Rev. A **57**, 120 (1998); G. Burkard, D. Loss, and D. P. DiVincenzo, Phys. Rev. B **59**, 2070 (1999).
[7] C. Yannouleas and U. Landman, Phys. Rev. Lett. **82**, 5325 (1999).
[8] S. Nagaraja, J.-P. Leburton, and R. M. Martin, Phys. Rev. B **60**, 8759 (1999).
[9] J. Kohlemainen, S. M. Reimann, M. Koskinen, and M. Manninen, Eur. Phys. J. B **13**, 731 (2000).
[10] A. Wensauer, O. Steffens, M. Suhrke, and U. Rössler, Phys. Rev. B **62**, 2605 (2000).
[11] A. Harju, S. Siljamäki, and R. M. Nieminen, Phys. Rev. Lett. **88**, 226804 (2002).
[12] F. R. Waugh, M. J. Berry, D. J. Mar, R. M. Westervelt, K. L. Campman, and A. C. Gossard, Phys. Rev. Lett. **75**, 705 (1995).
[13] A. W. Holleitner, C. R. Decker, H. Qin, K. Eberl, and R. H. Blick, Phys. Rev. Lett. **87**, 256802 (2001).
[14] J. M. Elzerman, R. Hanson, J. S. Greidanus, L. H. Willems van Beveren, S. De. Franceschi, L. M. K. Vandersypen, S. Tarucha, and L. P. Kouwenhoven, Phys. Rev. B **67**, 161308 (2003).
[15] L. Jacak, P. Hawrylak, A. Wójs, *Quantum Dots* (Springer, Berlin, 1998)
[16] For a review see, S. Viefers, P. Koskinen, P. Singa Deo, and M. Manninen, Physica E (Amsterdam) **21**, 1 (2004).
[17] A. Fuhrer, S. Lüscher, T. Ihn, T. Heinzel, K. Ensslin, W. Wegschelder, and M. Bichler, Nature (London) **413**, 822 (2001).
[18] N. B. Zhitenev, M. Brodsky, R. C. Ashoori, L. N. Pfeiffer, and K. W. West, Science **285**, 715 (1999).
[19] S. Bednarek, B. Szafran, K. Lis, and J. Adamowski, Phys. Rev. B **68**, 155333 (2003).
[20] A. Yacoby, M. Heiblum, D. Mahalu, and Hadas Shtrikman, Phys. Rev. Lett. **74**, 4047 (1995).
[21] K. Kobayashi, H. Aikawa, S. Katsumoto, and Y. Iye, Phys. Rev. B **68**, 235304 (2003).
[22] D. Schooss, A. Mews, A. Eychmüller, and H. Weller, Phys. Rev. B **49**, 17072 (1994).
[23] A. Mews, A. V. Kadavanich, U. Banin, and A. P. Alivisatos, Phys. Rev. B **53**, R13242 (1996).
[24] B. S. Monozon and P. Schmelcher, Phys. Rev. B **67**, 045203 (2003).
[25] B. J. Baelus, S. V. Yampolskii, and F. M. Peeters, Phys. Rev. B **66**, 024517 (2002).
[26] M Büttiker and C. A. Stafford, Phys. Rev. Lett. **76** 495 (1996).
[27] T. Chakraborty and P. Pietiläinen, Phys. Rev. B **50**, 8460 (1994).
[28] K. Niemielä, P. Pietiläinen, P. Hyvönen, and T. Chakraborty, Europhys. Lett. **36**, 533 (1996).
[29] S. M. Reimann and M. Manninen, Rev. Mod. Phys. **74**, 1283 (2002).
[30] B. Szafran, S. Bednarek, and J. Adamowski, Phys. Rev. B **67**, 045311 (2003); J. Phys.: Condens. Matter **15**, 4189 (2003).
[31] N. B. Zhitenev, R. C. Ashoori, L. N. Pfeiffer, and K. W. West, Phys. Rev. Lett. **79**, 2308 (1997).
[32] R. Hanson, B. Witkamp, L. M. K. Vandersypen, L. H. Willems van Beven, J. M. Elzerman, and L. P. Kouwenhoven, Phys. Rev. Lett. **91**, 196802 (2003).
[33] K. Ensslin, D. C. Driscoll, A. C. Gossard, and D. D. Awschalom, Nature (London) **414**, 619 (2001).
[34] B. Szafran, S. Bednarek, J. Adamowski, M. Tavernier, E. Anisimovas, and F. M. Peeters, Eur. Phys. J. D **28**, 373 (2004).
[35] A. H. MacDonald, S. R. E. Yang, and M. D. Johnson, Aust. J. Phys. **46**, 345 (1993).
[36] B. Szafran, F. M. Peeters, S. Bednarek, and J. Adamowski, Phys. Rev. B **69**, 125344 (2004).
[37] V. M. Bedanov and F. M. Peeters, Phys. Rev. B **49**, 2667 (1994).

Few-electron eigenstates of concentric double quantum rings

B. Szafran[1,2] and F. M. Peeters[1,*]
[1]*Departement Fysica, Universiteit Antwerpen, Groenenborgerlaan 171, B-2020 Antwerpen, Belgium*
[2]*Faculty of Physics and Applied Computer Science, AGH University of Science and Technology, al. Mickiewicza 30, 30-059 Kraków, Poland*

(Received 27 June 2005; revised manuscript received 26 August 2005; published 19 October 2005)

Few-electron eigenstates confined in coupled concentric double quantum rings are studied by the exact diagonalization technique. We show that the magnetic field suppresses the tunnel coupling between the rings, localizing the single-electron states in the internal ring and the few-electron states in the external ring. The magnetic fields inducing the ground-state angular momentum transitions are determined by the distribution of the electron charge between the rings. The charge redistribution is translated into modifications of the fractional Aharonov-Bohm period. We demonstrate that the electron distribution can be deduced from the cusp pattern of the chemical potentials governing the single-electron charging properties of the system. The evolution of the electron-electron correlations to the high field limit of a classical Wigner molecule is discussed.

DOI: 10.1103/PhysRevB.72.155316 PACS number(s): 73.21.La

I. INTRODUCTION

The phase shift of the electron wave function by the vector potential[1] results in oscillations of the quantum transport properties[2–6] of ring-shaped structures. The conductance[7] of metal and semiconductor rings is periodic in the external magnetic field with a period determined by the magnetic flux through the ring. On the other hand, in bound states of closed circular quantum rings, the single-electron spectrum exhibits periodic ground-state angular momentum transitions with the period of the flux quantum.[8] In confined interacting few-electron systems fractional Aharonov-Bohm (AB) periodicity of the spectrum was predicted[9,10] and subsequently observed in conductance oscillations measured[11] in a transport spectroscopy experiment. Discussion of the fractional periodicity in the context of the strength of the electron-electron interaction was given in Ref. 12. The fractional period for the interacting electron system is also found in realistic modeling of InGaAs self-assembled quantum rings.[13]

Recently, fabrication of self-assembled strain-free double concentric GaAs/AlGaAs quantum rings was reported.[14] Concentric coupled quantum ring structures can also be produced by the atomic force microscope tip oxidation technique.[4,11] In this paper we present an exact diagonalization study of the properties of few-electron states confined in concentric quantum rings. In the presence of inter-ring tunnel coupling the electron wave functions undergo hybridization, forming molecular orbitals similarly as in artificial molecules formed by lateral[15–19] or vertical[20–22] coupling of quantum dots. The magnetic field AB period will be significantly different for the internal and external rings. Therefore, the question arises, what will be the periodicity of the angular momentum transitions for such hybridized orbitals?

In the two-electron laterally coupled dots, the external magnetic field enhances the localization of the wave functions in each of the dots.[17] Similar is the effect of the electron-electron interaction favoring charge segregation. On the other hand, in concentric rings the electron-electron interaction will favor localization of the electrons in the external ring while the diamagnetic term of the Hamiltonian will tend to localize the electrons in the inner ring. We will show that the redistribution of the electrons between the rings affects the AB period of the angular momentum transitions, which can be extracted from conductance measurements[11] on rings connected to electrodes. Moreover, the angular momentum transitions result in characteristic cusp patterns of the chemical potential determining the single-electron charging of the structure. The alignment of the chemical potentials of the confined electrons with the Fermi level of the gate electrode can be detected in capacitance spectroscopy, which was used earlier to study the electronic structure of self-assembled quantum rings[23] incorporated in a charge tunable structure.

The present paper extends our previous work on the coupling between a quantum dot and a quantum ring.[24] For a single quantum ring, the envelope of the single-electron ground-state energy depends only on the strength of the confinement in the radial direction and not on the radius of the ring. For the radial ring confinement energy $\hbar\omega$, when the radius of the ring is large as compared to the range of the radial confinement, the ground-state envelope is approximately given[24] by $\sqrt{(\hbar\omega)^2+(\hbar\omega_c)^2}/2$, where ω_c is the cyclotron frequency. Therefore, a continuous evolution of the electron distribution between the two rings should be expected as a function of the magnetic field in contrast to the rapid ground-state charge redistributions found previously for a quantum dot coupled to a surrounding quantum ring.[24]

A study related to the present one was presented earlier for two concentric superconducting rings[25] in which the coupling between the rings was mediated by the magnetic self-field of the separate rings.

The paper is organized as follows. In Sec. II we present the model, the results for the single-electron coupling are given in Sec. III, and for the interacting electron systems in Sec. IV. Section V contains the summary and conclusions.

II. THEORY

We consider a two-dimensional model of circularly symmetric double concentric rings with confinement potential taken in the form

$$V(\rho) = \frac{m\omega^2}{2}\min[(\rho - R_1)^2, (\rho - R_2)^2], \quad (1)$$

where m is the effective electron band mass, R_1 and R_2 stand for the internal and external ring radii, ρ is the distance of the origin, and ω is the harmonic oscillator frequency for the lateral confinement of the electrons in each of the rings. Similar models were previously applied for laterally coupled dots.[17–19] In our calculations we take the GaAs value for the mass $m=0.067m_0$, the dielectric constant $\epsilon=12.4$, and assume $\hbar\omega=3$ meV. The adopted oscillator energy corresponds to a length $l=\sqrt{2\hbar/m\omega}=27.5$ nm which defines the width $d=2l$ of the considered rings. The Hamiltonian of a single electron in a perpendicular magnetic field (B), using the symmetric gauge, is

$$h = -\frac{\hbar^2}{2m}\left(\frac{d^2}{d\rho^2} + \frac{1}{\rho}\frac{d}{d\rho}\right) + \frac{\hbar^2 L^2}{2m\rho^2} + \frac{m\omega_c^2\rho^2}{8} - \frac{1}{2}\hbar\omega_c L + V(\rho), \quad (2)$$

where L is the angular momentum of the considered state, and $\omega_c=eB/m$. In the following we refer to the second, third, and fourth term of the Hamiltonian as the centrifugal, diamagnetic, and the orbital Zeeman terms. We neglect the Zeeman interaction of the electron spin with the magnetic field, which at high fields polarizes the spins of the confined electrons. The spin Zeeman interaction is decoupled from the orbital degree of freedom, it does not influence the tunnel coupling, and can be trivially accounted for as an energy shift linear in B.[24] The eigenstates of the N-electron Hamiltonian

$$H = \sum_{i=1}^{N} h_i + \sum_{i=1}^{N}\sum_{j>i}^{N} \frac{e^2}{4\pi\epsilon\epsilon_0 r_{ij}} \quad (3)$$

are found with a standard[26,27] exact diagonalization approach using the single-electron eigenstates of operator (2) to construct the basis elements in the form of Slater determinants. We use the numerical method as originally developed to discuss the coupling between a quantum dot and a quantum ring.[24] The single-electron Hamiltonian (2) is diagonalized using a finite difference scheme and the Coulomb matrix elements are integrated numerically.

III. SINGLE ELECTRON COUPLING

Let us first discuss the single-electron states in the coupled concentric rings. Figure 1 shows the potential felt by an electron in the $L=0$ and $L=6$ states as well as the lowest-energy orbitals (radial probability densities) for $R_1=120$ nm and $R_2=180$ nm in the absence of a magnetic field. In the lowest $L=0$ states the electron is equally probable to be found in both rings and the orbitals possess a clear bonding and antibonding character. On the other hand, for $L\neq 0$, the centrifugal potential pushes the electrons towards the outer ring. In Fig. 1 we show the result for $L=6$, which clearly shows that the lowest-energy orbital is shifted to the external ring. As a consequence, the electron in the excited-state orbital occupies predominantly the inner ring and the zero of

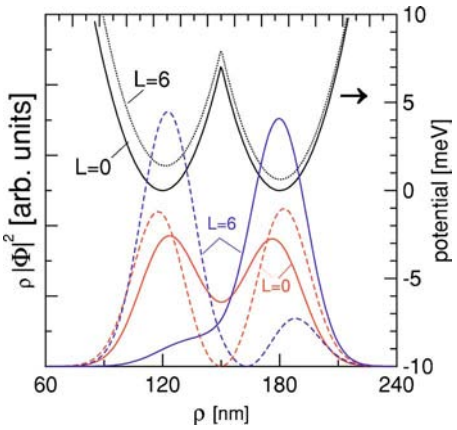

FIG. 1. (Color online) Radial profile of the confinement potential (black solid curve referred to the right vertical axis) of the two concentric rings for $R_1=120$ nm and $R_2=180$ nm at $B=0$. The black dotted curve shows the sum of the confinement potential and the centrifugal potential for $L=6$. Red (light gray) and blue (dark gray) curves show the square of the modulus of the two lowest-energy single-electron wave functions multiplied by Jacobian ρ at $B=0$ for $L=0$ and $L=6$, respectively. The lower-energy orbitals are given by the solid curves and the higher-energy orbitals by the dashed curves.

the wave function is displaced from the center of the barrier to the external ring. We see that the bonding-antibonding character of the lowest-energy orbitals occupying both rings is, for increasing L, replaced by a single-ring type of localization. Therefore, the effect of the centrifugal potential is to lift the tunnel coupling.

The energy levels are shown in Fig. 2 as functions of the inner ring radius R_1 for fixed $R_2=180$ nm. Note that for $R_1=0$, the system consists of a quantum dot surrounded by a quantum ring.[24] The lowest-energy level for $L=0$ and $B=0$ [see Fig. 2(a)] is then associated with the ring-localized state (of energy close to $\hbar\omega/2=1.5$ meV) and the excited state corresponds to an electron confined in the parabolic quantum dot (of energy $\hbar\omega=3$ meV). For $R_1>0$ the quantum dot is transformed to a quantum ring. The energy of the orbital, which is predominantly localized in the inner ring, first goes below $\hbar\omega/2$ and then returns to this value. Around $R_1=80$ nm the tunnel coupling appears between the internal and the external rings, leading to an energy gap between the two energy levels. Finally, for a single quantum ring ($R_1=R_2=180$ nm) the spectrum resembles the one-dimensional harmonic oscillator potential.[24] For $L=2$ at $R_1=0$ both the lowest-energy levels correspond to orbitals localized in the external ring. The energies are slightly shifted above $\hbar\omega/2$ and $3\hbar\omega/2$ by the centrifugal potential. The internal ring localized level becomes the first excited state near $R_1=30$ nm. The centrifugal potential lowers the height of the inter-ring tunnel barrier (see Fig. 1). Consequently, the avoided crossings between the $L=2$ energy levels ($R_1\simeq 100$ nm) are visibly larger than for $L=0$. A larger centrifugal shift of the energy levels and a stronger level interaction, a signature of a stronger tunnel coupling, is observed for $L=6$ [see Fig. 2(b)]. For $L=6$ and $B=0.5$ T the diamagnetic shift of the external ring-confined level is almost exactly

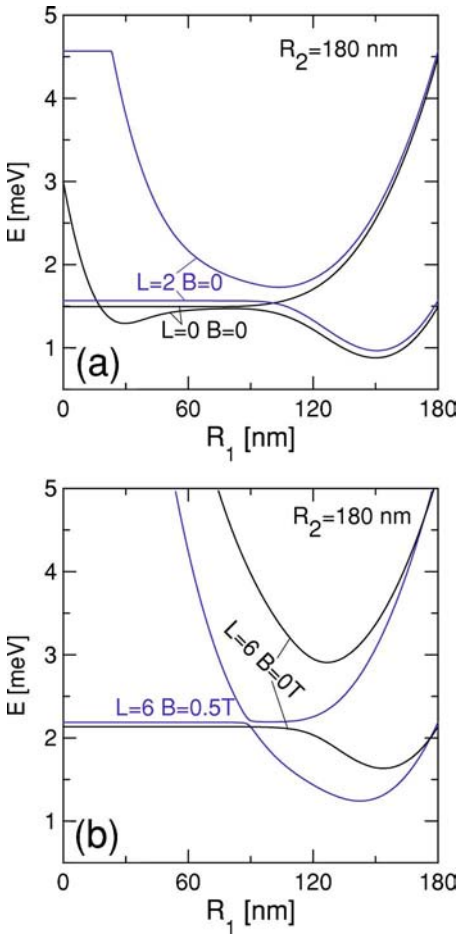

FIG. 2. (Color online) Two lowest single-electron energy levels for $L=0$, and $L=2$ at $B=0$ (a) and for $L=6$ at $B=0$ and 0.5 T (b), as functions of the internal ring radius for an external ring of radius $R_2=180$ nm.

cancelled by the orbital Zeeman term [compare the lowest black and blue curves at $R_1=0$ in Fig. 2(b)]. However, the Zeeman term dominates for the state localized in the internal ring. As a consequence, the energy levels change their order in a narrow anticrossing near $R_1=90$ nm.

The dependence of the single-electron energy spectrum on the external magnetic field is plotted in Figs. 3(a)–3(c) for fixed $R_2=180$ nm and different internal ring radii. For $R_1=60$ nm there is no tunneling between the rings and the spectrum is a simple sum of two single-ring spectra. The spectrum corresponding to the internal ring exhibits angular momentum transitions with a period of 0.214 T while the period of the one corresponding to the external ring is 0.0406 T. These periods correspond to the flux quantum passing through an effective one-dimensional ring of radius 55.4 nm and 180 nm, respectively. The ground state corresponds to the electron in the internal ring, except for $B\simeq 0.2$ T and $B\simeq 0.65$ T. The inner-ring localized states are favored by the $-(1/\rho)(d/d\rho)$ term of the kinetic energy.

For $R_1=100$ nm [see Fig. 3(b)] the inter-ring coupling is non-negligible. For comparison, the ground-state energy of the *single* quantum ring of radius 180 nm is also shown in Fig. 3(b) by the black curve. For $B>0.15$ T, sightly above the ground state, we observe more frequent angular momentum transitions than in the ground state. This energy band corresponds to the electron predominantly confined in the external ring. With increasing magnetic field, this band closely approaches the single-ring spectrum (cf. the black curve), which indicates that the electron becomes entirely localized in the external ring. Thus at high magnetic fields the spectrum of the internal and external rings become decoupled. Note that the energy band corresponding to the localization of the electron in the external ring becomes distinct only for $L>4$.

Energy levels with the same angular momentum change their order through avoided crossings. The lowest-energy levels, for $L\geqslant 2$, possess two minima, after and before the avoided level crossing. The wave functions and the potentials for the anticrossing of the $L=5$ energy levels [see the anticrossing of red lines near 0.38 T at Fig. 3(b)] are presented in Fig. 3(d). The $L=5$ eigenstate for $B=0.2$ T is the lowest-energy state of the external ring energy band [see Fig. 3(b) and the paragraph above] and its wave function is predominantly localized in the outer ring [see Fig. 3(d)]. At $B=0.38$ T, corresponding to the smallest distance between the anticrossing energy levels, the electron can be found with a comparable probability in both rings. After the avoided crossing the diamagnetic potential localizes the electron in the internal ring. For $B=0.7$ T the $L=5$ state is localized almost entirely in the inner ring [see purple curve in Fig. 3(d)] when it corresponds to the ground-state of the system [Fig. 3(b)]. Concluding, for $B=0$ and fixed nonzero L the lowest energy level is predominantly localized in the external ring due to the centrifugal potential. For high magnetic field, the lowest-energy state for a fixed L is transferred to the internal ring by the diamagnetic term of the Hamiltonian.

For $R_1=120$ nm [Fig. 3(c)] the coupling between the two rings is stronger and the difference between the centrifugal potentials in both rings is smaller. Consequently the two decoupled spectra of the internal and external ring are only distinguishable for $B>0.5$ T. The amount of electron charge localized in the internal ring [integrated over ρ from 0 to $(R_1+R_2)/2$] for the ground state is plotted in Fig. 4, together with the ground-state angular momentum. For low magnetic field the ground-state wave functions are almost equally distributed between the two rings and at high field they are entirely localized in the inner ring. Consequently, the period of the ground-state oscillations increases with B (see the slope of the black staircase in Fig. 4). Note that the decoupling of the spectra in Fig. 3(c) for $B>0.5$ T ($R_1=120$ nm) is accompanied by the transfer of the electron to the internal ring (see Fig. 4). For $R_1=140$ nm many more angular momentum transitions are needed before the electron becomes entirely localized in the inner ring.

At the end of this section we would like to explain the role of the adopted finite value of the rings' width for our results. The studied rings radii ($R\simeq 150$ nm) and width ($d=55$ nm) correspond to structures produced by the tip oxidation technique.[4] For instance, the ring of Ref. 4 is characterized by $R=132$ nm and $d=65$ nm. In the limit of infinite oscillator energy ($\hbar\omega$) the rings become strictly one-dimensional ($d\rightarrow 0$) and decoupled due to the infinite inter-

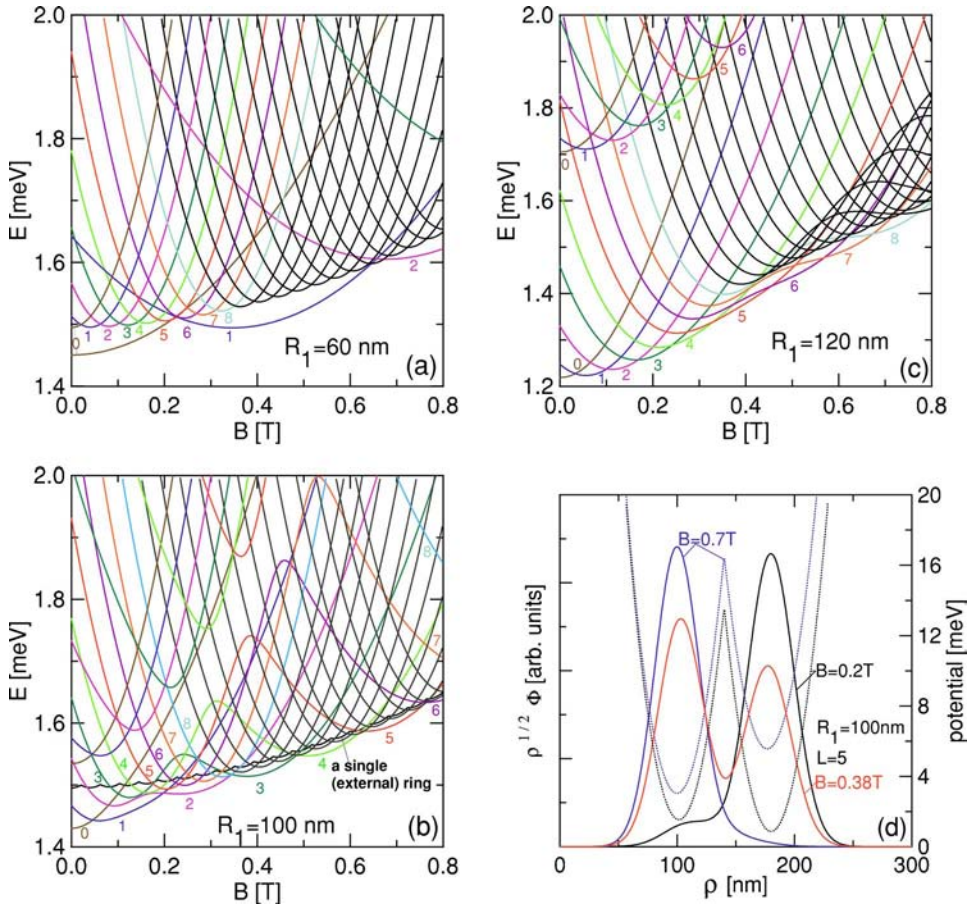

FIG. 3. (Color online) (a)–(c) Single electron spectrum for coupled rings with the external ring radius $R_2=180$ nm and the internal ring radius $R_1=60$ nm (a), 100 nm (b), and 120 nm (c). Energy levels corresponding to different angular momenta up to 8 were plotted with different colors. In (b) the ground state of a single ring with radius 180 nm is shown by the black curve. (d) Lowest energy $L=5$ wave function (solid lines) for $R_1=100$ nm, before ($B=0.2$ T) at (0.38 T) and after (0.7 T) the avoided crossings of the energy levels [cf. red lines in (b)] corresponding to states localized in the external and internal ring, respectively. Dotted curves refer to the right vertical axis and show the sum of the confinement, centrifugal, and diamagnetic potentials.

ring barrier. The energy levels of states confined in one-dimensional rings only depend on the magnetic flux[8] $E_i(L)=[\hbar^2/(2mR_i^2)](L-\Phi_i/\Phi_0)^2$, where $i=1$, 2 stands for the internal and external ring localization respectively, $\Phi_0=h/e$ is the flux quantum, and Φ_i corresponds to the flux through the radius R_i. It is clear that the localization of the lowest-energy level of a pair of one-dimensional rings will oscillate abruptly between internal and external rings when the magnetic field is increased. However, this switching is deprived of physical consequences since due to the infinite inter-ring barrier the electron is not allowed to release its energy tunneling from one ring to the other. Note that a trace of the discussed localization switching can be observed in Fig. 3(a) for negligible inter-ring tunnel coupling. Decoupled spectra with short appearances of the external ring localization in the lowest-energy state similar to Fig. 3(a) are obtained for $R_1=120$ nm, $R_2=180$ nm for d decreased from 55 nm [as in Fig. 3(c)] to 13.5 nm ($\hbar\omega=50$ meV). The rapid localization switching disappears for the nontrivial case of a non-negligible tunnel coupling [cf. Figs. 3(b)–3(d)].

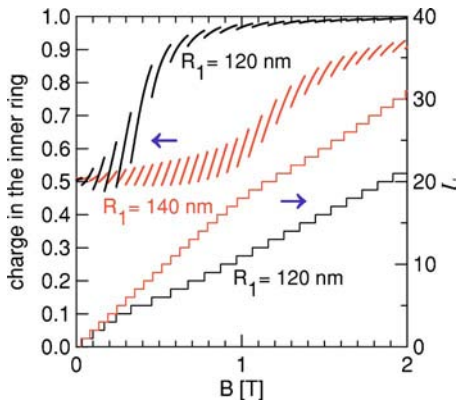

FIG. 4. (Color online) The discontinuous lines show the amount of charge localized in the internal ring for the single-electron ground state. The results correspond to the external radius $R_2=180$ nm and internal radius $R_1=120$ nm (black lines) and $R_1=140$ nm (red lines) as functions of the magnetic field. The staircases at the lower part of the figure are referred to the right axis and show the ground-state angular momentum.

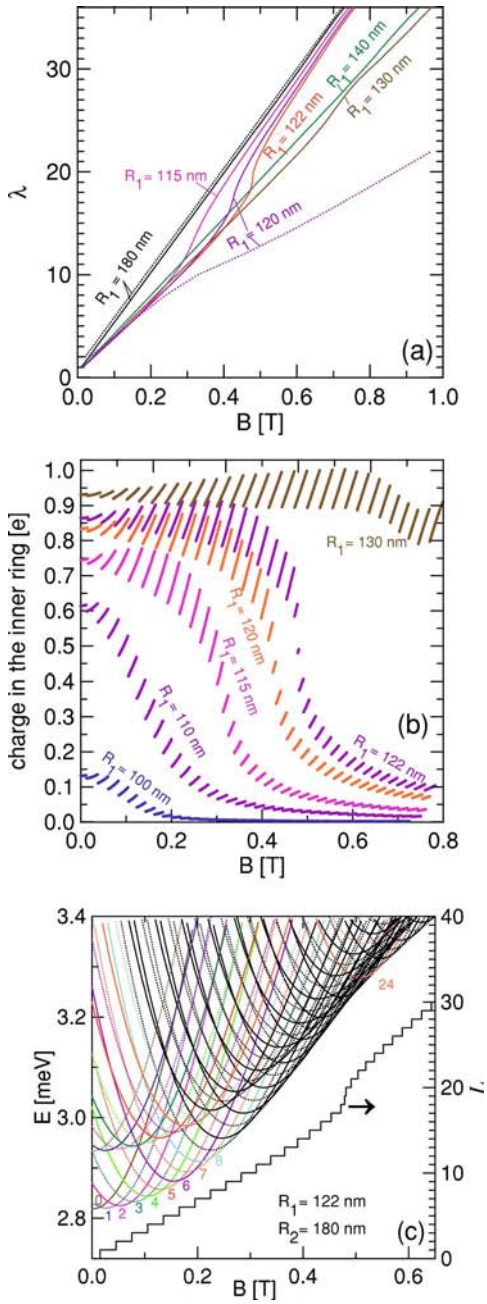

FIG. 5. (Color online) (a) Upper bound for the two-electron ground-state angular momentum for $R_2=180$ nm and various values of the inner ring radius. The dotted lines show the values in the absence of the electron-electron interaction. (b) Charge localized in the inner ring as function of the magnetic field for $R_2=180$ nm and different radii of the inner ring. (c) The two-electron energy spectrum for $R_1=122$ nm and $R_2=180$ nm. The spin singlets are plotted as solid lines and the triplets with dotted lines. In the bottom of the figure the ground-state angular momentum staircase is plotted.

IV. FEW-ELECTRON EIGENSTATES

Let us now discuss the effect of the electron-electron interaction on the ground-state properties of few-electron systems. We find that for the interacting two-electron system the ground-state angular momentum takes on all the subsequent integer values, such as for a single quantum ring. The upper

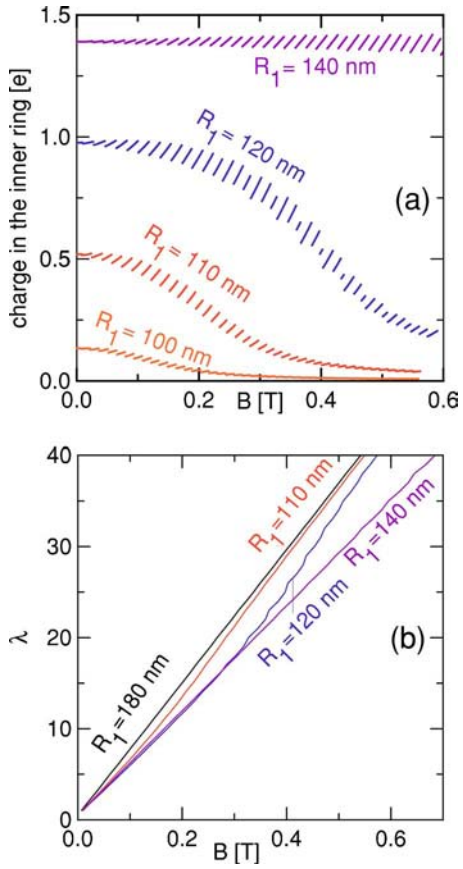

FIG. 6. (Color online) Three electrons in two concentric rings. (a) Charge localized in the inner ring for $R_2=180$ nm and various R_1 radii. (b) Upper bound for the ground-state angular momentum.

bound for the ground-state angular momentum of the two-electron system $\lambda \geqslant L$ is plotted in Fig. 5(a) as a function of the external magnetic field. In contrast to the single-electron problem, no influence of the inner ring on the ground-state angular momentum is observed for $R_1<90$ nm. This indicates that the Coulomb repulsion prevents the electrons from occupying the inner ring if its radius is too small. As a signature of the inter-ring coupling we see for $R_1=115$ nm, 120 nm, and 122 nm that the ground-state angular momentum increases initially more slowly than for the single $R=180$ nm ring, indicating the presence of electron charge in the internal ring. At a certain value of magnetic field, however, the lines change their slope and tend toward the values obtained for a single ring of radius 180 nm. In the discussed range of the magnetic field, the inter-ring coupling for the internal ring radii $R_1=130$ and 140 nm is preserved.

Dotted lines in Fig. 5(a) show the λ values for the noninteracting electron couple for a single ring with $R=180$ nm (black dots) and for the double ring with $R_1=120$ nm and $R_2=180$ nm (orange dots). For the single $R=180$ nm ring, the λ values for the interacting and noninteracting cases run parallel to one another. However, for $R=120$ nm the λ values for the noninteracting pair decreases its slope as the magnetic field is increased, while for the interacting pair an increase of the slope is observed instead. This is because for high magnetic fields the interacting electrons tend to occupy the external ring [cf. Fig. 5(b)] to minimize their mutual repulsion

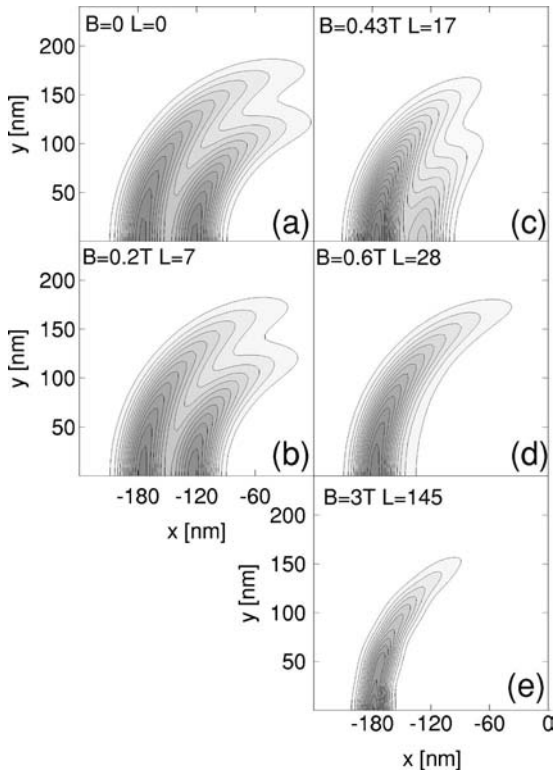

FIG. 7. Pair correlation function for two-electron ground state in concentric rings with radii $R_1=120$ nm and $R_2=180$ nm. One of the electrons is fixed at the point (180 nm,0).

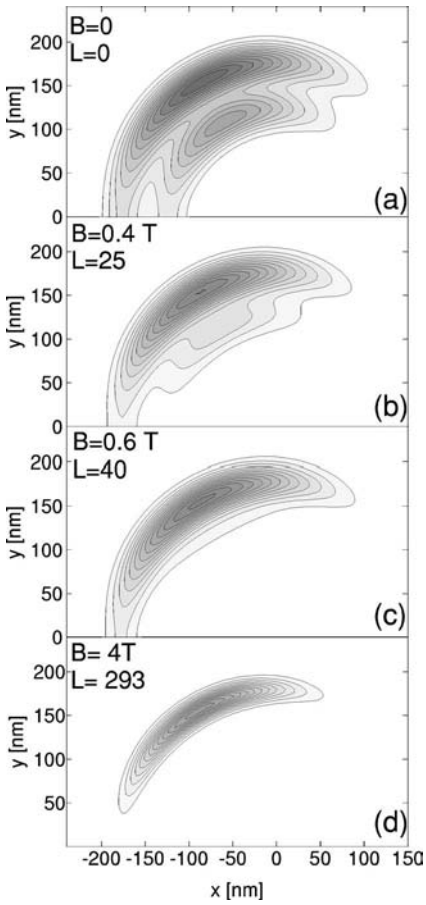

FIG. 8. Same as Fig. 7, but now for three electrons.

in contrast to the single-electron problem in which the diamagnetic term of the Hamiltonian promotes the localization in the inner ring (see Fig. 4).

The energy spectrum for $R_1=122$ nm, for which the localization of the charge in the external ring appears in the most abrupt way, is plotted in Fig. 5(c). Below $B=0.4$ T one can observe two bands of energy levels. In the ground state the spin singlets correspond to even angular momenta and the spin triplets to odd angular momenta. Opposite correspondence is found in the excited energy band. The two bands approach each other near $B=0.5$ T, but never cross. The relation between the ground-state spin and the even/odd parity of the angular momentum remains unchanged [cf. singlets and triplets of $L=24$ marked in orange in the right upper part of Fig. 5(c)].

The distribution of the charge between the rings in the three-electron system is qualitatively similar to the two-electron case. At zero magnetic field the electrons refuse to occupy the inner ring if its radius is too small [see Fig. 6(a)]. Some electron charge is present in the internal ring due to inter-ring tunneling, which is lifted by the application of the external magnetic field. The ground-state angular momentum at high magnetic field tends toward the value obtained for a single, external ring [see Fig. 6(b)]. For $R_1=140$ nm, in the range of the magnetic field presented in Fig. 6, the inter-ring coupling is not broken [cf. Figs. 5(a) and 5(b) for $R_1=130$ nm and $R_1=140$ nm]. In the high magnetic field limit, when the magnetic length becomes small compared to the size of the confining nanostructures, the charge distribution in few-electron systems can be identified[28] with the lowest-energy configuration of a classical system[29] of point-charge particles. Therefore, one should expect that in our model, assuming equal depths of both rings, the few-electron system will eventually become entirely localized in the external ring at still higher magnetic fields.

Next, we study the evolution of the ground-state electron-electron correlations with increasing magnetic field. For this purpose we consider the pair-correlation function plots given in Figs. 7 and 8 for two- and three-electron systems, respectively. The position of one of the electrons is fixed in the middle of the external ring, namely in the point (180 nm,0). For two electrons at zero magnetic field the second electron is found with an almost equal probability in the outer and inner rings opposite to the fixed electron [Fig. 7(a)]. For 0.6 T [Fig. 7(d)] the second electron occupies mainly the external ring with a small leakage of the probability density to the internal ring [cf. also the orange line in Fig. 5(b)]. On the other hand, in the three-electron system at $B=0$ there is already a pronounced shift of the pair-correlation function to the external ring [Fig. 8(a)]. Figs. 7 and 8 show that the infinite magnetic field limit is obtained in two steps: first the charge is removed from the internal ring and then the angular correlations between the electrons start to increase. The Wigner type of localization, i.e., separation of electron charges in the internal coordinates, increases with each ground-state angular momentum transition tending to the point-charge limit.

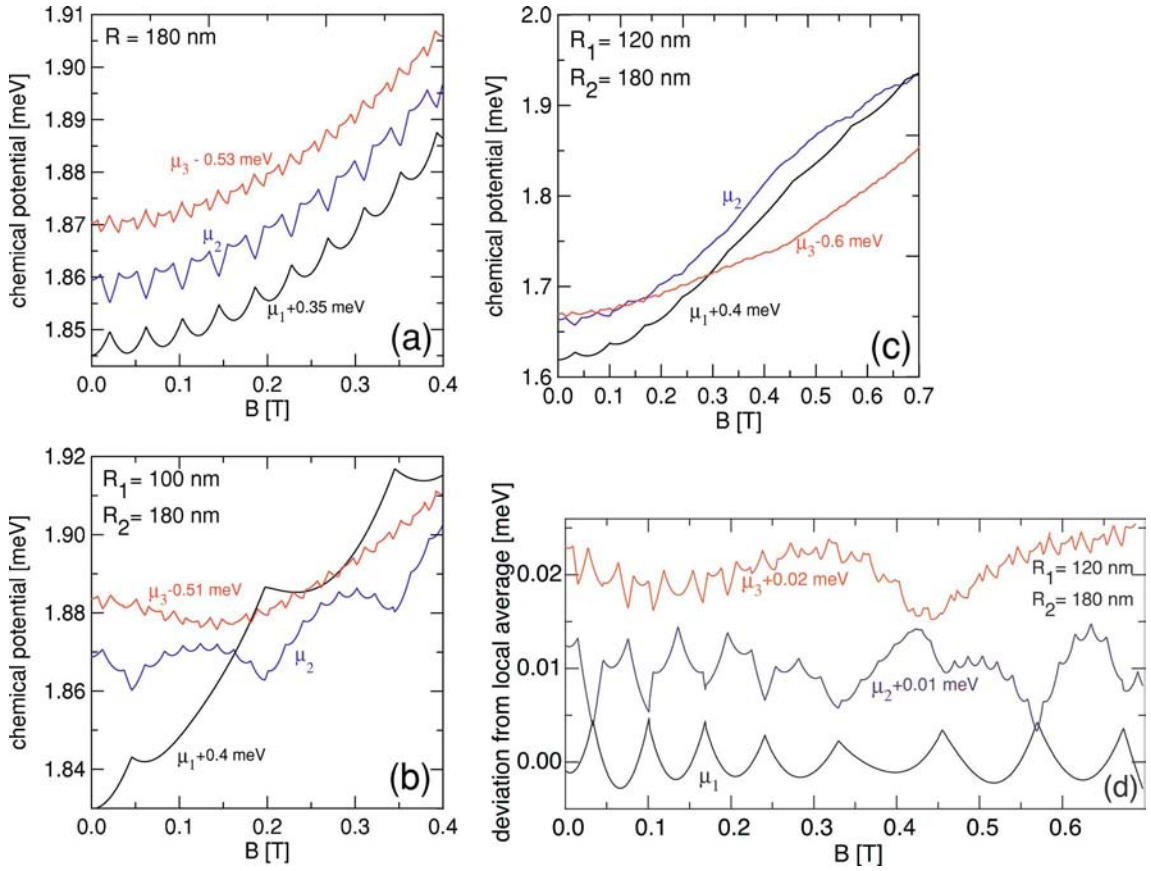

FIG. 9. (Color online) Magnetic field dependence of the chemical potentials for 1, 2, and 3 electron systems in a single ring of radius $R=180$ nm (a), in double concentric rings of external ring radius $R_2=180$ nm and internal ring radius $R_1=100$ nm (b), and $R_1=120$ nm. Chemical potentials for one and three electrons have been shifted for clarity. (d) Deviation of the chemical potentials from the local average (see text) for plot (c).

The above discussed AB oscillations associated with the angular momentum transitions can be measured through the magnetic field dependence of the conductance[11] as performed in phase-sensitive transport spectroscopy. Such transport measurements require contacts to be attached to the nanostructure. Connection of terminals to rings formed by the surface oxidation technique[4,11] is straightforward. On the other hand, attachment of electrodes to self-assembled rings[14,23] has not been reported so far. However, the ground-state angular momentum transitions can still be extracted from the chemical potential as measured in a capacitance experiment.[23] The magnetic field dependence of the chemical potentials μ_N, defined as the ground-state energy difference of N and $N-1$ electrons, is presented in Fig. 9. Figure 9(a) shows the chemical potential for a single quantum ring of radius 180 nm. For a single electron the chemical potential is equal to the ground-state energy. The potential exhibits cusps having a Λ shape at the angular momentum transitions. These Λ cusps are translated into V-shaped cusps of the chemical potential for the two-electron system. The angular momentum transitions in the two-electron system are twice as frequent[10] as for $N=1$, hence in the μ_2 plot we observe two Λ cusps per one V cusp. Similarly, in the cusps' pattern of the three-electron chemical potential we obtain three Λ's per two V's. Below 0.7 T for the double-ring structure with $R_1=140$ and $R_2=180$ nm, we obtain qualitatively the same spectrum of a single-ring type, only the AB oscillations period is increased due to the reduced effective R value. This is because for $R_1=140$ nm the inter-ring coupling is not broken by the magnetic field for $B<0.7$ T [see Figs. 4, 5(a), and 6(a)]. The occupied orbitals are equally distributed between the rings.

Figure 9(b), for the doubled ring with internal radius $R_1=100$ nm, corresponds to the situation when a small magnetic field localizes the single-electron ground states in the internal ring and ejects the entire charge of the two- and three- electron systems to the external ring [see Figs. 5(b) and 6(a)]. As a consequence, for μ_2 we observe seven to eight Λ cusps between each couple of V's. On the other hand, the pattern of cusps in the chemical potential of the three-electron system resembles the single-ring case [Fig. 9(a)], only below $B<0.1$ T a small perturbation of the pattern is observed.

Figure 9(c) shows the chemical potentials for $R_1=120$ nm, for which the inter-ring tunnel coupling is quite significant at $B=0$, but becomes suppressed in the studied range of magnetic field [see Figs. 4, 5(a), 5(b), and 6] for all considered N. Note that for $N=1$ and 2, the range of the chemical potential modification by the magnetic field is an order of magnitude larger than for a single ring [see Fig. 9(a)]. A distinctly larger range of chemical potential variation can also be noticed for $N=1$ in Fig. 9(b). This increase is due

to the magnetic field lifting of the inter-ring coupling present at $B=0$. For larger N the Coulomb repulsion weakens the tunnel coupling at $B=0$, which explains the weaker dependence of the envelopes of μ_3 and μ_2 in Fig. 9(b) and μ_3 in Fig. 9(c).

In order to extract the fine features of the cusps' pattern we fitted slowly varying sixth order polynomials to the chemical potentials in Fig. 9(c) and then subtracted from μ_N this local average provided by the fitted polynomial. The result is displayed in Fig. 9(d). For $N=1$ we see an enlargement of the AB oscillation period as the electron becomes localized in the inner ring. The low magnetic field Λ-V cusp sequences for $N=2$ and 3 resemble the single-ring localization [see Fig. 9(a)]. For $B>0.45$ T when both electrons are ejected to the external ring and the single electron is localized in the inner ring, we see in μ_2 several Λ's per one V, as in Fig. 9(b). For μ_3 the single-ring type of pattern is found above $B>0.45$ T. In the transition region ($0.35\ \mathrm{T}<B<0.45\ \mathrm{T}$) the cusp structure is less pronounced. This is due to the fact that in the B range corresponding to the transition of the electrons to the external ring, the angular momentum increases very fast, tending toward the angular momentum of the ground state in the single quantum ring [see Figs. 5(a), 5(c), and 6] of radius $R=180$ nm.

V. SUMMARY AND CONCLUSIONS

We studied the coupling between concentric rings for the few-electron eigenstates using the exact diagonalization approach. We find that the strength of the tunnel coupling decreases with angular momentum since the centrifugal potential favors the localization of the electrons in the external ring. At high magnetic field, for which the ground state corresponds to high angular momentum, the tunnel coupling between the rings is suppressed and the energy spectrum becomes decoupled into spectra of separate external and internal rings. The ground state for the single electron becomes entirely localized in the inner ring due to the diamagnetic term of the Hamiltonian, enhancing the localization of the electron orbits. In contrast, the few-electron states at high magnetic field become localized in the external ring to minimize their mutual Coulomb repulsion. In our model, assuming a similar radial confinement potential near the centers of both rings, we find that the order of the spin-orbital ground-state symmetries is not perturbed by the inter-ring coupling, only the stability intervals of the subsequent ground states are affected by the coupling. The modification of the electron distribution between the external and internal rings is translated into the frequency of the ground-state angular momentum transitions on the magnetic field scale. The electron distribution can be extracted from the cusp patterns of the single-electron charging lines, i.e., the chemical potential dependence on the magnetic field. Suppression of the tunnel inter-ring coupling and localization of the ground states in one of the rings under the influence of a magnetic field is accompanied by a distinctly stronger increase of the chemical potentials compared to the charging spectra in which the charge distribution between the rings is not modified.

ACKNOWLEDGMENTS

This work was supported by the Flemish Science Foundation (FWO-Vl) and the Belgian Science Policy and the EU-network of excellence SANDiE. B.S was supported by the EC Marie Curie IEF Project No. MEIF-CT-2004-500157.

*Electronic address: Francois.Peeters@ua.ac.be

[1] Y. Aharonov and D. Bohm, Phys. Rev. **115**, 485 (1959).
[2] R. A. Webb, S. Washburn, C. P. Umbach, and R. B. Laibowitz, Phys. Rev. Lett. **54**, 2696 (1985).
[3] G. Timp, A. M. Chang, J. E. Cunningham, T. Y. Chang, P. Mankiewich, R. Behringer, and R. E. Howard, Phys. Rev. Lett. **58**, 2814 (1987).
[4] A. Fuhrer, S. Lüscher, T. Ihn, T. Heinzel, K. Ensslin, W. Wegscheider, and M. Bichler, Nature (London) **413**, 822 (2001).
[5] W. G. van der Wiel, Yu. V. Nazarov, S. De Franceschi, T. Fujisawa, J. M. Elzerman, E. W. G. M. Huizeling, S. Tarucha, and L. P. Kouwenhoven, Phys. Rev. B **67**, 033307 (2003).
[6] S. Pedersen, A. E. Hansen, A. Kristensen, C. B. Sorensen, and P. E. Lindelof, Phys. Rev. B **61**, 5457 (2000).
[7] M. Büttiker, Y. Imry, R. Landauer, and S. Pinhas, Phys. Rev. B **31**, 6207 (1985).
[8] S. Viefers, P. Koskinen, P. Singa Deo, and M. Manninen, Physica E (Amsterdam) **21**, 1 (2004).
[9] T. Chakraborty and P. Pietiläinen, Phys. Rev. B **50**, 8460 (1994).
[10] K. Niemielä, P. Pietiläinen, P. Hyvönen, and T. Chakraborty, Europhys. Lett. **36**, 533 (1996).
[11] U. F. Keyser, C. Fühner, S. Borck, R. J. Haug, M. Bichler, G. Abstreiter, and W. Wegscheider, Phys. Rev. Lett. **90**, 196601 (2003).
[12] A. Emperador, F. Pederiva, and E. Lipparini, Phys. Rev. B **68**, 115312 (2003).
[13] J. I. Climente, J. Planelles, and F. Rajadell, J. Phys.: Condens. Matter **17**, 1573 (2005).
[14] T. Mano, T. Kuroda, S. Sanguinetti, T. Ochiai, T. Tateno, J. Kim, T. Noda, M. Kawabe, K. Sakoda, G. Kido, and N. Koguchi, Nano Lett. **5**, 425 (2005).
[15] C. Yannouleas and U. Landman, Phys. Rev. Lett. **82**, 5325 (1999).
[16] S. Nagaraja, J.-P. Leburton, and R. M. Martin, Phys. Rev. B **60**, 8759 (1999).
[17] A. Harju, S. Siljamäki, and R. M. Nieminen, Phys. Rev. Lett. **88**, 226804 (2002).
[18] M. Marlo, A. Harju, and R. M. Nieminen, Phys. Rev. Lett. **91**, 187401 (2003).
[19] A. Wensauer, O. Steffens, M. Suhrke, and U. Rössler, Phys. Rev. B **62**, 2605 (2000).
[20] J. J. Palacios and P. Hawrylak, Phys. Rev. B **51**, 1769 (1995).
[21] M. Pi, A. Emperador, M. Barranco, F. Garcias, K. Muraki, S. Tarucha, and D. G. Austing, Phys. Rev. Lett. **87**, 066801 (2001).
[22] B. Partoens and F. M. Peeters, Phys. Rev. Lett. **84**, 4433 (2000); Europhys. Lett. **56**, 86 (2001).

[23] A. Lorke, R. J. Luyken, A. O. Govorov, J. P. Kotthaus, J. M. Garcia, and P. M. Petrof., Phys. Rev. Lett. **84**, 2223 (2000).
[24] B. Szafran, F. M. Peeters, and S. Bednarek, Phys. Rev. B **70**, 125310 (2004).
[25] B. J. Baelus, S. V. Yampolskii, and F. M. Peeters, Phys. Rev. B **66**, 024517 (2002).
[26] S. M. Reimann and M. Manninen, Rev. Mod. Phys. **74**, 1283 (2002).
[27] M. B. Tavernier, E. Anisimovas, F. M. Peeters, B. Szafran, J. Adamowski, and S. Bednarek, Phys. Rev. B **68**, 205305 (2003).
[28] B. Szafran, F. M. Peeters, S. Bednarek, and J. Adamowski, Phys. Rev. B **69**, 125344 (2004).
[29] V. M. Bedanov and F. M. Peeters, Phys. Rev. B **49**, 2667 (1994).

In-plane magnetic-field-induced Wigner crystallization in a two-electron quantum dot

B. Szafran,[1,2] F. M. Peeters,[1,*] S. Bednarek,[2] and J. Adamowski[2]
[1]*Departement Fysica, Universiteit Antwerpen, (Campus Drie Eiken), B-2610 Antwerpen, Belgium*
[2]*Faculty of Physics and Nuclear Techniques, AGH University of Science and Technology, al. Mickiewicza 30, 30-059 Kraków, Poland*
(Received 21 June 2004; revised manuscript received 31 August 2004; published 23 December 2004)

The orbital effects of the in-plane magnetic field on a two-electron harmonic quantum dot are studied using a variational method. For flat quantum dots the singlet-triplet transitions appearing in a perpendicular magnetic field are absent in a magnetic field oriented parallel to the plane of confinement. Instead, a degeneracy of orbital energies for symmetric and antisymmetric states at high in-plane magnetic field is observed. This degeneracy is due to the formation of Wigner molecules in the laboratory frame of reference with charge islands elongated along the direction of the magnetic field and localized within the plane perpendicular to it.

DOI: 10.1103/PhysRevB.70.235335 PACS number(s): 73.21.−b, 73.22.Gk

I. INTRODUCTION

Epitaxially grown quantum dots[1] usually have a flat geometry with a confinement in the growth direction much stronger than the in-plane confinement. Application of a magnetic field oriented along the growth direction leads to a number of extensively studied[2] effects, i.e., angular momentum and spin transitions, which are observed in transport spectroscopy[3] as cusps in the single-electron charging lines. A high perpendicular magnetic field induces separation of electron charges, i.e., Wigner crystallization, which for circular dots appears only in the internal degrees of freedom. Laboratory-frame Wigner crystallization is a realizable feature of the ground state only at the angular momentum transitions.[5] On the other hand, Wigner molecules can be observed in anisotropic quantum dots if the system possesses a nondegenerate classical[4] counterpart reproducing the symmetry of the confinement potential.[5,6] The pinning of Wigner molecules by a local potential cavity[7,8] or by an external charged defect[9] was studied recently. In this paper we consider the breaking of the rotational symmetry of the quantum dot by the application of an in-plane magnetic field, and we show that it can result in a laboratory-frame Wigner localization.

The effect of the external magnetic field on the electron system is proportional to its flux through the area encircled by the electrons. Therefore, the orbital effects of the in-plane magnetic field are weaker than those of the perpendicular field and in the limit of a strictly two-dimensional confinement the in-plane magnetic field does not influence the orbital wave functions. Such an in-plane magnetic field has been applied experimentally[10–12] to investigate spin effects (Zeeman splitting and spin-orbit[13,14] interactions). Nevertheless, the electron wave functions in real dots have a finite spread in the growth direction. In pillar quantum dots based on $Al_xGa_{1-x}As/In_xGa_{1-x}As$ double barrier heterostructures[15] the quantum well has a width of 12 nm, and the width of the GaAs quantum well in the planar vertical dot[16] is about 17 nm. The lateral quantum dots[17] are based on a gated two-dimensional electron gas (2DEG) formed at a $GaAs–nAl_xGa_{1-x}As$ heterojunction. The vertical spread of the electron wave function in the 2DEG for typical values of the electron density and dopant concentration is also of the order 10–15 nm.[18] As a consequence, the orbital effects of the field are nonzero and can be visible for instance in the diamagnetic shifts[12] of chemical potentials. The role of the in-plane magnetic field for the attenuation of tunneling between vertically[19] and laterally[20] coupled dots has been pointed out.

The effect of the in-plane magnetic field on few-electron systems in a single dot has not been studied so far. The purpose of the present paper is to provide such a study for the two-electron system—the simplest few-electron eigenproblem. We show that although for strong vertical confinement and relatively weak magnetic fields the orbital related triplet-singlet energy difference (the exchange energy[20]) is positive and approximately constant, its limit value in the high magnetic field falls to zero, which results from the separation of the electron charges appearing due to Wigner crystallization. In vertical and lateral quantum dots the confinement in the growth direction has a rectangular or triangular shape. In the present paper we are interested in the qualitative effects of the in-plane field, so we consider a harmonic confinement potential that largely simplifies the calculations due to the separation of the center-of-mass motion.

This paper is organized as follows. The next section outlines the theory and the method to solve the Hamiltonian eigenvalue problem. In Sec. III the results and discussion are given. The summary and conclusions are presented in Sec. IV.

II. THEORY

We consider a pair of electrons in a three-dimensional harmonic quantum dot, rotationally symmetric with respect to the z axis and subject to a magnetic field oriented along the x direction. We apply the Landau gauge $\mathbf{A}=(0,-Bz,0)$ under which the Hamiltonian reads

$$H = -\hbar^2(\nabla_1^2+\nabla_2^2)/2m + m\omega^2(x_1^2+y_1^2+x_2^2+y_2^2)/2 + m(\omega_z^2+\omega_c^2)(z_1^2+z_2^2)/2 + i\hbar\omega_c(z_1\partial/\partial y_1 + z_2\partial/\partial y_2) + e^2/4\pi\epsilon\epsilon_0|\mathbf{r}_1-\mathbf{r}_2|, \quad (1)$$

where $\hbar\omega_z$ is the confinement energy in the z direction, $\hbar\omega$ is

the energy of confinement in the (x,y) plane, m is the electron band mass, $\omega_c = eB/m$ is the cyclotron frequency, and ϵ is the dielectric constant. For our numerical calculations material data of GaAs are used $m=0.067$ and $\epsilon=12.9$. We study the orbital effects neglecting the spin Zeeman interaction, which, however, can be trivially accounted for.

Introducing center-of-mass $\mathbf{R}=(\mathbf{r}_1+\mathbf{r}_2)/2$ and relative position $\mathbf{r}=\mathbf{r}_1-\mathbf{r}_2$ vectors, one can separate the Hamiltonian into a sum of center-of-mass and relative Hamiltonians $H=H_{cm}+H_{rel}$ with

$$H_{cm} = -\hbar^2\nabla_{cm}^2/2M + M\omega^2(X^2+Y^2)/2 + M(\omega_z^2+\omega_c^2)Z^2/2 + i\hbar\omega_c Z\,\partial/\partial Y \tag{2}$$

and

$$H_{rel} = -\hbar^2\nabla_{rel}^2/2\mu + \mu\omega^2(x^2+y^2)/2 + \mu(\omega_z^2+\omega_c^2)z^2/2 + i\hbar\omega_c z\,\partial/\partial y + e^2/4\pi\epsilon\epsilon_0 r, \tag{3}$$

where $M=2m$ and $\mu=m/2$. The two-electron wave function can be written as a product of center-of-mass and relative eigenfunctions

$$\Psi(\mathbf{r}_1,\mathbf{r}_2) = \Phi_{cm}[(\mathbf{r}_1+\mathbf{r}_2)/2]\Phi_{rel}(\mathbf{r}_1-\mathbf{r}_2). \tag{4}$$

It can be verified by a direct calculation that the ground-state energy of the center-of-mass motion equals $E_{cm}=\hbar\{\omega+[\omega_c^2+(\omega+\omega_z)^2]^{1/2}\}/2$, and that the ground-state wave function reads (up to a normalization constant)

$$\Phi_{cm}(\mathbf{R}) = \exp(-b_x X^2 - b_y Y^2 - b_z Z^2 + ib_{zy}ZY), \tag{5}$$

with $b_x=M\omega/2\hbar$, $b_y=M\omega\sqrt{1+\omega_c^2/(\omega_z+\omega)^2}/2\hbar$, $b_z=M\omega_z\sqrt{1+\omega_c^2/(\omega_z+\omega)^2}/2\hbar$, and $b_{zy}=M\omega_c\omega/(\omega_z+\omega)\hbar$.

The relative Hamiltonian (3) commutes with the parity operator $(\mathbf{r}\rightarrow-\mathbf{r})$. States with even (odd) parity are symmetric (antisymmetric) with respect to the interchange of electrons and therefore correspond to spin singlets (triplets). The relative Hamiltonian commutes also with operators of inversion in x direction $(x\rightarrow-x)$ and in the plane perpendicular to the magnetic field $[(y,z)\rightarrow-(y,z)]$. In the following we will label the states by their parities in x and y directions put in parentheses by the first and second descriptor, respectively [for instance, (even,odd) stands for a state even in x direction and odd in the (y,z) plane].

In the absence of the electron-electron interaction the contribution of the diamagnetic $(m\omega_c^2z^2/2)$ and the paramagnetic $(i\hbar\omega_c z\,\partial/\partial y)$ terms describing the in-plane magnetic field in Hamiltonians (1)–(3) can be evaluated analytically. For the center-of-mass Hamiltonian (2) and the wave function (5) the expectation values of the diamagnetic and paramagnetic terms equal $M\omega_c^2/8b_z=\hbar\omega_c^2/4\omega_z\sqrt{1+\omega_c^2/(\omega_z+\omega)^2}$ and $-\hbar\omega_c b_{zy}/4b_z=-\hbar\omega\omega_c^2/2(\omega_z+\omega)\omega_z\sqrt{1+\omega_c^2/(\omega_z+\omega)^2}$, respectively. In the limit of infinite ω_z the electrons become confined two-dimensionally in the $z=0$ plane, which leads to the vanishing of the diamagnetic and paramagnetic contributions (it is also evident from the form of the corresponding terms in the Hamiltonian). In order to maintain the values of the magnetic contributions to the energy, ω_c has to grow simultaneously with ω_z. For the ω_c/ω_z ratio kept constant the diamagnetic contribution is approximately linear in ω_c and the paramagnetic contribution is approximately constant.

TABLE I. Convergence of the energy estimates obtained with wave function (6) to the exact ground-state energy (last row) of the relative Hamiltonian as function of M (the number of terms used in the wave function is K) for $B=0$ and a spherically symmetric confinement potential with $\hbar\omega=\hbar\omega_z=3$ meV.

M	K	E(meV)
0	1	8.6100
2	5	8.4336
6	30	8.4187
14	204	8.4145
22	650	8.4134
exact		8.4134

In order to solve the eigenequation for the relative motion Hamiltonian in the presence of the interaction we use the variational method with the following trial wave function:

$$\Phi_{rel}(\mathbf{r}) = \exp(-\alpha x^2 - \beta y^2 - \gamma z^2 + iczy) \sum_{i,j,k=0}^{i+j+k\leqslant M} d_{ijk}x^i y^j z^k, \tag{6}$$

where α, β, γ, c are the nonlinear parameters and d_{ijk} is the linear variational parameter, M controls the number of basis elements. In the absence of the interaction, the wave function (6) reproduces exactly the analytic eigenfunctions using a finite number of terms in the expansion. In this sense the present approach is equivalent to the three-dimensional generalization of the method used by Drouvelis *et al.*[22,23] for two-dimensional anisotropic quantum dots with perpendicular magnetic field. Similar single-electron wave function was used by Harju *et al.*[21] for the configuration-interaction study of the electron pair in two-dimensional laterally coupled quantum dots.

The exact wave function for the s-type states in a harmonic-oscillator confinement potential is asymptotically linear in the limit $r\rightarrow0$ (has a cusp at $r=0$), which is related to the Coulomb interaction singularity. Since r cannot be developed in a MacLaurin series in Cartesian coordinates the present and previously used wave functions[21–23] cannot account for this linearity in the nearest neighborhood of the origin. We have performed test calculations in order to estimate the importance of this shortcoming. For this purpose we have solved the eigenequation for Hamiltonian (1) for $B=0$ and a spherically symmetric potential $\hbar\omega=\hbar\omega_z=3$ meV in a numerically exact manner with a finite difference method. Table I shows the convergence of the energy estimates obtained with the wave function (6) to the exact ground-state eigenvalue. Comparison of the wave functions is presented in Fig. 1. For $M=6$ the wave function has a shallow local minimum at the origin and the maximum of the wave function is shifted to the right with respect to the exact solution. For $M=22$ the local minimum gets almost as deep

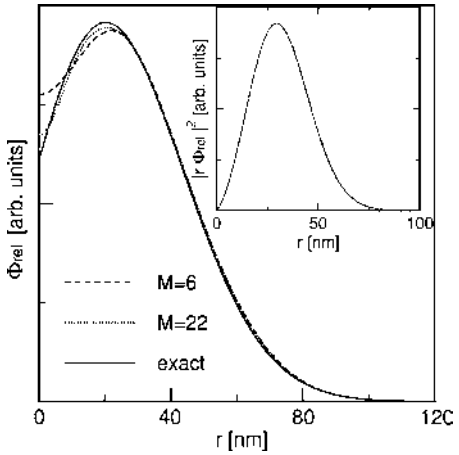

FIG. 1. Ground-state wave function of the relative Hamiltonian calculated for the parameters used in Table I. Solid line shows the exact wave function, the dashed (dotted) line is the wave function obtained by the variational method for $M=6(M=22)$. Inset: comparison of the exact radial probability density (solid line) with the dependence obtained variationally with $M=22$ (open circles).

as in the exact solution, the wave function becomes linear between 5 and 15 nm, and the position of the maximum of the wave function is improved with respect to the $M=6$ wave function. The expectation value of the energy is a functional of the radial probability density, which is depicted in the inset of Fig. 1. We can see that the exact radial probability density and the one calculated for $M=22$ are indistinguishable, which explains the high precision of the energy estimates (cf. Table I). The region of the trial wave function nonlinearity around the origin can be made arbitrarily small, and a numerically exact value of the energy and a nearly exact radial probability density are obtained. Therefore the application of the proposed wave function is well justified. The cusp shortcoming concerns also the states of p symmetry, but its importance is smaller since for p states the functions vanish at the origin. Wave functions of higher angular momentum have no cusps at the origin. The cusps in the exact s and p symmetry states dissapear[24] in the Wigner crystallization limit for which a Coulomb hole is formed in the relative wave function near $r=0$.

III. RESULTS AND DISCUSSION

A. Spherical quantum dot

We consider first the effect of the magnetic field on a spherical quantum dot. The lowest energy levels for all parity symmetries calculated with respect to the lowest Landau level are plotted in Fig. 2 as function of the external magnetic field. The solid (dotted) lines correspond to states of even (odd) total parity, i.e., to singlet (triplet) states. In the absence of a magnetic field the ground state corresponds to the angular momentum quantum number $L=0$, the lowest excited states of (even, odd) as well as with (odd, even) parity correspond to $L=1$. The lowest (odd, odd) energy level corresponds to $L=2$. The magnetic field breaks the spherical symmetry of the system so only the x-component

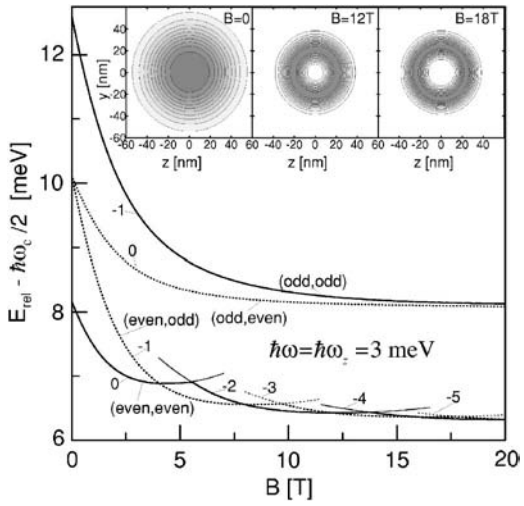

FIG. 2. Energy eigenvalues of the relative Hamiltonian (3) calculated with respect to the lowest Landau level for a spherical quantum dot with $\hbar\omega=\hbar\omega_z=3$ meV (Zeeman effect neglected). The solid and dotted lines show the singlet and triplet energy levels, respectively. In parentheses the parity of the corresponding eigenstates in the x direction and within the (y, z) plane is given. The numbers indicate the x component of the angular momentum in $\hbar$ units. The inset shows the lowest singlet probability density integrated over the x direction for magnetic fields $B=0$, 12, and 18 T.

of the angular momentum is quantized. Figure 2 shows that angular momentum and spin transitions appear in the ground state. The x component of angular momentum of the lowest singlet (triplet) states takes values of even (odd) parity integers (in $\hbar$ units). The angular momentum transitions and the singlet-triplet oscillations are qualitatively similar to the effects appearing in two-dimensional circular quantum dots in the presence of a perpendicular magnetic field.[23,25] The origin of the singlet-triplet oscillations in two-electron two-dimensional quantum dots is well understood. The increase of the magnetic field pushes the maximum of the relative wave function toward the origin (in the three-dimensional case—towards the x axis) increasing the mean value of the Coulomb interelectron repulsion. In consequence the state of a higher angular momentum (with stronger electron separation) acquires lower energy beyond some critical value of the magnetic field. The ground-state angular momentum (without the spin Zeeman term) takes the subsequent integer values as the magnetic field increases. The lowest-energy states of the odd (even) angular momentum are realized in the triplet (singlet) spin configuration,[25] which leads to the singlet-triplet oscillations.

On the other hand, the order of the lowest singlet and triplet energy levels that are odd in the x direction is not affected by the field (cf. Fig. 2). Here, the magnetic-field-induced localization of the relative wave function around the x axis does not essentially decrease the electron-electron distance since in these states the electrons are separated in the x direction. The driving force for the singlet-triplet oscillations is therefore absent in this branch of energy levels.

The inset to Fig. 2 shows the contours of the relative probability density for the lowest singlet state integrated over the x direction. Note that in the integration the minimum of

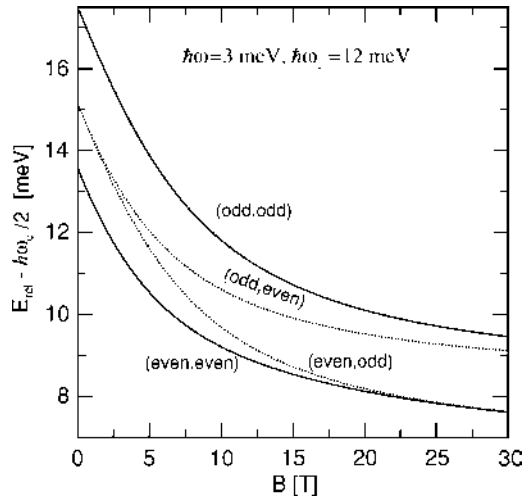

FIG. 3. Energy eigenvalues of the relative Hamiltonian calculated with respect to the lowest Landau level for a flat quantum dot with $\hbar\omega=3$ meV and $\hbar\omega_z=12$ meV. The solid and dotted lines show the singlet and triplet energy levels, respectively. In parentheses the parity of the corresponding eigenstates in the x direction and within the (y,z) plane is given.

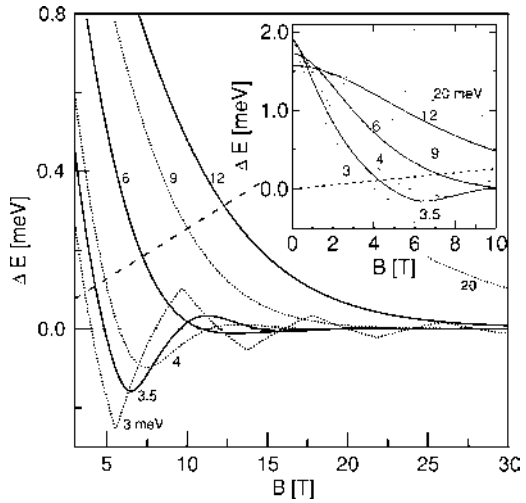

FIG. 4. Triplet-singlet energy difference (without the spin Zeeman effect) as function of the magnetic field for $\hbar\omega=3$ meV and various confinement energies in the z direction. The thick dashed line shows the spin Zeeman splitting between the triplet and the singlet states. The inset shows the low-magnetic-field region.

the probability density at the origin for $B=0$ (cf. Fig. 1) disappears. The lowest singlet states for $B=0$, 12, and 18 T correspond to the x component of the angular momentum equal to 0, $-2\hbar$, and $-4\hbar$, respectively. For nonzero angular momentum, the probability density is totally removed from the x axis. The densities exhibit perfect circular symmetry around the x axis, although it is not evident from the form of the Landau-gauge Hamiltonian [cf. Eq. (3)]. This result can serve as an additional test of the reliability of the numerical approach applied.

B. Flat quantum dot

The low-energy spectrum for a flat quantum dot with $\hbar\omega=3$ meV and $\hbar\omega_z=12$ meV is plotted in Fig. 3 (Zeeman effect neglected). For this value of the z confinement energy the spread of the electron charge density in the z direction $2\Delta z=2\langle z^2\rangle^{1/2}=\sqrt{2\hbar/m\omega_z}$ is about 13.75 nm. The magnetic field lifts the degeneracy of the triplet energy levels, which for $B=0$ correspond to states with z-component angular momentum equal to $\pm\hbar$. In the presence of a magnetic field oriented along the x direction none of the components of the angular momentum commute with the Hamiltonian and therefore none of them are quantized. The external magnetic field leads to singlet-triplet degeneracy in contrast to singlet-triplet oscillations observed in a spherical dot (cf. Fig. 2). Figures 2 and 3 show that the lowest singlet as well as the lowest triplet states have even x direction parity, independently of the value of the magnetic field and the strength of the electron-electron interaction.

The singlet-triplet energy splitting in the absence of the spin Zeeman effect is shown in more detail in Fig. 4. The exchange energy for the spherical quantum dot has a discontinuous derivative when angular momentum transitions appear in the lowest singlet or triplet states. For small anisotropy of the confinement potential (cf. the line for $\hbar\omega_z=3.5$ meV), the exchange energy becomes a smooth function of the magnetic field. The oscillations of the energy difference around zero have a decreasing amplitude with growing confinement energy in the z direction. For $\hbar\omega_z\geqslant 8$ meV the oscillations disappear and the exchange energy decreases monotonically to zero with the external field. The thick dashed line in Fig. 4 shows the spin Zeeman splitting between the singlet and triplet states ($-B\hbar g^*\mu_B$ with the effective Landé factor $g^*=-0.44$). The crossing of this line with the exchange energy curves indicate the value of the magnetic field for which the triplet becomes the ground state.

The inset to Fig. 4 shows the exchange energy in the low magnetic field region. For $B=0$ T the singlet-triplet energy splitting is a decreasing function of the strength of confinement in the z direction. As the z size of the quantum dot is decreased the system starts to approach the strictly two-dimensional limit in which the singlet-triplet splitting for $\hbar\omega=3$ meV is 1.3 meV. The increase of the z confinement energy affects more strongly the energy of the singlet state, increasing the value of the wave function at the origin (corresponding to both electrons localized in the same position). The triplet wave function vanishes at the origin due to the Pauli exclusion principle.

Let us now look at the origin behind the magnetic-field-induced singlet-triplet degeneracy for the dot with $\hbar\omega_z=12$ meV. The contour plots in Fig. 5 show the relative probability density integrated over x (left panel) and z (right panel) coordinates for the lowest singlet state. The quasi-three-dimensional plots at the right-hand side of Fig. 5 show the surface in the $z>0$ half space at which the probability density falls to one-fifth of its maximum value. Region inside the surface contains roughly 90% of the probability. For $B=0$ T the probability density integrated over the x direction exhibits local maxima outside the $y=0$ line (cf. left panel of the contour plot in Fig. 5). The magnetic field transforms them into separated islands on the (y, z) plane. For $B=0$ T

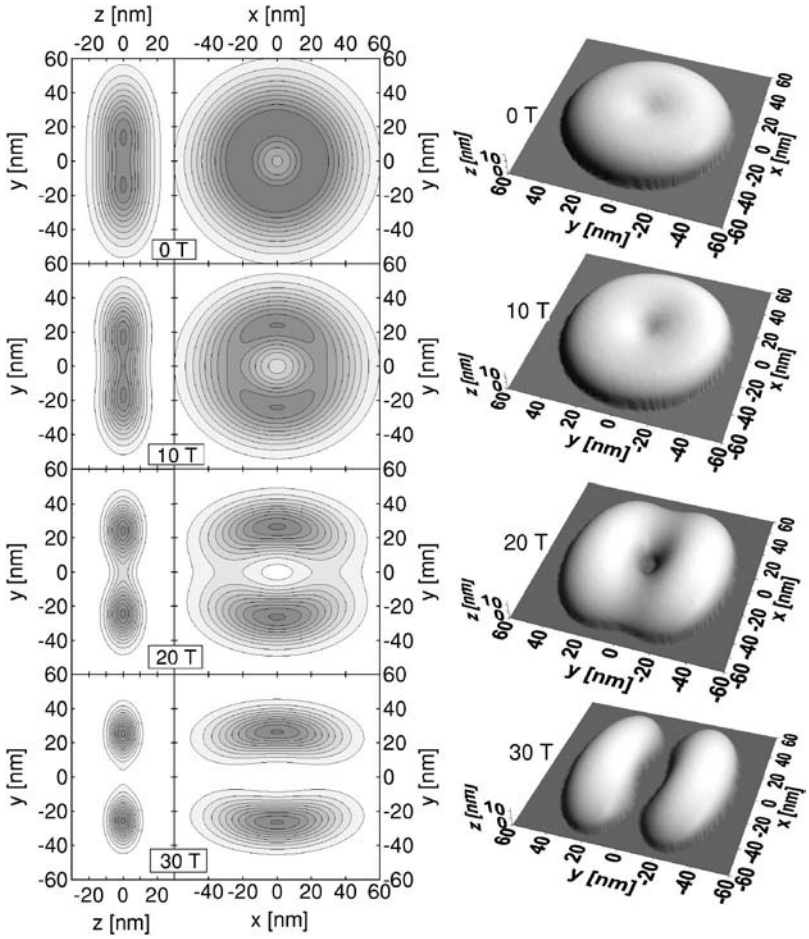

FIG. 5. Contour plots at the left side of the figure shows the relative motion probability density for the lowest singlet state integrated over the x direction (left panel) and over the z coordinate (right panel) for $\hbar\omega=3$ meV, $\hbar\omega_z=12$ meV, and different magnetic fields. Larger values of density are marked with darker colors. At the right side of the figure we show the surface at which the probability density takes one-fifth of its maximum value.

the density integrated over the z coordinate is circular symmetric (cf. right panel of the contour plot in Fig. 5). For the flat quantum dot the integration over the z coordinate does not fill in the central local maximum as in the spherical case (cf. Fig. 1 and inset of Fig. 2 for $B=0$ T). When a magnetic field is applied, the density loses its circular symmetry and is transformed into two maxima elongated along the direction of the magnetic field (x) and becomes strongly localized in the direction perpendicular to the field. The region in which the probability density is nonzero at high magnetic field resembles two beans put along the x axis near the $z=0$ plane.

Figure 6 shows the relative probability density for the triplet state [of odd parity in the (y,z) plane and of even parity in the x direction]. For $B=0$ the y and z degrees of freedom are decoupled and the wave function is simply of odd parity in the y direction and even in z direction.[26] The plots for $B=0$ T show that the density vanishes near the $y=0$ plane and that it forms two semiround islands parallel to the x axis localized around the $z=0$ plane. Magnetic field makes the islands thinner, longer, and less oval. For $B=30$ T the probability densities for the triplet and singlet states become almost identical, which is the reason for the singlet-triplet degeneracy at high magnetic field (cf. Fig. 3).

For the sake of physical interpretation it is useful to look at the ground-state charge density in the laboratory frame of reference. The charge density can be extracted from the two-electron wave function by integration with Dirac δ functions

$$n(\mathbf{r}) = \langle \Psi(\mathbf{r}_1,\mathbf{r}_2)|\delta(\mathbf{r}-\mathbf{r}_1)+\delta(\mathbf{r}-\mathbf{r}_2)|\Psi(\mathbf{r}_1,\mathbf{r}_2)\rangle$$
$$= 2\int d\mathbf{r}_1 |\Phi_{cm}((\mathbf{r}_1+\mathbf{r})/2)|^2 |\Phi_{rel}(\mathbf{r}_1-\mathbf{r})|^2. \quad (7)$$

Figure 7 shows the comparison of the probability densities of the center-of-mass and relative ground states and the two-electron charge densities (divided for comparison by two) integrated over the z direction for the potential parameters of Figs. 5 and 6.[27] The noninteracting density (divided by two) and the center-of-mass density come from solutions of the same Schrödinger equations, the only difference is that the center of mass is twice heavier, which results in a stronger localization of the center-of-mass density. On the other hand, the mass that enters the relative Hamiltonian is half of the electron mass, which along with the repulsive Coulomb potential results in a weaker localization of the relative charge density. The interacting two-electron charge density calculated according to expression (7) is more weakly localized than the center-of-mass density but the localization is stronger than for the relative wave function. The integration of the relative charge density with the center-of-mass density fills the Coulomb hole visible in the relative density (cf. right panel of Fig. 5 for $B=0$ T). The effect of the Coulomb interaction on the electron localization can be estimated from a comparison of the interacting and noninteracting charge densities.

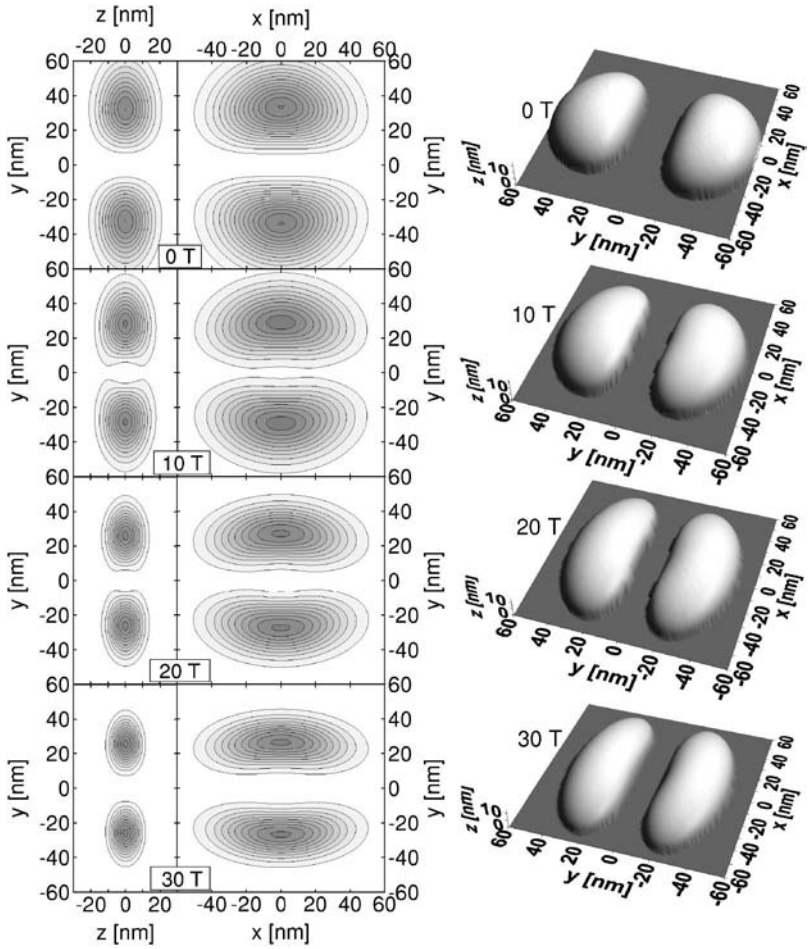

FIG. 6. The same as Fig. 5 but now for the lowest triplet state.

The evolution of the ground-state charge density $[n(\mathbf{r})]$ with the in-plane magnetic field, which is presented in Fig. 8. The two local maxima of the probability density visible for the relative eigenstate (cf. left plot for $B=0$ T in Fig. 5) merge into a central maximum when integrated over the relative probability density with the center-of-mass density. For $B=10$ T the limits of the charge pool become squeezed in the direction perpendicular to the field. The appearance of the maximum elongated along the $x=0$ axis (cf. right plot for $B=10$ T) is due to the formation of the two maxima in the relative density (cf. right plot in Fig. 5 for $B=10$ T). Plots for $B=20$ T and $B=30$ T show a distinct separation of the electron charges, i. e., Wigner crystallization. The single-electron charge islands formed under the influence of the in-plane field form stripes elongated along the direction of the applied field. The extent of the charge density is not essentially changed along the direction of the field.

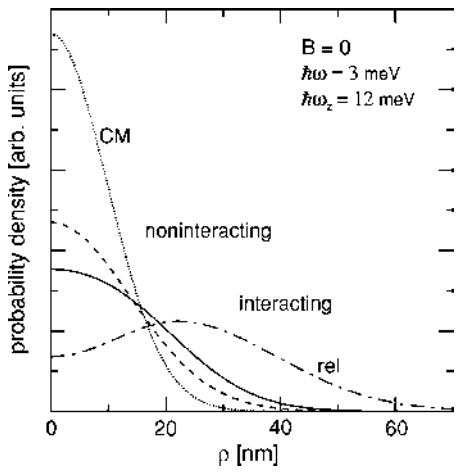

FIG. 7. Probability densities of the ground state of the center of mass (CM) and relative (rel) Hamiltonians, and the charge density of the noninteracting and interacting system of two electrons integrated over the z direction as a function of the radial coordinate $\rho=\sqrt{x^2+y^2}$ for $\hbar\omega=3$ meV, $\hbar\omega_z=12$ meV, and $B=0$ T. The two-electron charge densities have been divided by 2.

The magnetic-field-induced singlet-triplet degeneracy can be conveniently explained in the single-electron picture as due to the vanishing overlap between the wave functions of the two electrons. In the absence of the overlap the exchange interaction disappears leading to the observed spin degeneracy. The wave function separation is due to the strong localization of the single-electron charge islands in the direction perpendicular to the field. The present effect is similar to the singlet-triplet degeneracy induced by the in-plane magnetic field for laterally coupled quantum dots.[19,20] For coupled dots the in-plane magnetic field induces stronger localization in each of the quantum dots, which results in a decreasing tunnel coupling (an increase of the effective height of the interdot barrier), which eventually leads to the

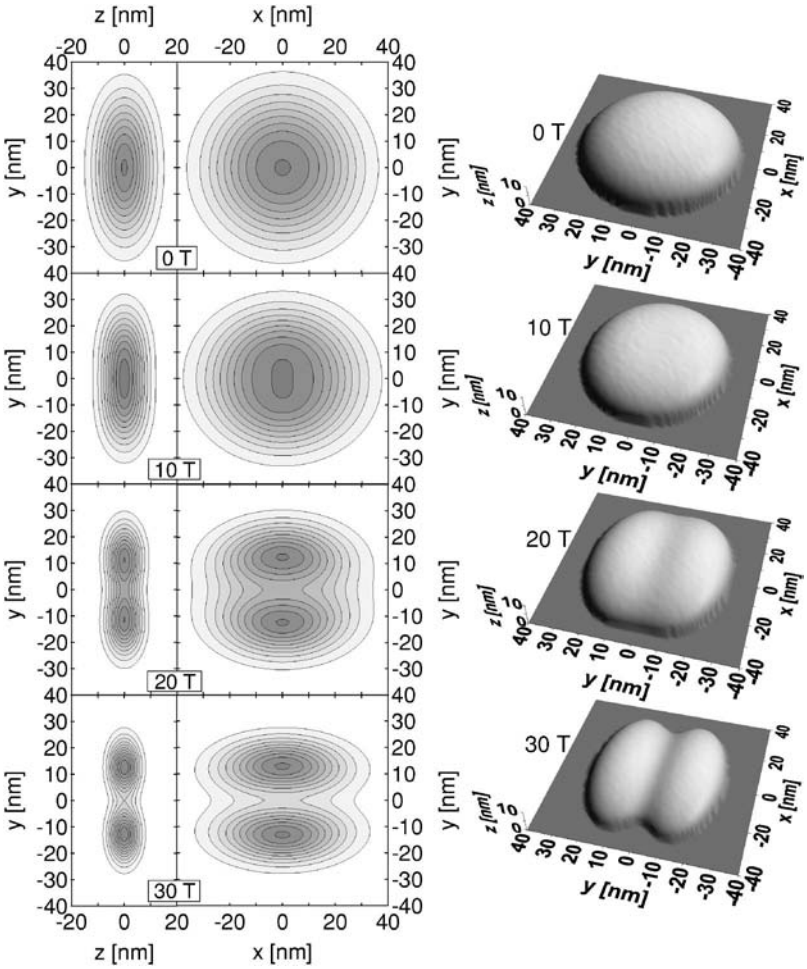

FIG. 8. Contour plots at the left side of the figure show the two-electron probability densities $[n(\mathbf{r})]$ integrated over the x (left panel) and z coordinates (right panel) for $\hbar\omega=3$ meV, $\hbar\omega_z=12$ meV. The surface plots at the right side of the figure show the surface at which the charge density takes one-fifth of its maximum value.

separation of the single-electron wave functions. The separation accompanied with the singlet-triplet degeneracy appears also without the in-plane field for the thick interdot barrier[28] as well as in large quasi-one-dimensional quantum dots.[28,29] Drouvelis *et al.*[23] found the ground-state singlet-triplet degeneracy for large anisotropy in a *small* two-dimensional quantum dot in the absence of the external magnetic field. For strong anisotropy this model[23] gives a *strictly* one-dimensional potential, for which the Coulomb interaction is extremely strong, leading to Wigner crystallization even for dots of relatively small size.

Since the laboratory frame separation is accompanied by a singlet-triplet degeneracy one can use the vanishing value of the exchange energy to propose a criterium for the magnetic-field-induced Wigner crystallization. Figure 9 shows the triplet-singlet energy difference (Zeeman effect neglected) on the $(\hbar\omega_z, B)$ plane for $\hbar\omega=3$ meV. The magnetic field for which the exchange energy becomes negligible is a distinctly growing function of $\hbar\omega_z$. The magnetic field above which the exchange energy falls below 0.1 meV for $\hbar\omega_z>4$ meV can be very well approximated by a linear dependence $B=1.6(\hbar\omega_z-1.266\ \text{meV})$ T/meV. The value of the magnetic-field-inducing Wigner crystallization is an increasing function of $\hbar\omega$—the confinement energy in the (x,y) plane. For $\hbar\omega_z>\frac{4}{3}\hbar\omega$ the exchange energy falls to 0.1 meV at $B=1.24(\hbar\omega_z-0.37\ \text{meV})$ T/ meV, $B=2.1(\hbar\omega_z-1.72\ \text{meV})$

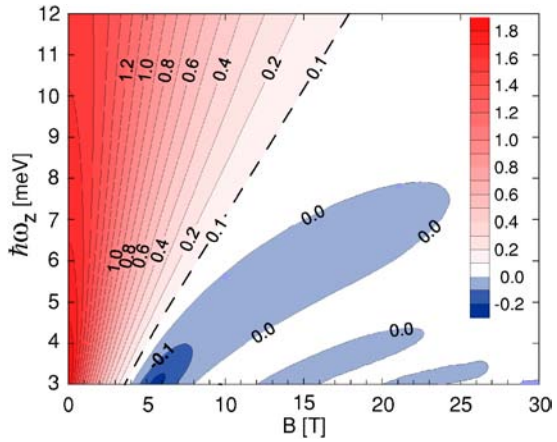

FIG. 9. (Color online) Triplet-singlet energy difference as a function of the magnetic field and vertical confinement energy for $\hbar\omega=3$ meV. Blue (white and red) regions correspond to the triplet (singlet) ground state for the spin Zeeman effect neglected. The dashed line shows the values of B and $\hbar\omega_z$ for which the triplet-singlet energy difference is equal to 0.1 meV. Color scale is given at the right-hand side of the figure.

T/meV, $B=2.95(\hbar\omega_z-3.74$ meV) T/meV for $\hbar\omega=2$, 5, and 10 meV, respectively.

In spherical quantum dots (cf. Fig. 2) as well as in circular two-dimensional quantum dots in a perpendicular magnetic field[23,25] singlet-triplet oscillations are observed instead of the above degeneracy. But in these systems the separation of the electron charges appears in the inner degrees of freedom not in the laboratory frame, so that the picture of vanishing overlap between the single-electron wave functions does not apply (it would imply breaking of the symmetry of the external potential).

In the present paper we have used a harmonic confinement potential in the growth direction. The potential in real dots has often a quantum-well or a triangular form. Although the shape of the confinement in the growth direction should not have a qualitative influence on the results, one should expect quantitative differences except in the region where the magnetic field is so strong that the magnetic length ($\sqrt{2\hbar/eB}=36.28/\sqrt{B}$ nm$\sqrt{T}$) is much smaller than the range of the vertical confinement. In quantum wells the energy spacings between the lowest-energy levels are larger than that for the harmonic-confinement potential. The spacings between the lowest-energy levels for an infinite quantum well with width 13.75 nm (corresponding to a similar vertical spread of the electron wave function for $\hbar\omega_z=12$ meV) equal 22 meV. Therefore, the in-plane magnetic field values inducing Wigner crystallization in dots with well-like vertical confinement will be larger than the ones found in this paper for the harmonic-confinement potential.

IV. SUMMARY AND CONCLUSIONS

We have studied the orbital effects due to the external magnetic field oriented along the *x* axis on two electrons confined within a harmonic three-dimensional quantum dot rotationally symmetric with respect to the *z* axis. Calculations used explicitly the center-of-mass separation and were performed with Gaussian trial wave functions. In flat quantum dots a high in-plane magnetic field leads eventually to spin degeneracy (in the absence of the spin Zeeman interaction) instead of spin-triplet oscillations, which are obtained for magnetic field oriented along the axis of a cylindrical symmetric quantum dot. The spin degeneracy is due to Wigner crystallization induced in the laboratory frame by the in-plane magnetic field. For flat quantum dots and low magnetic fields the orbital effects have initially a negligible effect on the singlet-triplet energy splitting. In the high-magnetic-field limit, when Wigner molecules are formed, all the singlet-triplet splitting can be *strictly* attributed to spin-related effects. Nevertheless, between the low-field and molecular regimes there exists a magnetic field interval for which the exchange energy rapidly changes with the magnetic field.

ACKNOWLEDGMENTS

This paper was partly supported by the Polish Ministry of Scientific Research and Information Technology in the framework of the solicited grant PBZ-MIN-008/P03/2003, the Flemish Science Foundation (FWO-Vl), the Belgian Science Policy, and the University of Antwerpen (VIS and GOA). The first author is supported by the Foundation for Polish Science (FNP) and by Marie Curie IEF Project No. MEIF-CT-2004-500157.

*Electronic address: francois.peeters@ua.ac.be

[1] L. Jacak, P. Hawrylak, and A. Wójs, *Quantum Dots* (Springer Berlin, 1998).
[2] S. M. Reimann and M. Manninen, Rev. Mod. Phys. **74**, 1283 (2002).
[3] L. P. Kouwenhoven, D. G. Austing, and S. Tarucha, Rep. Prog. Phys. **64**, 701 (2001).
[4] V. M. Bedanov and F. M. Peeters, Phys. Rev. B **49**, 2667 (1994).
[5] B. Szafran, F. M. Peeters, S. Bednarek, and J. Adamowski, Phys. Rev. B **69**, 125344 (2004).
[6] M. Manninen, M. Koskinen, S. M. Reimann, and B. Mottelson, Eur. Phys. J. D **16**, 381 (2001).
[7] B. Reusch and R. Egger, Europhys. Lett. **64**, 84 (2003).
[8] A. D. Güçlü, J.-S. Wang, and H. Guo, Phys. Rev. B **68**, 035304 (2003).
[9] B. Szafran and F. M. Peeters, Europhys. Lett. **66**, 701 (2004).
[10] J. A. Folk, S. R. Patel, K. M. Birnbaum, C. M. Marcus, C. I. Duruöz, and J. S. Harris Jr., Phys. Rev. Lett. **86**, 2102 (2001).
[11] R. Hanson, B. Witkamp, L. M. Vandersypen, L. H. Willems van Beveren, J. M. Elzerman, and L. P. Kouwenhoven, Phys. Rev. Lett. **91**, 196802 (2003).
[12] R. M. Potok, J. A. Folk, C. M. Marcus, V. Umansky, M. Hanson, and A. C. Gossard, Phys. Rev. Lett. **91**, 016802 (2003).
[13] B. I. Halperin, A. Stern, Y. Oreg, J. N. H. J Cremers, J. A. Folk, and C. M. Marcus, Phys. Rev. Lett. **86**, 2106 (2001).
[14] M. Valín-Rodriguez, A. Puente, and L. Serra, Phys. Rev. B **69**, 085306 (2004).
[15] S. Tarucha, D. G. Austing, T. Honda, R. J. van der Hage, and L. P. Kouwenhoven, Phys. Rev. Lett. **77**, 3613 (1996).
[16] R. C. Ashoori, H. L. Stormer, J. S. Weiner, L. N. Pfeiffer, S. J. Pearton, K. W. Baldwin, and K. W. West, Phys. Rev. Lett. **68**, 3088 (1992).
[17] J. Schmid, J. Weis, K. Eberl, and K. v. Klitzing, Phys. Rev. Lett. **84**, 5824 (2000).
[18] F. Stern and S. Das Sarma, Phys. Rev. B **30**, 840 (1984).
[19] D. Bellucci, M. Rontani, F. Troiani, G. Goldoni, and E. Molinari, Phys. Rev. B **69**, 201308 (2004).
[20] G. Burkard, D. Loss, and D. P. Di Vicenzo, Phys. Rev. B **59**, 2070 (1999).
[21] A. Harju, S. Siljamäki, and R. M. Nieminen, Phys. Rev. Lett. **88**, 226804 (2002).
[22] P. S. Drouvelis, P. Schmelcher, and F. K. Diakonos, Europhys. Lett. **64**, 232 (2003).
[23] P. S. Drouvelis, P. Schmelcher, and F. K. Diakonos, Phys. Rev. B

69, 155312 (2004); **69**, 035333 (2004).
[24] B. Szafran, J. Adamowski, and S. Bednarek, Physica E (Amsterdam) **5**, 185 (2000).
[25] M. Dineykhan and R. G. Nazmitdinov, J. Phys.: Condens. Matter **11**, L83 (1999).
[26] This wave function is *not* the eigenfunction of the *z* component angular momentum. However, it can be constructed from a superposition of degenerate wave functions with the *z*-component angular momentum $\pm\hbar$ at $B=0$.
[27] The charge densities are normalized with the Jacobian ρ.
[28] S. Bednarek, T. Chwiej, J. Adamowski, and B. Szafran, Phys. Rev. B **67**, 205316 (2003).
[29] B. Szafran, F. M. Peeters, S. Bednarek, T. Chwiej, and J. Adamowski, Phys. Rev. B **70**, 035401(2004).

Spatial ordering of charge and spin in quasi-one-dimensional Wigner molecules

B. Szafran,[1,2] F. M. Peeters,[1] S. Bednarek,[2] T. Chwiej,[1,2] and J. Adamowski[2]
[1]*Departement Natuurkunde, Universiteit Antwerpen (Campus Drie Eiken), B-2610 Antwerpen, Belgium*
[2]*Faculty of Physics and Nuclear Techniques, AGH University of Science and Technology, al. Mickiewicza 30, 30-059 Kraków, Poland*
(Received 19 January 2004; published 2 July 2004)

Few-electron systems confined in quasi-one-dimensional quantum dots are studied by the configuration interaction approach. We consider the parity symmetry of states forming Wigner molecules in large quantum dots and find that for the spin-polarized Wigner molecules it strictly depends on the number of electrons. We investigate the spatial spin ordering in the inner coordinates of the quantum system and conclude that for small dots it has a short-range character and results mainly from the Pauli exclusion principle while the Wigner crystallization in large dots is accompanied by spin ordering over the entire length of the dot.

DOI: 10.1103/PhysRevB.70.035401 PACS number(s): 73.21.La, 73.20.Qt

I. INTRODUCTION

Strong confinement of charge carriers in two directions results in reduction of their degrees of freedom to a single one, i.e., in quasi-one-dimensional motion. Such one-dimensional systems are realized typically in split-gate[1,2] and cleaved-edge overgrowth[3] semiconductor quantum wires, as well as in carbon nanotubes,[4] but can also be realized in finite-size systems, i.e., in anisotropic quantum dots[5] or quantum rings.[6] There is a renewed interest in the one-dimensional systems related to the recent progress of vapour-liquid-solid fabrication of quantum wires of very high quality.[7–9]

The present paper is devoted to electron systems confined in one-dimensional quantum dots and in particular to their Wigner crystallization[10] appearing when the electron-electron interaction dominates over the kinetic energy. Wigner electron solids (Wigner molecules) are predicted to appear in large dots[11] or in strong magnetic fields.[12] In the Wigner molecules the charge density separates into distinct charge maxima each corresponding to one of the confined electrons. Formation of Wigner molecules in the ground-state charge density in one-dimensional quantum dots was previously obtained in exact diagonalization[13–15] and the density functional approach.[16] In one-dimensional dots the Wigner localization appears in the laboratory frame, in contrast to the inner-coordinate crystallization appearing in circular quantum dots,[12] including quantum rings. Transport properties of Wigner crystals formed in open infinite one-dimensional systems have also been studied.[17,18] The Luttinger liquid formalism has been applied[19] to quantum wires with box-like boundary conditions, i.e., to the one-dimensional quantum dots. Melting of classical one-dimensional Wigner crystals has recently been described.[20]

We study the quasi-one-dimensional quantum dots using a configuration interaction approach with the effective electron-electron interaction potential which we derived recently.[21] This work is a generalization of our exact two-electron study[15] to a larger number of electrons. In the weak confinement limit the ground state becomes nearly degenerate with respect to the spin configuration of the electron system.[14,15] Similar approximate degeneracy has been found in quantum rings of large radius.[22] In this paper we study the parity symmetry of the nearly degenerate states forming Wigner molecules in large dots. We show that for spin-polarized electrons the Wigner localization is formed only for one (even or odd) spatial parity of the state strictly dependent on the number of electrons. We present this dependence in the form of a theorem for which we provide a rigorous analytical proof. The found dependence of the parity of one-dimensional Wigner molecule states on the number of electrons is similar to the appearance of the magic angular momenta states for which Wigner crystallization is possible in circular dots.[23,24] Furthermore, we discuss an inhibition of Wigner crystallization by a perturbation of the confinement potential through a central inversion-invariant potential well.

Magnetic spin ordering of electrons in one-dimensional space has been extensively studied[25] in Hubbard models which, in one dimension with only nearest-neighbor hopping interactions, predict the appearance of a low-spin ground state.[26] This is a consequence[26] of the Lieb-Mattis theorem[27] which implies that without spin-dependent interactions the ground state of one-dimensional electron systems corresponds to the lowest possible spin quantum number ($S=0$ or $1/2$). This feature generally does not have to result in any spatial spin ordering. In this paper we use the exact numerical solution of the Schrödinger equation to investigate the spatial distribution of spins in the one-dimensional quantum dot and the relation between the charge and spatial spin ordering in the Wigner crystallization limit. We find that Wigner crystallization is accompanied by a long-range spin-ordering in the inner coordinates of the system instead of a spin-symmetry breaking predicted by the density functional theory.[16,28] In the ground-state this ordering has a clear antiferromagnetic character.

This paper is organized as follows. In Sec. II we present the theoretical method. Section III contains the results for the Wigner localization and ground state degeneracy of the few electron systems. In Sec. IV we present proof for the dependence of the parity of spin-polarized Wigner molecules on the number of electrons. Section V contains a discussion of the effect of a central defect on Wigner crystallization. In Sec. VI the study of spin ordering is presented. Section VII contains our summary and conclusions.

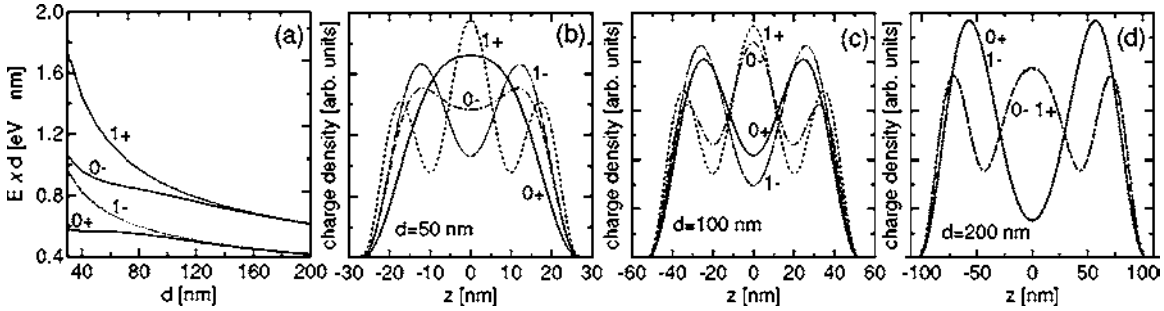

FIG. 1. (a) Lowest energy levels multiplied by the dot length for $N=2$. Numbers close to the curves denote the total spin quantum number of the corresponding states and signs +, − stand for even and odd parity symmetry. (b), (c), (d) Charge density of 0+, 1−, 1+, and 0− states plotted with solid, dotted, dashed, and dash-dotted lines for $d=50$, 100, and 200 nm, respectively.

II. THEORY

We consider N electrons confined in a quasi-one-dimensional quantum dot with strong lateral harmonic-oscillator confinement potential. The Hamiltonian of the system reads

$$H=\sum_{i=1}^{N} h_i+\sum_{i=1}^{N}\sum_{j>i}^{N}\frac{\kappa}{r_{ij}}, \tag{1}$$

where h stands for the single-electron Hamiltonian

$$h=-\frac{\hbar^2}{2m^*}\nabla^2+\frac{m^*\omega^2}{2}(x^2+y^2)+V(z), \tag{2}$$

$V(z)$ is the confinement potential in the z direction. For a large lateral harmonic-oscillator confinement energy ($\hbar\omega$) the movement of electrons in the (x,y) plane is frozen to the harmonic-oscillator ground state. Then, one can perform integration[21] over the lateral degrees of freedom which results in the following Hamiltonian:

$$H=N\hbar\omega+\sum_{i=1}^{N} h_i^{1D}+\sum_{i=1}^{N}\sum_{j>i}^{N}(\pi/2)^{1/2}(\kappa/l)$$
$$\times \mathrm{erfc}(z_{ij}/2^{1/2}l)\exp(z_{ij}^2/2l^2), \tag{3}$$

where $z_{ij}=|z_i-z_j|$ and

$$h^{1D}=-\frac{\hbar^2}{2m^*}\frac{d^2}{dz^2}+V(z) \tag{4}$$

is the single-electron one-dimensional Hamiltonian. In the following we will neglect the first term in Eq. (3), i.e., the lateral confinement energy which is independent of the form of wave functions in the z direction. The last term in Eq. (3) is the effective interaction energy[21] for electrons in a quasi-one-dimensional environment resulting from integration of the Coulomb potential over the lateral coordinates, m^* is the effective mass, $\kappa=e^2/4\pi\varepsilon_0\varepsilon$, ε is the dielectric constant, and $l=\sqrt{\hbar/m^*\omega}$. We assume $V(z)=V_{\mathrm{well}}(z)$, a rectangular potential well of depth $V_0=200$ meV, and width d. We adopt GaAs material parameters, i.e., $m^*=0.067\,m_{e0}$, $\epsilon=12.4$ as well as $\hbar\omega=10$ meV ($l=10.66$ nm) for the lateral confinement energy. Calculations have been performed for $N=2,\ldots,5$ electrons by the configuration interaction approach with a basis set of Slater determinants built with single-electron spin orbitals. Spatial single-electron wave functions have been obtained by numerical diagonalization of the finite-difference version of the single-electron one-dimensional Hamiltonian (4) on a mesh of points. In construction of the Slater determinants with required spin and parity symmetries we use the spatial wave functions of up to eight lowest-energy single-electron states which results in a Slater determinant basis size of up to 1520 elements and an accuracy better than 0.01 meV.

The present approach is based on the assumption that only the lowest state of the lateral (x,y) quantization is occupied. We performed test calculations for two, three and four electrons to check the validity of this approach. We allowed the electrons to occupy also the p-type lowest excited state of the lateral quantization with angular momentum $\pm\hbar$. Inclusion of p states not only allows for determination of the critical well length above which the p shell is emptied, but it is also helpful to estimate the importance of the angular correlations in the x-y plane. The Coulomb matrix elements were evaluated using effective interaction potentials derived with the use of the Fourier transform technique.[21] We have obtained the following results: the p shell is left empty for $d>39$ and 41 nm for $N=3$ and 4, respectively (for two electrons the p shell is never occupied). Accounting for the x-y correlations via inclusion of the p-type orbitals in the configuration interaction basis lowers the two-electron total energy estimates by 0.18, 0.12, 0.01, and 10^{-4} meV for $d=40,50,100$, and 200 nm, respectively. These "lateral correlation energies" for the same values of d are equal to 0.4, 0.3, 0.08, and 4×10^{-3} meV for $N=3$, and 1.18, 0.67, 0.23, and 0.03 for $N=4$, respectively. The energy overestimation in the range of d studied further is never significant and the present approach is nearly exact in the Wigner localization regime.

III. GROUND STATE DEGENERACY AND WIGNER CRYSTALLIZATION

In this paper we label the states by their total spin S and parity quantum numbers using the notation: $S\pm$, where the positive (negative) sign stands for even (odd) parity. We discuss only the lowest-energy states for a given spin-orbital symmetry. Figure 1(a) shows the lowest energy levels of the two-electron system multiplied by the dot length d as functions of d. For large dots the states 0+ and 1− as well as

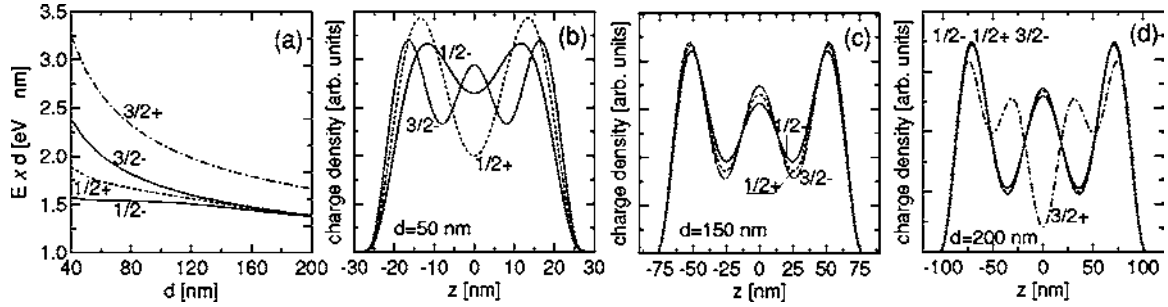

FIG. 2. (a) Lowest energy levels multiplied by the dot length for $N=3$. (b), (c), (d) Charge density of $1/2-$, $1/2+$, and $3/2-$ states plotted with solid, dashed, and dotted lines for $d=50$, 150, and 200 nm, respectively. In (d) the charge density of the $3/2+$ state is shown by the dash-dotted curve.

$0-$ and $1+$ become mutually degenerate. For large values of d potential energy related to penetration of electrons into the barrier region is negligible, the kinetic energy scales as $1/d^2$ and the Coulomb energy as $1/d$. Therefore, the product of energy and dot length for large d behaves as $f(d)=C+D/d$ function, where the constants C and D are related to the Coulomb and kinetic energy, respectively. The energy levels of the degenerate pairs of states tend to different constants in the infinite d limit which is apparently due to different values of the Coulomb interaction in these pairs of states. The evolution of the charge density for growing length of the dot is shown in Figs. 1(b)–1(d). For large dots [cf. Fig. 1(d)] the charge densities of the degenerate pairs of states become identical. In the ground state the charge density has two pronounced maxima which indicates the separation of electron charges into two charge islands, i.e., the Wigner crystallization. Figure 1 shows that the singlet-triplet degeneracy obtained previously[15] for the two-electron ground-state appears also in the first excited state.

Figure 2(a) shows the energy levels and Figs. 2(b)–2(d) the charge density for the lowest-energy states of the three-electron system for increasing d. For three electrons the Wigner molecule is formed in states $1/2-$, $1/2+$, and $3/2-$ which become degenerate for large d. In the state $3/2+$ the charge density exhibits four maxima [cf. Fig. 2(d)], which apparently prevents this state to be degenerate with the ground state.

In the four-electron system the ground state corresponds to $0+$ symmetry. The states $1-$, $1+$, and $2+$ for large dots [cf. Fig. 3(a)] tend to the degeneracy with the ground state. The charge densities of these states for large dots present four distinct maxima [cf. Fig. 3(d)]. Energy levels corresponding to states $0-$ and $2-$ are separated by a significant energy distance from the ground state [cf. Fig. 3(a)] and in large dots they correspond to identical charge densities with five maxima. The ground state charge density evolution obtained for $N=3$ and 4 is in a qualitative agreement with the results of Ref. 13.

Finally, in the five-electron system the ground state of $1/2+$ symmetry becomes degenerate with $1/2-$, $3/2+$, $3/2-$, and $5/2+$ states [cf. Fig. 4(a)] forming Wigner molecules for large dots [cf. Figs. 4(b)–4(d)]. The spin polarized state of odd parity $5/2-$ does not become degenerate with the ground-state and its charge density in large dots forms six maxima [cf. Fig. 4(d)].

In the entire d range and for all electron numbers studied the order of the lowest energy levels for given total spin quantum numbers (neglecting the parity) follow the order of the spin quantum numbers, which is in agreement with the theorem of Lieb and Mattis.[27] In large dots the ground-state degeneracy appears. In Ref. 14 the degeneracy was interpreted in terms of a vanishing tunnel coupling between the local minima of the total N-dimensional potential energy. The present results indicate that the nearly degenerate states possess the same charge density in the laboratory frame. Moreover, we observe the following regularities. In the limit of Wigner localization the ground state of the N-electron system appears for N different pairs of the spin and parity quantum numbers.[29] For even electron numbers $N=2$ and 4, N charge maxima are formed only for even parity states with

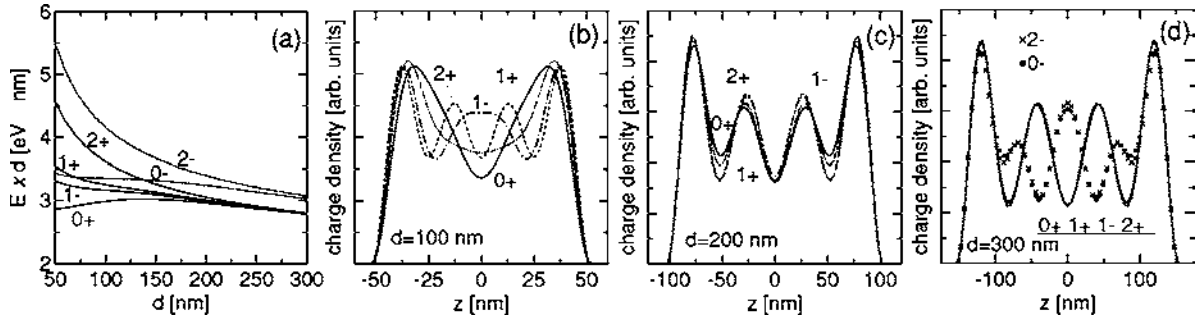

FIG. 3. (a) Four-electron energy levels multiplied by the dot length. (b), (c), (d) Charge density of $0+$, $1-$, $1+$, and $2+$ four-electron states plotted with solid, dash-dotted, dotted, and dashed lines for $d=100$, 200, and 300 nm, respectively. In (d) the charge densities of $2-$ and $0+$ states are marked with crosses and dots, respectively.

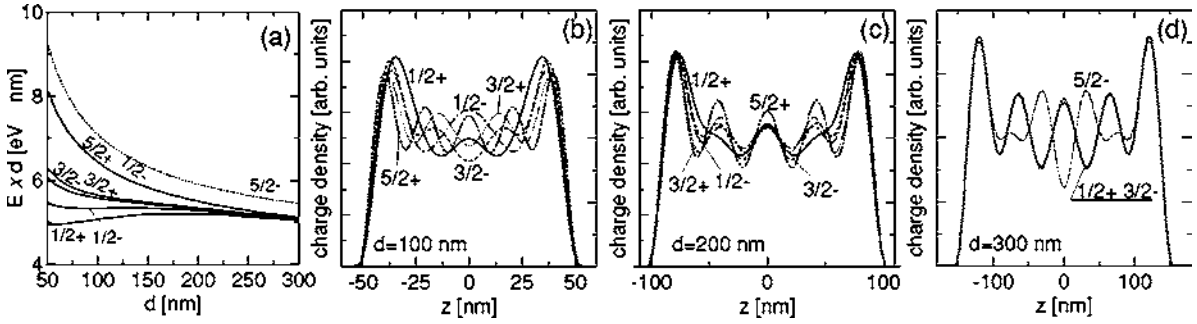

FIG. 4. (a) Five-electron energy levels multiplied by the dot length. Even (odd) parity levels are plotted with solid (dotted) lines. (b), (c) Charge density of $1/2+$, $1/2-$, $3/2+$, $3/2-$, and $5/2+$ states plotted with solid, dash-dotted, dotted, dashed, and dash-double-dot lines for $d=100$ and 200 nm, respectively. In (d) the charge density of the $1/2+$, $3/2-$, and $5/2-$ state is shown by solid, dashed, and dotted lines, respectively [charge densities of $1/2-$, $3/2+$, and $5/2+$ are almost identical with the $1/2+$ and $3/2-$ charge densities are therefore omitted in (d) for the sake of clarity].

$S=0$, while the odd parity zero-spin states possess $N+1$ charge maxima [cf. Figs. 1(d) and 3(d)]. The spin-polarized Wigner-localized state can only be formed for one (even or odd) parity. Namely, the parity of the spin-polarized Wigner molecule state is even for four and five electrons and odd for two and three electrons. The charge density of the spin-polarized state of the other parity exhibits $N+1$ maxima, i.e., the state does not form a Wigner molecule and as a consequence does not become degenerate with the ground state even for large dots. This conclusion will be cast into a theorem in the next section.

IV. PARITY OF SPIN-POLARIZED WIGNER MOLECULE STATES

Here we give an analytical proof of the theorem: *for an odd number of electrons $N=2M+1$ as well as for an even number of electrons $N=2M$ the parity of one-dimensional spin-polarized Wigner-molecule state is even (odd) for even (odd) value of the integer M.*

We will present here the proof for an odd number of electrons (the proof for even N can be easily deduced from the present demonstration). For odd N one of the electrons resides near the center of the dot (point $z_0=0$, cf. Fig. 5), and the others occupy spatially symmetric sites to the left and right of the dot around points which satisfy $z_k=-z_{-k}$ for $k=\pm1,\pm2,\ldots,\pm M$. In the Wigner phase the total charge density possesses N maxima corresponding to the separate single-electron charge densities. A single-electron density $|\psi_k(z)|^2$ is localized around point z_k. In the Wigner limit the overlap between the single-electron charge densities vanishes (the proof is only valid when this overlap is negligible), so the total charge density can be expressed as their sum. Since the total charge density is symmetric with respect to the origin the following equality holds:

$$|\psi_k(-z)|^2 = |\psi_{-k}(z)|^2, \tag{5}$$

which results in the following relation for the single-electron wave functions:

$$\psi_k(-z) = e^{i\phi_k}\psi_{-k}(z), \tag{6}$$

where the phase ϕ_k is a real number. Relation (6) with changed sign of k reads:

$$\psi_{-k}(-z) = e^{i\phi_{-k}}\psi_k(z). \tag{7}$$

Phases ϕ_k and ϕ_{-k} are not independent. Changing the sign of z in Eq. (7) and making use of relation (6) we arrive at

$$\psi_{-k}(z) = e^{i\phi_{-k}}\psi_k(-z) = e^{i(\phi_{-k}+\phi_k)}\psi_{-k}(z), \tag{8}$$

hence,

$$\phi_k = -\phi_{-k}, \tag{9}$$

up to an unimportant multiple of 2π. Considering relation (6) for $k=0$ and reminding that we arrive at the same value $\psi_0(0)$ (nonzero for odd N) approaching the origin from both positive and negative sides we arrive at $\phi_0=0$ and consequently ψ_0 is an even parity function

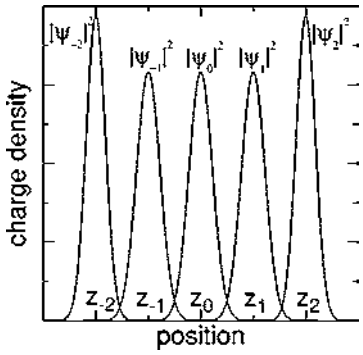

FIG. 5. Illustration to the proof that for $N=2M+1$ or $N=2M$ electrons the parity of the spin-polarized state which exhibits Wigner localization is accordant with the parity of M.

$$\psi_0(-z) = \psi_0(z). \tag{10}$$

Since the considered state is spin polarized the spin and spatial parts of the wave function can be separated into a product

$$\chi(z_1,\sigma_1,\ldots,z_N,\sigma_N) = \alpha(\sigma_1)\alpha(\sigma_2)\cdots\alpha(\sigma_N) \times \Psi(z_1,z_2,\ldots,z_N), \tag{11}$$

where α is an eigenfunction of the single-electron spin z-component operator. The spatial wave function Ψ can be written as a Slater determinant[30]

$$\Psi(z_1,z_2,\ldots,z_N) = \begin{vmatrix} \psi_{-M}(z_1) & \psi_{-M+1}(z_1) & \ldots\psi_{M-1}(z_1) & \psi_M(z_1) \\ \psi_{-M}(z_2) & \psi_{-M+1}(z_2) & \ldots\psi_{M-1}(z_2) & \psi_M(z_2) \\ \cdots & & & \\ \psi_{-M}(z_N) & \psi_{-M+1}(z_N) & \ldots\psi_{M-1}(z_N) & \psi_M(z_N) \end{vmatrix}. \tag{12}$$

We apply the parity operator on Ψ and make use of properties (6) and (9) obtaining

$$\Psi(-z_1,-z_2,\ldots,-z_N) = \begin{vmatrix} e^{-i\phi_M}\psi_M(z_1) & e^{-i\phi_{M-1}}\psi_{M-1}(z_1) & \ldots e^{i\phi_{M-1}}\psi_{-M+1}(z_1) & e^{i\phi_M}\psi_{-M}(z_1) \\ e^{-i\phi_M}\psi_M(z_2) & e^{-i\phi_{M-1}}\psi_{M-1}(z_2) & \ldots e^{i\phi_{M-1}}\psi_{-M+1}(z_2) & e^{i\phi_M}\psi_{-M}(z_2) \\ \cdots & & & \\ e^{-i\phi_M}\psi_M(z_N) & e^{-i\phi_{M-1}}\psi_{M-1}(z_N) & \ldots e^{i\phi_{M-1}}\psi_{-M+1}(z_N) & e^{i\phi_M}\psi_{-M}(z_N) \end{vmatrix}. \tag{13}$$

Phase factors can be extracted from each of the determinant columns, which yields

$$\Psi(-z_1,-z_2,\ldots,-z_N) = e^{-i(\phi_M+\phi_{M-1}+\ldots+\phi_{-M+1}+\phi_{-M})} \times \begin{vmatrix} \psi_M(z_1) & \psi_{M-1}(z_1) & \ldots\psi_{-M+1}(z_1) & \psi_{-M}(z_1) \\ \psi_M(z_2) & \psi_{M-1}(z_2) & \ldots\psi_{-M+1}(z_2) & \psi_{-M}(z_2) \\ \cdots & & & \\ \psi_M(z_N) & \psi_{M-1}(z_N) & \ldots\psi_{-M+1}(z_N) & \psi_{-M}(z_N) \end{vmatrix}. \tag{14}$$

The phases in front of the determinant in Eq. (14) cancel according to property (9). Exchanging M pairs of corresponding columns in the determinant we arrive at Eq. (12) but multiplied by $(-1)^M$, which proofs that the parity of spin-polarized one-dimensional Wigner molecule state is determined by the odd or even value of M.

We have found that two- and four-electron zero-spin states can form a Wigner-localized charge density only for even spatial parity. We are unable to proof in general that the zero-spin state with Wigner localization has to be of even parity for even N. But for $N=2$ such a proof is easily given. In this case the spin and spatial parts of the wave function can be separated as follows:

$$\chi^{0+}(z_1,\sigma_1,z_2,\sigma_2) = [\alpha(\sigma_1)\beta(\sigma_2) - \alpha(\sigma_2)\beta(\sigma_1)] \times [\psi_1(z_1)\psi_{-1}(z_2) + \psi_{-1}(z_1)\psi_1(z_2)]. \tag{15}$$

Applying the parity operator to the spatial part of this wave function and making use of the properties of the single-electron wave functions given earlier we find that this wave function is of even parity. Moreover, it follows that construction of a symmetric spatial wave function for odd-parity singlet (zero-spin) two-electron states (0−) requires at least three single-electron functions, for instance, the function

$$\Psi^{0-}(z_1,z_2) = \psi_0(z_1)\psi_1(z_2) + \psi_1(z_1)\psi_0(z_2) - \psi_0(z_1)\psi_{-1}(z_2) - \psi_{-1}(z_1)\psi_0(z_2), \tag{16}$$

is of odd parity provided that we take zero phase shifts in relation (6). Indeed, the 0− state for $N=2$ exhibits three charge maxima [see Fig. 1(d)]. Moreover, construction of a triplet antisymmetric spatial wave function with even parity (1+) also requires at least three localized functions, for instance

$$\Psi^{1+}(z_1,z_2) = \psi_0(z_1)\psi_1(z_2) - \psi_1(z_1)\psi_0(z_2) + \psi_0(z_1)\psi_{-1}(z_2) - \psi_{-1}(z_1)\psi_0(z_2), \tag{17}$$

possesses the required symmetries for zero phase shifts in relation (6). The charge density corresponding to wave functions (16) and (17) is the same provided that the overlaps between the functions ψ_i are negligible. Figure 1(d) shows that the charge densities of the states 0− and 1+ are indeed indistinguishable. The area below the central maximum of the probability density of degenerate 0− and 1+ states in Fig. 1(d) is two times larger than the area below each of the extreme maxima, which can be interpreted by saying that one of the electrons stays in the neighborhood of the center of the system with 100% probability while probabilities of finding the other one at the left or right end of the well are equal to 50%. This feature is in agreement with the probability amplitudes (16) and (17). Although in the wave functions (16) and (17) the electron positions are separated, this separation has a nonclassical character since the charge maxima at the left and right ends of the dot correspond to subelectron charges. Therefore, we do not refer to this separation as Wigner localization. Average electron-electron distances in states described by wave functions (16) and (17) are smaller

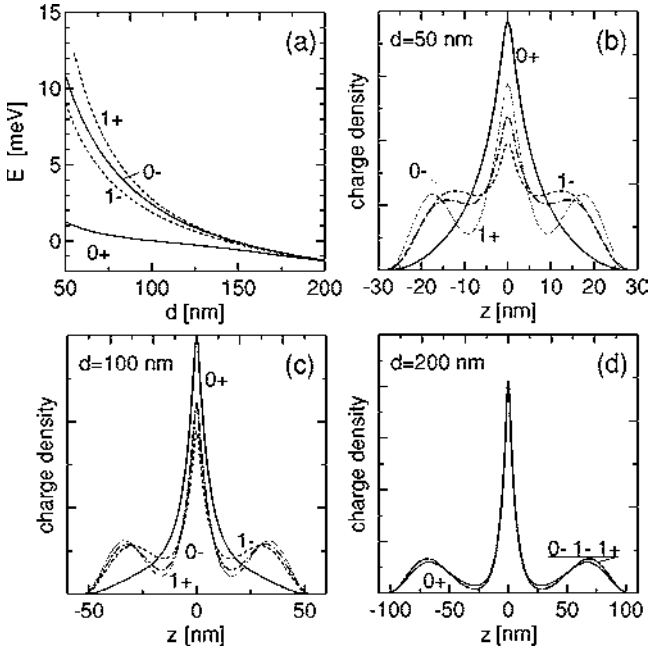

FIG. 6. (a) Lowest energy levels for $N=2$ as functions of the length of the well with a central attractive cavity [Eq. (18)]. Numbers close to the curves denote the total spin quantum number of the corresponding states and signs +, − stand for even and odd parity symmetry, respectively. (b), (c), (d) Charge density of 0+, 1−, 1+, and 0− states plotted with solid, dotted, dashed, and dash-dot curves for $d=50$, 100, and 200 nm, respectively.

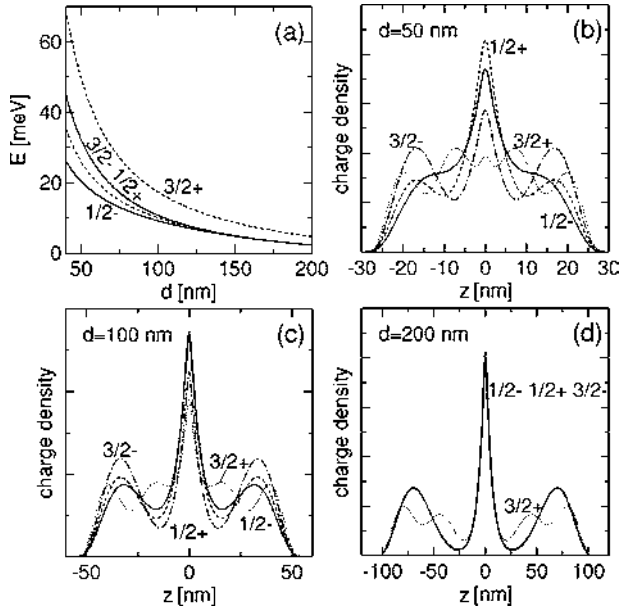

FIG. 7. (a) Lowest energy levels for $N=3$ as function of the length of the well with a central attractive cavity [Eq. (18)]. Numbers close to the curves denote the total spin quantum number of the corresponding states and signs +, − stand for even and odd parity symmetry. (b),(c),(d) Charge density of 0+, 1−, 1+, and 0− states plotted with solid, dotted, dashed, and dash-dot curves for $d=50$, 100, and 200 nm, respectively.

than in states 0+, 1− with two charge maxima, which leads to a larger value of the Coulomb interaction energy and consequently to an energy separation between pairs of degenerate states 0+,1− and 0−,1+ presented in Fig. 1(a) in the weak confinement limit.

V. WIGNER CRYSTALLIZATION IN THE PRESENCE OF A DEFECT POTENTIAL

The presence of defects can significantly perturb the Wigner crystallization in large systems. We consider here a thin attractive cavity just deep enough to bind one electron. The perturbed quantum dot potential is of the form

$$V(z) = V_{\text{well}}(z) + V_{\text{defect}}(z), \tag{18}$$

where $V_{\text{defect}}(z)=-50$ meV for $|z|<1$ nm and $V_{\text{defect}}(z)=0$ for $|z|>1$ nm. The assumption that the defect is localized in the center of the system does not perturb the inversion invariance of the total potential.

Figure 6(a) shows that contrary to the unperturbed quantum well potential [cf. Fig. 1(a)] the 0− and 1+ states become degenerate with the 0+ and 1− states. Figures 6(b)–6(d) show the evolution of the charge densities of the four considered states with increasing size of the system. For large well thickness [cf. Fig. 1(d)] the charge densities of these states become indistinguishable. One of the electrons is trapped by the potential of the central cavity which results in the sharp central peak of the charge density. The probabilities to find the other electron at the left or right side of the origin are equal. This differs essentially from the two-electron Wigner molecule charge density in the unperturbed dot [cf. Fig. 1], for which the probability to find an electron in the center of the well was negligible and for which each of the two charge maxima could be associated with an integer electron charge. The formation of three maxima in the charge density is possible for all states [cf. Eqs. (16) and (17), for 0− and 1+ states, similar formulas can be given for the other two]. Therefore, the ground state tends to a fourfold degeneracy in contrast to the double degeneracy for the unperturbed dot [cf. Fig. 1(a)].

Figure 7 shows the lowest energy levels and corresponding charge density evolution for the three-electron system. Contrary to the two-electron system the central defect does not perturb the number of charge maxima, Wigner localization appears similarly as for the unperturbed dot [cf. Fig. 2] for $1/2+$, $1/2-$, and $3/2-$ states which become degenerate in the Wigner localization limit. State $3/2+$, which according to the theorem given in Sec. IV cannot form a Wigner phase lies higher in energy, like for the unperturbed dot.

The influence of the central attractive defect is qualitatively different for odd and even electron number. For an odd number of electrons it simply enhances the localization of the central electron, and does not influence the ground state degeneracy. While for even N it destroys Wigner crystallization leading to the appearance of an extra charge maximum corresponding to subelectron charge and allows more states to become degenerate with the ground state.

VI. SPATIAL SPIN ORDERING IN THE WIGNER LIMIT

It is interesting to look whether the low-spin ground states exhibit any spatial antiferromagnetic ordering of the electron

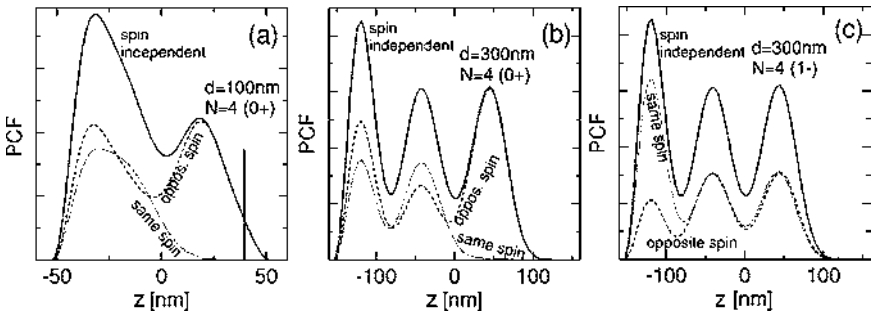

FIG. 8. PCFs for four electrons in state 0+ [(a),(b)] and state 1− with $S_z=\hbar$ (c) for $d=100$ (a) and 300 nm [(b),(c)]. One of the electrons is fixed and its position is marked by a thin vertical line. Solid curves show the spin-independent PCF, dashed (dotted) curves show the opposite (same) spin PCF.

spins. For even number of electrons and arbitrary dot length the ground state corresponds to zero total spin. In this case the spin-up and spin-down densities are exactly equal to each other, so that spin ordering is not visible in the laboratory frame of reference. In order to investigate a possible spin ordering in the zero-spin ground states one has to look into the inner coordinates of the quantum system. We use here the spin-dependent pair correlation functions (PCFs) defined for a given state by the expectation values

$$F_{\mathrm{PCF}}^{\mathrm{same}}(z_a,z_b)=\left\langle \sum_{i=1}^{N}\sum_{j>i}^{N}\delta(z_a-z_i)\,\delta(z_b-z_j) \times\left(|\alpha(\sigma_i)\alpha(\sigma_j)\rangle\langle\alpha(\sigma_i)\alpha(\sigma_j)| + |\beta(\sigma_i)\beta(\sigma_j)\rangle\langle\beta(\sigma_i)\beta(\sigma_j)|\right)\right\rangle, \quad (19)$$

and

$$F_{\mathrm{PCF}}^{\mathrm{oppo}}(z_a,z_b)=\left\langle \sum_{i=1}^{N}\sum_{j>i}^{N}\delta(z_a-z_i)\,\delta(z_b-z_j) \times\left(|\alpha(\sigma_i)\beta(\sigma_j)\rangle\langle\alpha(\sigma_i)\beta(\sigma_j)| + |\beta(\sigma_i)\alpha(\sigma_j)\rangle\langle\beta(\sigma_i)\alpha(\sigma_j)|\right)\right\rangle, \quad (20)$$

where α and β stand for spin-up and spin-down eigenstates, respectively. Functions (19) and (20) give the probability of finding at positions z_a and z_b a pair of electrons with the same (19) or opposite (20) spins. The sum of functions (19) and (20) gives the spin-independent PCF.

Figure 8(a) shows the PCF plots for the four-electron ground state in a small quantum dot [cf. Fig. 3(b)] with $d=100$ nm. The position of one of the electrons is fixed near the right end of the dot [position marked by the thin vertical line in Fig. 8(a)]. We see that the probability of finding an electron with the same spin in the neighborhood of the fixed-position electron is zero, which is a signature of the Pauli exclusion principle. At the left side of the dot probabilities of finding an electron with the same or opposite spin as the one of the fixed position electron are nearly equal. For the total zero-spin states in relatively small dots the spin ordering in the inner coordinates is of short range and results from the Pauli exclusion. We only found a long-range inner-coordinate spin ordering in the Wigner crystallization limit. Figure 8(b) shows the plot for the four-electron ground state with $d=300$ nm. The charge density of the system exhibits four distinct maxima [cf. Fig. 3(d)]. We fix the position of one of the electrons at the rightmost density maximum [cf. the vertical line in Fig. 8(b)]. The probability that the electron in the adjacent maximum has the opposite spin is nearly 100%. The spin-dependent PCFs also differ for the two charge maxima at the left of the origin. An electron confined at the first (second) charge maximum to the left of the origin is more probable to have the same (opposite) spin as the one of the fixed electron. The ordering is of a probabilistic character, so that the antiferromagnetic order of spins is the most probable to be found, but the probability is not 100%. The spin ordering in this state has a clearly antiferromagnetic character and its range covers the entire length of the dot. A similar inner-coordinate antiferromagnetic order was previously found for quantum rings.[6]

The 100% probability of finding the opposite spin in the charge maximum adjacent to the maximum associated with the fixed electron presented in Fig. 8(b) is not, as one could naively expect, related to the Pauli exclusion. In Fig. 8(c) we plotted the PCF for the 1− state, which becomes degenerate with the ground 0+ state in the weak confinement limit. We see that in this state the spin of electrons confined in the two central maxima is independent of the spin of the electron at the rightmost maximum. However, in this state one may expect that the electrons at the opposite ends of the dot have the same spin, which means that also in this state a long-range spin ordering exists, even if it is not of antiferromagnetic origin.

For odd number of electrons the difference between spin-up and spin-down densities appears in the laboratory frame. This is qualitatively different from quantum rings, which in fact are endless structures. Figure 9(a) shows the spin densities for a relatively small dot length of $d=100$ nm [too small for the ground state Wigner localization to appear, cf. Fig. 4(b)]. The spin-up electrons tend to gather at the extreme left and right ends of the dot as well as in its center. The spin-down density is minimal in the center of the dot, and the overall spin density (difference of the spin-up and spin-down densities) exhibits antiferromagnetic sign oscillations within the dot. These sign oscillations are due to the electron-electron interaction since in the noninteracting electron system the majority spin-up density is nowhere smaller than the spin-down density. For larger systems [$d=250$ nm, cf. Fig. 9(b)] the antiferromagnetic spin oscillations become more pronounced. However, for even larger d [cf. Figs. 9(c) and 9(d)], for which the Wigner molecule appear in the $1/2+$ ground state, the typically antiferromagnetic

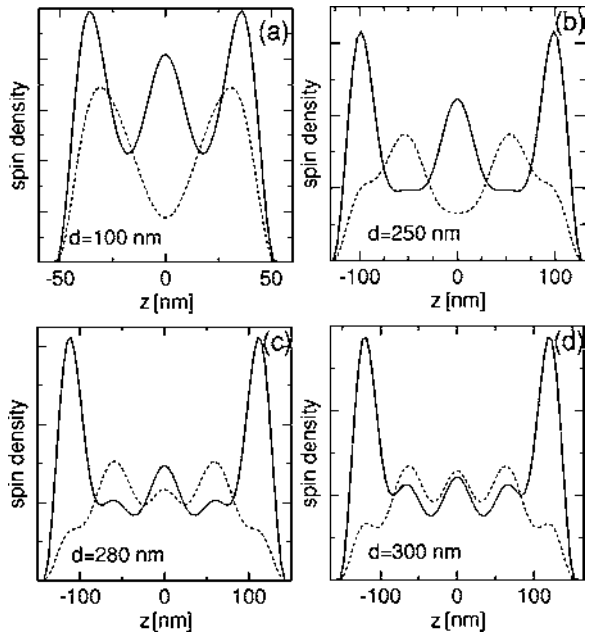

FIG. 9. Spin-up (solid lines) and spin-down (dashed lines) densities for the ground-state 5-electron system $1/2+$ with $S_z=\hbar/2$ for different system sizes.

real-space spin ordering with the spin orientation changing between the adjacent charge maxima vanishes.

Let us look at the spin distribution in the inner coordinates of the 5-electron $1/2+$ ground state. Figure 10(a) shows the PCF plots for $d=100$ nm. Electrons of the same spin as the fixed electron do not appear in its close neighborhood, but are more probable to be found at the center of the dot than electrons of opposite spin. Probability of finding an electron at the opposite side of the dot is independent of its spin. The spin order in this relatively small dot ($d=100$ nm) is clearly short range which is similar as for the case of four electrons in a small dot [cf. Fig. 8(a)]. The PCF plots for opposite spins at the left end of the dot start to differentiate for $d=200$ nm [cf. Fig. 8(b)]. For $d=300$ nm, for which Wigner localization is observed [cf. Fig. 4(d)], the PCF plots show a long-range antiferromagnetic spin ordering. Notice the growth of the PCF plot for the same spin direction in the closest neighborhood of the fixed-position electron from $d=200$ to 300 nm in Figs. 8(b) and 8(c). Pauli exclusion plays a less significant role for larger distances between the charge maxima.

Density-functional studies[16,28] predict the appearance of interlocked waves of opposite spins in the laboratory frame for long quasi-one-dimensional dots. The appearance of the spin-density wave for even electron number amounts in spin symmetry breaking. Recently,[16] it was found that for even N the formation of the spin density wave in the density functional theory accompanies the Wigner crystallization. But in the present study we find that for the exact solution spin symmetry is conserved and Wigner crystallization is associated with the inner space spin ordering. In the exact solution the interlocked spin densities in the laboratory frame can only be observed for odd numbers of electrons, but the presented five-electron case shows that this effect is not necessarily related with Wigner crystallization. In the exact solution the electrons with opposite spins avoid one another in the inner space. A mean field approach can only account for this effect by symmetry breaking. The reason for the occurrence of spin symmetry breaking in the mean field approach for large single-dimensional dots are similar to the origin of the broken spatial symmetry mean field solutions for the magnetic field induced Wigner crystallization in circular structures.[12]

In large systems the spin-independent PCF plots become identical for all states degenerate with the ground state [cf. spin-independent PCFs for the four-electron degenerate $0+$ and $1-$ states in Figs. 8(b) and 8(c)]. This means that in Wigner-molecule states electrons avoid one another with the same efficiency independently of their spins. As a matter of fact this is the origin of the appearance of the ground state degeneracy in the Wigner molecule regime. One-dimensional Wigner molecules present pronounced magnetic properties related to the long-range spin ordering in the inner coordinate space. This ordering for different degenerate spin eigenstates may be typical for ferromagnetic, antiferromagnetic or even an other form of order. Due to the vanishing energy spacing between the different spin states the spin magnetic properties of Wigner molecules are of a very soft character. The Wigner molecules should be extremely susceptible to any spin-dependent interactions. In particular, even a weak additional effect promoting the spin-polarized phase can result in spin polarization of the system. A possible spin polarization of the one-dimensional electron gas has been found[2] in transport measurements.

VII. CONCLUSIONS AND SUMMARY

We have studied the ground and excited states of electron systems confined in quasi-one-dimensional quantum dots using an exact diagonalization approach. For large systems we found Wigner localization which appears not only in the

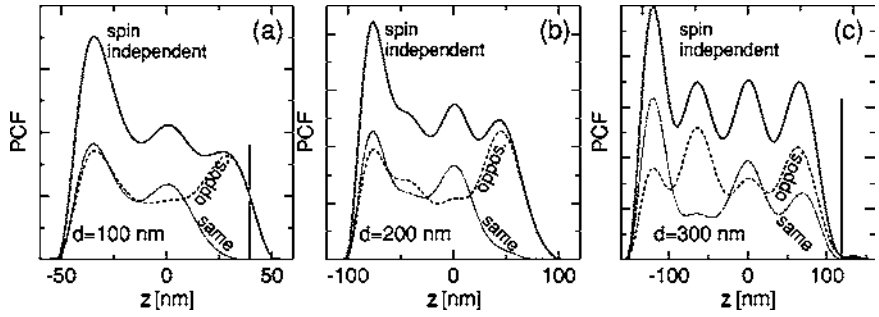

FIG. 10. PCFs for five electrons in the state $1/2+$ for $d=100$ (a), 200 (b), and 300 nm (c). The position of the fixed electron is marked by a thin vertical line. Solid lines show the spin-independent PCF, dashed (dotted) lines show the opposite (same) spin PCF.

ground state but also for several excited states which eventually leads to the degeneracy of the ground state in the large d limit. We have considered spin and spatial parity of states forming Wigner molecules. We have shown that the parity of the spin-polarized state which forms a Wigner molecule is strictly determined by the number of electrons.

We have discussed the effect of a central attractive defect which destroys Wigner crystallization for an even number of electrons allowing more states to become degenerate with the ground state in the weak confinement limit. For odd electron numbers the central defect enhances the localization of the electron occupying the central position in the Wigner molecule and does not affect the ground state degeneracy.

We have investigated the spin-ordering effects associated with Wigner crystallization. We have found that for small dots the spatial spin ordering in the inner coordinates has a short-range character and results mainly from the Pauli exclusion principle. The long-range spatial spin order appears only in the Wigner molecule regime when the electrons occupy distinct sites within the quantum dot. We conclude that in one-dimensional quantum dots the Wigner crystallization is a necessary condition for the long range spin ordering to appear. We have identified the effect of spin symmetry breaking observed in the density functional theory as a tendency of the mean field method to mimic the internal-space spin ordering present in the exact solution for the Wigner molecule regime.

ACKNOWLEDGMENTS

This paper has been partly supported by the Polish Ministry of Scientific Research and Information Technology in the framework of solicited Grant No. PBZ-MIN-008/P03/2003, by the Flemish Science Foundation (FWO-Vl), the Belgian Science Policy and the University of Antwerpen (VIS and GOA). B.S. was supported by the Foundation for Polish Science (FNP) and T.C. was partially supported by the Marie Curie Training Site Programme of the European Union.

[1] S. Tarucha, T. Honda, and T Saku, Solid State Commun. **94**, 413 (1995).
[2] K. J. Thomas, J. T. Nicholls, M. Y. Simmons, M. Pepper, D. R. Mace, and D. A. Ritchie, Phys. Rev. Lett. **77**, 135 (1996).
[3] A. Yacoby, H. L. Stormer, N. S. Wingreen, L. N. Pfeiffer, K. W. Baldwin, and K. W. West, Phys. Rev. Lett. **77**, 4612 (1996).
[4] A. Bachtold, C. Strunk, J.-P. Salvetat, J.-M. Bonard, L. Forro, T. Nussbaumer, and C. Schonenberger, Nature (London) **397**, 673 (1999).
[5] L. Jacak, P. Hawrylak, and A. Wójs, *Quantum Dots* (Springer, Berlin, 1998).
[6] S. Viefers, P. Koskinen, P. Singha Deo, and M. Manninen, Physica E (Amsterdam) **21**, 1 (2004).
[7] M. S. Gudiksen, L. J. Lauhon, J. Wang, D. C. Smith, and C. M. Lieber, Nature (London) **415**, 617 (2002).
[8] Y. Wu, R. Fan, and P. Yang, Nano Lett. **2**, 83 (2002).
[9] M. T. Björk, B. J. Ohlsson, T. Sass, A. I. Persson, C. Thelander, M. H. Magnusson, K. Deppert, L. R. Wallenberg, and L. Samuelson, Nano Lett. **2**, 82 (2002).
[10] F. P. Wigner, Phys. Rev. **46**, 1002 (1934).
[11] R. Egger, W. Häusler, C. H. Mak, and H. Grabert, Phys. Rev. Lett. **82**, 3320 (1999).
[12] S. M. Reimann and M. Manninen, Rev. Mod. Phys. **74**, 1283 (2002).
[13] K. Jauregui, W. Häusler, and B. Kramer, Europhys. Lett. **24**, 581 (1993).
[14] W. Häusler and B. Kramer, Phys. Rev. B **47**, 16 353 (1993).
[15] S. Bednarek, T. Chwiej, J. Adamowski, and B. Szafran, Phys. Rev. B **67**, 205316 (2003).
[16] E. Räsanen, H. Saarikoski, V. N. Stavrou, A. Harju, M. J. Puska, and R. M. Nieminen, Phys. Rev. B **67**, 235307 (2003).
[17] L. I. Glazman, I. M. Ruzin, and B. I. Shklovskii, Phys. Rev. B **45**, 8454 (1992).
[18] H. J. Schulz, Phys. Rev. Lett. **71**, 1864 (1993).
[19] F. Anfuso and S. Eggert, Phys. Rev. B **68**, 241301 (2003).
[20] G. Piacente, I. V. Schweigert, J. J. Betouras, and F. M. Peeters, Solid State Commun. **128**, 57 (2003).
[21] S. Bednarek, B. Szafran, T. Chwiej and J. Adamowski, Phys. Rev. B **68**, 045328 (2003).
[22] M. Koskinen, M. Manninen, B. Mottelson, and S. M. Reimann, Phys. Rev. B **63**, 205323 (2001).
[23] P. A. Maksym, Phys. Rev. B **53**, 10 871 (1996).
[24] C. G. Bao, W. Y. Ruan, and Y. Y. Liu, Phys. Rev. B **53**, 10 820 (1996).
[25] E. B. Kolomeisky and J. P. Straley, Rev. Mod. Phys. **68**, 175 (1996).
[26] H. Tasaki, J. Phys.: Condens. Matter **10**, 4353 (1998).
[27] E. Lieb and D. Mattis, Phys. Rev. **125**, 164 (1962).
[28] S. M. Reimann, M. Koskinen, P. E. Lindelof, and M. Manninen, Physica E (Amsterdam) **2**, 648 (1998).
[29] The approximate ground-state degeneracy of a N electron system in large one-dimensional dot equals 2^N (taking into account the degeneracies with respect to the z component of the total spin) as reported already in Ref. 14. For four and five electrons also higher-energy states for a given spin and parity quantum numbers (not discussed in the present paper) become degenerate with the ground state. We have determined the parity of these states. Namely, the four-electron ground state becomes degenerate with second $1-$ and $0+$ states and the five-electron ground state becomes degenerate with the second $1/2-, 3/2-, 1/2+$, and $3/2+$ symmetry states as well as with the third $1/2+$ state.
[30] A single determinant is sufficient to describe the spin-polarized Wigner molecule formed by N electrons localizated around N space sites. See also the discussion of the electron-electron correlation given in Ref. 15.

Parity symmetry and energy spectrum of excitons in coupled self-assembled quantum dots

B. Szafran,* S. Bednarek, and J. Adamowski
Faculty of Physics and Nuclear Techniques, University of Mining and Metallurgy (AGH), Cracow, Poland
(Received 22 November 2000; published 5 September 2001)

A theoretical study is presented for excitons in coupled self-assembled InGaAs quantum dots. We have proposed a model of an isolated single quantum dot based on the assumption of the Gaussian distribution of indium concentration. The same distribution, with the parameters fixed for the single dot, has been applied to vertically stacked coupled quantum dots in order to study the exciton properties, which result from the interdot coupling. The exciton lowest-energy levels have been calculated with use of the many-element variational basis, which includes the two-particle correlation effects. We have discussed the symmetry with respect to the parity of the exciton wave functions in the coupled quantum dots. We have shown that—in a general case—these wave functions do not possess the definite one-particle parity. Only for very small interdot distance the ground-state wave function exhibits the approximate one-particle parity. The nature of splitting of the photoluminescence lines in the coupled quantum dots is discussed. The present theory applied to a description of photoluminescence spectra in coupled self-assembled InGaAs quantum dots leads to a very good agreement with the experimental data.

DOI: 10.1103/PhysRevB.64.125301 PACS number(s): 73.23.−b

I. INTRODUCTION

A three-dimensional confinement of charge carriers in semiconductor quantum dots (QD's) results in a space quantization of energy levels.[1] Electron systems confined in QD's are called artificial atoms,[2,3] since they show atomiclike properties, e.g., their energy spectrum is discrete. Among various types of QD's, the self-assembled QD's are the subject of an extensive study[4–28] because of their possible applications in semiconductor lasers. It is expected[13] that the self-assembled QD's used as active regions in the semiconductor lasers will provide low-threshold currents, a high gain, and an improved thermal stability of the devices. The coupled QD's (Refs. 14–21) can be treated as artificial molecules. The coupling between the QD's should be useful in optical applications, because it leads to an appearance of additional spectral lines. The positions of these lines can be changed by choosing different interdot distances in a technological process.

The present study has been inspired by the recent measurements[21] of exciton-related radiative transitions in vertically stacked InGaAs self-assembled QD's.[21] The experimental results,[21] obtained with use of the state-filling photoluminescence spectroscopy,[22] show a strong dependence of the photoluminescence spectra on the distance between the dots. In the state-filling spectroscopy,[22] the exciting light of large intensity is used to fill as many electron-hole states as possible; so, all the allowed radiative transitions can be detected. In recent measurements,[9,10] carried out on a single self-assembled QD, the fine structure of the luminescence spectrum has been observed as a function of the excitation power, i.e., as a function of the number of the confined excitons. In the case of the coupled QD's, the experimental spectra[21] have been taken from a sample containing a large number of QD's. Then, the fine structure is not observed, since the inhomogeneous broadening of the luminescence lines is larger than the fine-structure splitting[9] and the energetic positions of the lines do not show any visible dependence on the number of confined excitons. Therefore, at this level of the experimental resolution, a theory of a single exciton should be sufficient for the interpretation of these measurements.[21]

A theoretical description of the excitons in the single dots was elaborated for self-assembled InAs/GaAs QD's (Ref. 29) and for InP and CdSe nanocrystals[30] in the framework of the pseudopotential approach. In Ref. 31, the excitons in the coupled QD's were studied as candidates for a reliable preparation of entangled states in solid-state systems.

The present paper is devoted to theoretical study of parity symmetry and spectral properties of the exciton in isolated and coupled self-assembled quantum dots. The paper is organized as follows. In Sec. II, we formulate a theoretical model of the exciton in a single QD. In Sec. III, we generalize this approach to the case of the coupled QD's. In Sec. IV we present the results and discussion and in Sec. V we give the summary.

II. SINGLE QUANTUM DOT

In this section, we formulate and parametrize a model of a single QD, which will be used in the following sections for a description of exciton states in coupled QD's. Most of theoretical papers[2,11,12,23–28] dealing with the QD's use the two-dimensional model of the QD. Such a model does not allow for a description of the coupling between vertically stacked QD's. In order to describe the coupling between the QD's aligned in the growth direction, we have proposed a three-dimensional model of a single, isolated $In_XGa_{1-X}As$ QD. The present model is based on the recent understanding[32] of the growing process of the self-assembled QD's. During the growing process, InAs deposited on the GaAs substrate first forms a thin wetting layer and next InAs island. This nanostructure is subsequently covered with GaAs. Due to the indium diffusion[32] the self-assembled QD's are made of the $In_XGa_{1-X}As$ alloy with a spatially varying indium concentration. In this paper, we propose a model that takes into

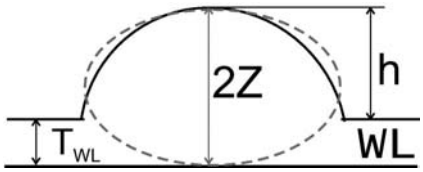

FIG. 1. Schematic of a single QD. Dashed line shows the contour of the indium-concentration Gaussian distribution function with range Z in the growth direction, h is the height of the QD and T_{WL} is the thickness of the wetting layer (WL).

account a spatial modulation of the indium concentration in the nanostructure. The present model is based on the assumption of the Gaussian distribution of indium concentration in the QD. Explicitly, we assume that indium concentration X in the single isolated QD is described by the Gaussian function of the cylindrical symmetry

$$X(\rho,z)=X_0\exp(-\rho^2/R^2-z^2/Z^2), \tag{1}$$

where $\rho^2=x^2+y^2$, X_0 is the indium concentration at the center of the dot, R is the dot ''radius,'' and Z is the half of its ''height.'' The real self-assembled QD's are not symmetric with respect to the inversion of the z axis (Fig. 1). Therefore, parameter $2Z$ can be treated as the effective height of the dot, which partially takes into account the presence of the wetting layer (Fig. 1). The $In_XGa_{1-X}As$ island in the GaAs matrix is responsible for the potential confining the charge carriers in the quantum dot. The conduction-valence-band offset ratio for the InAs/GaAs interface was estimated to be 70/30.[33] Therefore, we assume the confinement potential to be parametrized as follows:

$$V_e(\rho,z)=-0.7\Delta E_g X(\rho,z) \tag{2}$$

for the electrons and

$$V_h(\rho,z)=-0.3\Delta E_g X(\rho,z) \tag{3}$$

for the holes, where $\Delta E_g=E_g^{\mathrm{GaAs}}-E_g^{\mathrm{InAs}}$, E_g^{GaAs}, and E_g^{InAs} are the GaAs and InAs energy gaps, respectively. In the present calculations, we take on $E_g^{\mathrm{GaAs}}=1.5196$ eV (Ref. 34) and $E_g^{\mathrm{InAs}}=0.4105$ eV.[35]

Here, we briefly comment on the choice of the confinement potential [Eqs. (2) and (3)]. The application of the cylindrically symmetric Gaussian potential allows us to describe the three-dimensional confinement of the charge carriers in the QD's, and to take into account a finite depth of the confinement potential and an approximate parabolicity of the potential near the dot center. The properties of the one- and two-electron systems in the spherically symmetric, Gaussian confinement potential have been studied in detail in our recent paper.[36]

Finally, in accordance with the assumed indium-concentration distribution [Eq. (1)], we introduce the following space dependence of the electron and hole effective masses:

$$m_{e,h}(\rho,z)=m_{e,h}^{\mathrm{InAs}}X(\rho,z)+m_{e,h}^{\mathrm{GaAs}}[1-X(\rho,z)], \tag{4}$$

where $m_e^{\mathrm{InAs}}=0.023m_0$,[37] $m_e^{\mathrm{GaAs}}=0.0667m_0$,[38] $m_h^{\mathrm{InAs}}=0.41m_0$,[39] $m_h^{\mathrm{GaAs}}=0.5m_0$,[40] and m_0 is the electron rest mass.

Equations (2)–(4) express the effective confinement potentials for electrons and holes and the spatial modulation of their band masses by a single indium distribution function (1). The parameters of this function (X_0, R, and Z) will be extracted from the experimental photoluminescent data for a single isolated QD. Such a procedure implicitly takes into account the strain effects[7] and the indium concentration given by Eq. (1) has an effective meaning. The same parametrization, with values of parameters fixed for a single dot, will be applied to coupled double QD's. Therefore, the Gaussian distribution function [Eq. (1)] can be treated as an universal function, which allows us to include the most important effects for the real nanostructures.

In the case of the position-dependent effective masses,[41] the Hamiltonian of the electron-hole pair confined in the single QD has the following form (in atomic units):

$$H=-\frac{1}{2}\nabla_e\frac{1}{m_e(\mathbf{r}_e)}\nabla_e+V_e(\rho_e,z_e)-\frac{1}{2}\nabla_h\frac{1}{m_h(\mathbf{r}_h)}\nabla_h + V_h(\rho_h,z_h)-\frac{1}{\varepsilon r_{eh}}, \tag{5}$$

where $\mathbf{r}_e$ and $\mathbf{r}_h$ are the position vectors of the electron and hole, respectively, and $r_{eh}=|\mathbf{r}_e-\mathbf{r}_h|$. Since the dielectric properties of GaAs and InAs are similar, we have adopted the average value[5] $\varepsilon=12.5$ of the static dielectric constant for the $In_XGa_{1-X}As$ alloy for all values of X. Throughout the present paper, the conduction-band minimum of GaAs is the reference energy level for the electron and the GaAs valence-band maximum is the reference energy level for the hole [cf. Eqs. (2) and (3)].

Probability p of radiative transition from the exciton state described by the wave function $\Phi(\mathbf{r}_e,\mathbf{r}_h)$ is proportional to the integral[42]

$$p\sim\left|\int d\mathbf{r}_e d\mathbf{r}_h\Phi(\mathbf{r}_e,\mathbf{r}_h)\,\delta(\mathbf{r}_e-\mathbf{r}_h)\right|^2. \tag{6}$$

In the present paper, we consider the optically active exciton states, i.e., the states, from which the radiative transitions (electron-hole recombination) are allowed. For these transitions the initial states correspond to zero total angular momentum, since otherwise integral (6) vanishes.

We note that Hamiltonian (5) commutes with the operator of the z component of the total angular momentum and the parity operator. Both these quantities are conserved in the framework of the present model. However, because of the presence of the Coulomb-interaction potential in Eq. (5), the one-particle operators of parity and z component of angular momentum do not commute with the Hamiltonian. Due to the small size of the self-assembled QD's the one-particle energies are considerably larger than to the Coulomb-interaction contribution. Moreover, the energy separations between the one-particle shells of different angular momenta are also large with respect to the Coulomb term. On the contrary, in the coupled QD's, the energy spacings between

the one-particle states of opposite parities can be arbitrarily small. Thus, it should be expected that the Coulomb interaction essentially perturbs the one-particle parity. In this paper, we concentrate our attention on the problem of parity, which arises for the coupled QD's. Therefore, we construct the exciton wave functions of zero total angular momentum, using the eigenstates of one-particle angular momentum, which is a reasonable approximation in the problem considered. We shall label the exciton states by the one-particle z-component angular momentum quantum number m and use the following dependence of the wave function $\Psi(\mathbf{r}_e,\mathbf{r}_h)$ on azimuthal angles φ_e and φ_h:

$$\chi_m(\varphi_e,\varphi_h)=\exp[im(\varphi_e-\varphi_h)]. \tag{7}$$

In the following, we consider the lowest-energy optically active exciton states with $m=0$, 1, 2, and 3 labeled by s, p, d, and f, respectively. In Eq. (7), the signs of the angular momentum quantum number for the electron and the hole are chosen to be opposite, i.e., z component of the total angular momentum for the exciton is zero. All the states considered are symmetric with respect to the in-plane inversion, i.e., the change of sign of x and y coordinates of both the particles. Therefore, the total parity of the exciton is entirely determined by the z parity.

The eigenvalue problem for the exciton confined in the single QD has been solved by variational means with the trial wave function of the form

$$\Phi_1(\mathbf{r}_e,\mathbf{r}_h)=\rho_e^m\rho_h^m\chi_m(\varphi_e,\varphi_h) \times\sum_{jkln} c_{jkln}f_{jkln}(\rho_e,\rho_h,z_e,z_h,z_{eh}), \tag{8}$$

which is expanded in the Gaussian basis

$$f_{jkln}(\rho_e,\rho_h,z_e,z_h,z_{eh})=\exp(-\alpha_j^e\rho_e^2-\alpha^h\rho_h^2-\beta_k^e z_e^2 -\beta_l^h z_h^2-\gamma^z z_{eh}^2), \tag{9}$$

where $z_{eh}=z_e-z_h$. In Eq. (9), variational parameters α_j^e and α^h (β_k^e and β_l^h) describe the localization of the electron and the hole in the x-y plane (z direction), and γ^z accounts for the correlation of the relative motion in the z direction. Wave function Φ_1 partially includes the radial correlation between the electron and hole, since it cannot be separated into a product of ρ_e and ρ_h dependent functions. However, it neglects the angular correlation.

In order to check a quality of trial wave function (8) we have performed test calculations for the exciton ground-state energy E_0 using a more general variational wave function, which explicitly includes the in-plane electron-hole distance. For $m=0$ this wave function has the form

$$\Phi_0(\mathbf{r}_e,\mathbf{r}_h)=\sum_{jklnp} c_{jklnp}\exp(-\alpha_j^e\rho_e^2-\alpha_k^h\rho_h^2-\beta_l^e z_e^2-\beta_n^h z_h^2 -\gamma_p^\rho\rho_{eh}^2-\gamma^z z_{eh}^2), \tag{10}$$

where $\rho_{eh}^2=(x_e-x_h)^2+(y_e-y_h)^2$ and variational parameters γ_p^ρ are responsible for the in-plane correlation. Putting $\gamma_p^\rho=0$ in Eq. (10) we obtain wave function (8) for $m=0$. The results of the test calculations reported in Table I show that the neglect of the angular correlation yields the ground-state energy estimate with the uncertainty less than 2 meV. For comparison the estimated widths of photoluminescence peaks[21] amount to several meV. Therefore, basis (8) with the neglected angular correlation and smaller number of elements (cf. Table I) is sufficient for the present purposes. The results presented in this paper have been obtained with the use of basis (8), in which the sums run over $j,k,n=1,2$, $l=1,\ldots,3$, and $p=0$ (cf. Table I). The energy eigenvalues E_m calculated for given angular momentum quantum number m are used to determine the energy of the radiative interband transition, which is defined as $h\nu_m=E_g^{\mathrm{GaAs}}+E_m$.

The values of the parameters describing the indium-concentration distribution in Eq. (1) have been obtained from the adjustment of the calculated transition energies to the experimental data[21] for the isolated QD's. For this purpose we have used the photoluminescence spectrum[21] taken at the interdot distance of ~ 15 nm, for which the QD's can be treated as spatially separated and uncoupled. The values obtained are $X_0=0.66$, $Z=0.92$ nm, and $R=24.9$ nm. The comparison of the calculated and measured[21] radiative-transition energies for the isolated quantum dot is presented in Table II. The further description of the vertical coupling

TABLE I. Convergence of ground-state energy estimates E_0 for an exciton confined in a single QD with increasing number of basis elements. In the first five columns, the upper limits of the corresponding sums in Eq. (10) are listed. According to Eq. (10), labels j, k, l, n, and p denote the different Gaussians dependent on ρ_e, ρ_h, z_e, z_h, and ρ_{eh}, respectively. N is the total number of basis elements used in the calculations. The numbers in the first row correspond to basis (8) used in the latter part of the present paper. Energy is expressed in meV.

j	k	l	n	p	N	E_0
2	2	3	2		24	−241.93
3	3	4	4		144	−242.22
3	3	4	4	1	144	−243.21
3	3	4	4	2	288	−243.59
3	3	4	4	3	432	−243.70

TABLE II. Calculated energy eigenvalues E_m of the optically active exciton states for the single QD, energy spacings ΔE between the consecutive energy levels, and calculated radiative-transition energies $h\nu_{calc}$. The measured transition energies $h\nu_{expt}$ are extracted from the photoluminescence-peak positions (Ref. 21) taken for the separated QD's ($a=15$ nm). The states involved in the transitions are quoted in the first column. Energy is expressed in meV.

	E_m	ΔE	$h\nu_{calc}$	$h\nu_{expt}$
s-s	−241.9		1277.7	1278.2
p-p	−197.2	44.8	1322.4	1322.2
d-d	−159.7	37.5	1359.9	1359.4
f-f	−125.9	33.8	1393.7	1394.4

TABLE III. Calculated lowest-energy levels of the electron, E_e, and hole, E_h, states in the single QD (the mutual Coulomb interaction omitted). The separations $\Delta E_{e,h}$ between the consecutive energy levels are also quoted. Energy is expressed in meV.

	E_e	ΔE_e	E_h	ΔE_h
s	−118.3		−101.4	
p	−89.0	28.3	−93.0	8.5
d	−64.1	25.9	−84.7	8.3
f	−40.7	23.4	−76.6	8.1

between the QD's requires an accurate modeling of the confinement in the growth direction. In this context, we have to emphasize that the value of Z we have obtained from our fit very well agrees with the experimental result.[21] The height h of the dot was estimated by the transmission-electron spectroscopy[21] to be smaller than 2 nm, whereas the wetting-layer thickness $T_{WL}=0.54$ nm (Ref. 21) (cf. Fig. 1, where $h=2Z-T_{WL}$). Table II shows that the differences between the calculated and measured radiative-transition energies do not exceed 0.5 meV, which is considerably less than the experimental uncertainty.

Table II shows that energy spacings ΔE between the subsequent energy levels decrease with the increasing energy of the interband transitions. According to our interpretation, three effects of comparable importance are responsible for this behavior. If the energy of the electron-hole pair state increases, the charge carriers become more weakly localized and in consequence (i) the effect of the nonparabolicity of the confinement potential becomes stronger,[36] (ii) the electron and hole effective masses become larger with the increasing distance from the dot center [cf. Eq. (4)], (iii) the Coulomb interaction between the confined charge carriers decreases. In Table III, we have listed the energy levels of the quantum-dot confined electron and hole calculated with the neglect of their mutual Coulomb interaction. The spacings between the hole energy levels are much smaller than those for the electron, which results from the larger effective mass of the hole. We also see that—contrary to the case of the parabolic confinement—the energy levels are not equally spaced. The effective nonparabolicity of the confining potential is consideraby smaller for the hole, which results from the larger localization of the heavy hole near the dot center.

III. COUPLED QUANTUM DOTS

The parametrization obtained in Sec. II for the single QD enables us to discuss exciton states in coupled QD's. For this purpose we have extended the model formulated in Sec. II to the case of vertically stacked QD's. Accordingly, the indium-concentration distribution in the two coupled, vertically stacked QD's has been expressed as follows:

$$X(\rho,z)=X_0\exp[-\rho^2/R^2-(z-a/2)^2/Z^2] + X_0\exp[-\rho^2/R^2-(z+a/2)^2/Z^2], \qquad (11)$$

where a is the distance between the centers of the QD's. We note that the model of the coupled QD's does not contain any new fitting parameter. The shape of the potential confining the charge carriers in the coupled QD's, obtained from Eqs. (2) and (11), is schematically displayed in Fig. 2(a). Figure 2(b) shows the geometry of the coupled-dot nanostructure. In Eq. (11), the values of parameters X_0, R, and Z are the same as for the single QD (Sec. II). In this section, we are using the same formulas for the confinement potentials, effective masses, and Hamiltonian as those given in Sec. II. In these formulas, we substitute concentration distribution function (1) by Eq. (11). For the exciton confined in the coupled quantum dots we propose the following trial wave function:

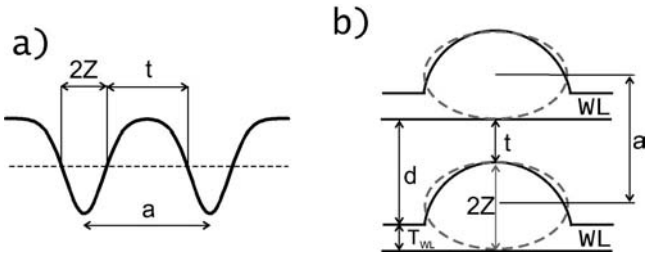

FIG. 2. Schematic of coupled QD's. The barrier and spacer thicknesses are denoted by t and d, respectively, a is the interdot-center distance. Plot (a) shows the profile of the confinement potential in the growth direction and plot (b) shows the geometry of the two coupled dots.

$$\Phi_2(\mathbf{r}_e,\mathbf{r}_h)=\rho_e^m\rho_h^m\chi_m(\varphi_e,\varphi_h) \times\sum_{n_e=0}^{1}\sum_{n_h=0}^{1}\sum_{jkln} c_{jkln}^{n_e n_h} f_{jkln}[\rho_e,\rho_h,z_e +(-1)^{n_e}(a/2),z_h+(-1)^{n_h}(a/2),z_{eh}], \qquad (12)$$

which is a generalization of the form given by Eq. (8). Wave function (12) allows for a description of the electron and hole states of both even and odd parity. Due to the presence of the Coulomb-interaction term in Hamiltonian (5), the exact wave functions are *not* eigenfunctions of the one-particle parity operators. Therefore, they do not possess a definite symmetry with respect to the change of sign of the z coordinate of one particle only. However, Hamiltonian (5) is invariant with respect to the simultaneous change of sign of both the coordinates z_e and z_h. Thus, the electron-hole wave functions possess a definite *total* parity. The symmetry with respect to the total parity applied to Eq. (6) yields the following selection rules: radiative transition is allowed (forbidden) for the initial state of even (odd) parity. Therefore, only the states of the even total parity are optically active.

The thickness of the barrier between the QD's is a more appropriate parameter for a description of the interdot coupling than the distance between the dot centers, since the self-assembled QD's do not possess well-defined centers. In the framework of the present model, thickness t of the interdot barrier is defined as follows: $t=a-2Z$ [cf. Fig. 2(a)], where a is the interdot-center distance. The experimental results[21] have been given as functions of spacer thickness d. These two parameters are related by $t=d+T_{WL}-2Z$

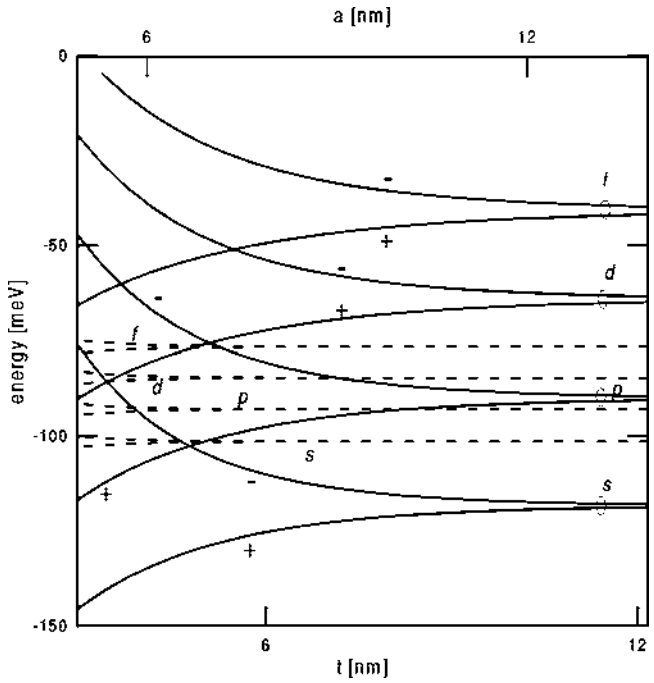

FIG. 3. Calculated one-particle energy levels of the electron (solid curves) and the hole (dashed curves) as functions of barrier thickness t (distance a between the centers of the dots). Signs + and − correspond to the states of even and odd z parity, respectively, and symbols s, p, d, and f denote the angular momentum quantum numbers $m=0$, 1, 2, and 3, respectively.

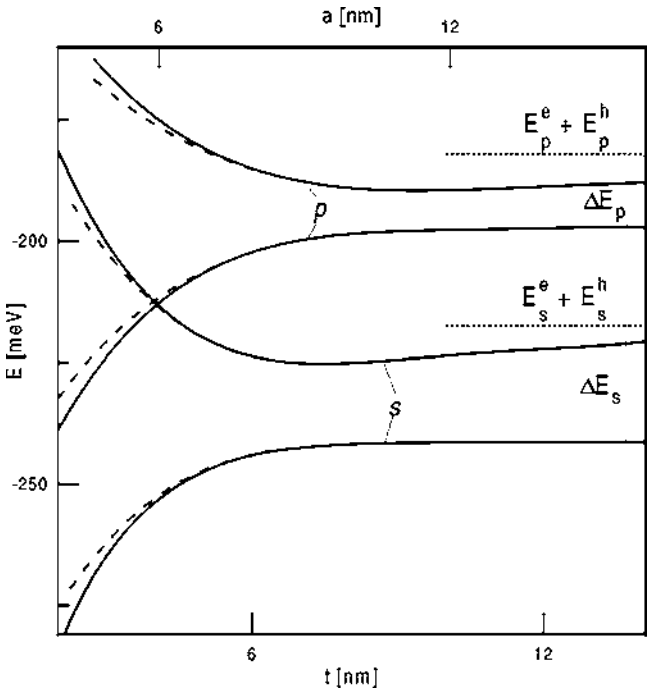

FIG. 4. Calculated energy of s and p states of the exciton confined in the coupled In_XGaAs_{1-X} QD's as a function of barrier thickness t (interdot-center distance a). Solid (dashed) curves show the results for the even-parity optically active (odd-parity optically inactive) states. Dotted lines (labeled by $E_s^e+E_s^h$ and $E_p^e+E_p^h$) display the sums of the energies of the electron and the hole localized in the different infinitely separated QD's. ΔE_s and ΔE_p are the electron-hole Coulomb-interaction energies for s and p states, respectively.

[cf. Fig. 2(b)], which yields the following relation between the spacer thickness and the interdot-center distance: $d=a-T_{WL}$.

IV. RESULTS AND DISCUSSION

In Fig. 3, we have plotted the calculated energy levels of the electron and hole confined in the coupled QD's (with the electron-hole Coulomb interaction omitted) as functions of the barrier thickness (interdot-center distance). For large interdot distances the energy levels are twofold degenerate. When the distance between the dots decreases, the degeneracy with respect to the parity is lifted. The energies of even- (odd-) parity states decrease (increase) with the decreasing interdot separation. The resulting splitting of the energy levels is much larger for the electron than for the hole and only weakly depends on the angular-momentum quantum number.

Figure 4 presents the dependence of the eight lowest-energy levels for the s and p states of the exciton confined in the coupled QD's (with the Coulomb interaction included) on the barrier thickness. The solid curves correspond to the optically active states of even total parity and the dashed curves corespond to the states of odd total parity, from which the radiative transitions are forbidden. For large barrier thickness the lowest-energy s and p levels as well as the higher-energy levels are twofold degenerate. This degeneracy is lifted by the interdot coupling for small interdot separations. In the limit $t\rightarrow\infty$ the exciton ground-state energy becomes equal to the ground-state energy of the exciton confined in the single QD (cf. Table I). Similarly, the energy of lower p level becomes equal to the energy of p state of the exciton in the separated QD (cf. Table II). In the same limit, the higher-energy levels of both angular symmetries tend to the corresponding sums of the energies for the noninteracting electron and hole confined in the separated QD's (cf. Table II). These limit values marked by the dotted lines in Fig. 4 correspond to the dissociated exciton.

Figures 5, 6, and 7 display the contours of the probability amplitudes, i.e., the electron-hole wave functions $\Phi_2(\mathbf{r}_e=(0,0,z_e),\mathbf{r}_h=(0,0,z_h))$ for the four lowest-energy states of s symmetry. In these figures, the coordinates corresponding to the centers of the QD's are marked by the dashed straight lines and the white (dark gray) areas correspond to the lowest (highest) values of the wave functions [in plots (a) through (d), the shades of gray do not correspond to the same values of the wave function]. Figures 5, 6, and 7 show the asymmetry in the electron and hole probability distribution, which results from the stronger localization of the hole due to its larger mass.

Let us consider the case of large interdot distances (Fig. 5). In the two lowest-energy degenerate states [Figs. 5(a) and 5(b)], the values of Φ_2 differ only in signs, i.e., these states are characterized by the same probability density. The identical property holds true for the two degenerate excited states [cf. Figs. 5(c) and 5(d)]. The probability amplitudes for the

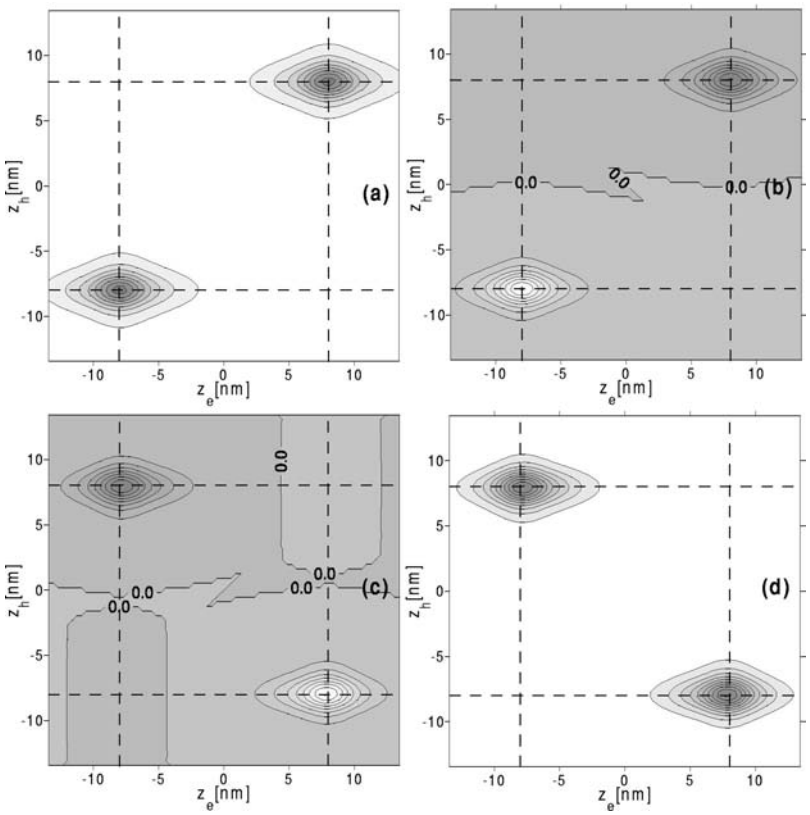

FIG. 5. Contours of *s* exciton wave functions $\Phi_2(\mathbf{r}_e=(0,0,z_e),\mathbf{r}_h=(0,0,z_h))$ for interdot-center distance $a=16$ nm, plotted along the z axis as functions of the electron z_e and hole z_h coordinates for (a) the ground state and the (b) first, (c) second, and (d) third excited state. White (dark gray) areas correspond to the lowest (highest) values of the wave functions. The shades of gray express the relative values of the wave functions, but are not the same in plots (a)–(d). In plots (a) and (d) [and also in 6(a) and 7(a)], the wave functions equal zero in the white areas, whereas in all the other plots the contours corresponding to the wave function equal to zero are denoted by 0.0. Dashed straight lines correspond to the coordinates of the dot centers.

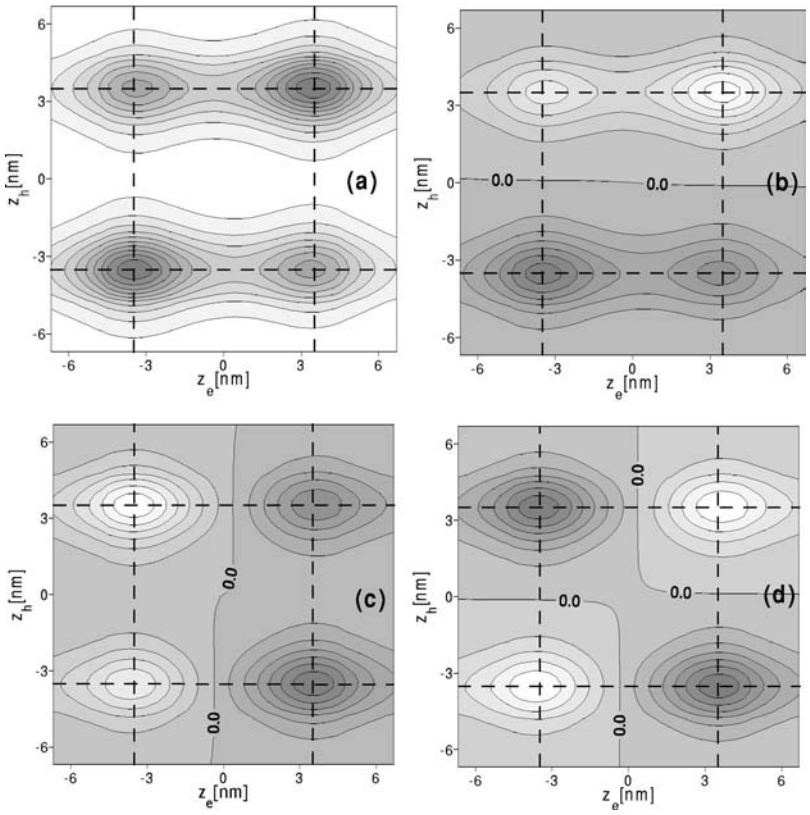

FIG. 6. Contours of *s* exciton wave functions for interdot-center distance $a=7$ nm. The symbols have the same meaning as in Fig. 5.

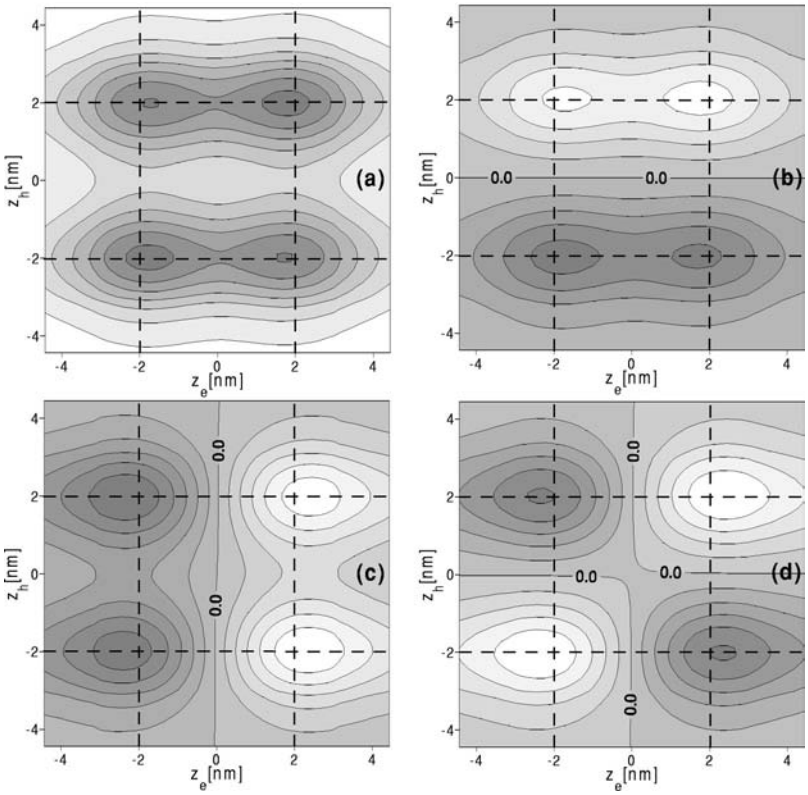

FIG. 7. Contours of *s* exciton wave functions for interdot-center distance $a=4$ nm. The symbols have the same meaning as in Fig. 5.

degenerate ground state possess extrema on the straight line $z_e=z_h$ and those for the degenerate excited states possess extrema on the straight line $z_e=-z_h$. This means that the twofold degenerate ground state corresponds to the electron-hole pair confined in the same quantum dot, whereas in the twofold degenerate excited state, the electron is confined in one QD and the hole is confined in the other. Therefore, in the limit of large interdot distances, the two pairs of degenerate states correspond to essentially different physical situations, i.e., the bound exciton and the dissociated exciton. The ground-state wave functions inside a single QD show the inversion symmetry with respect to the dot center [Figs. 5(a) and 5(b)]. The excited-state wave functions are slightly spread out in the direction of the other QD, in which the oppositely charged particle is localized [Figs. 5(c) and 5(d)]. We note that for large interdot distances the exciton wave functions do not show any trace of the symmetry with respect to the one-particle parity. Obviously, these wave functions are symmetric with respect to the simultaneous change of sign of both the z_e and z_h coordinates.

If the distance between the dots decreases, the energy of the excited state slightly lowers (cf. Fig. 4), which results from the increasing attraction between the electron and hole localized in different dots. This effect is not observed in the ground state, in which both the charge carriers are confined in the same QD. Therefore, in the case of large interdot distances, the only effective coupling is the long-range Coulomb coupling between the charge carriers localized in the different QD's. Figure 4 shows that for the barrier thickness $t \lesssim 8$ nm the higher-energy branches begin to grow and the degeneracy is lifted. In Fig. 6, we have plotted the exciton wave function for the four lowest-energy states in the case of intermediate distance between the dots ($a=7$ nm). The results of Fig. 6 show that the correlation in the relative electron-hole motion is weaker than in the case of large interdot distances. In the two lowest-energy states [Figs. 6(a) and 6(b)], both the particles still prefer to occupy the same QD, but there appears a nonzero probability of occupation of different dots. In the third and fourth excited states [Figs. 6(c) and 6(d)], both the particles exhibit the tendency of avoiding each other, but with the nonvanishing probability of occupation of the same QD.

In Fig. 7, the shapes of the exciton wave functions are shown for a small interdot-center distance ($a=4$ nm). In this case, the wave functions begin to exhibit a definite parity with respect to the change of sign of the single *z* coordinate. The ground-state wave function is approximately even in both the z_e and z_h coordinates [Fig. 7(a)]. The first excited state [Fig. 7(b)] corresponds to the even-parity electron state and odd-parity hole state. On the contrary, in the second excited state [Fig. 7(c)], the electron possesses the odd parity and the hole possesses the even parity, whereas in the third excited state [Fig. 7(d)] both the particles possess the odd parity.

According to the results of Figs. 5, 6, and 7, the one-particle description of the parity symmetry is approximately true only for small interdot distances, i.e., in the limit of the strong interdot coupling. In a general case, the one-particle parity is not well-defined. Therefore, one has to be very careful when describing the symmetry of the exciton for the coupled QD's, especially when using one-particle methods, e.g., LDA approach,[18] which cannot reproduce the total exciton parity. In particular, we can expect that—for some in-

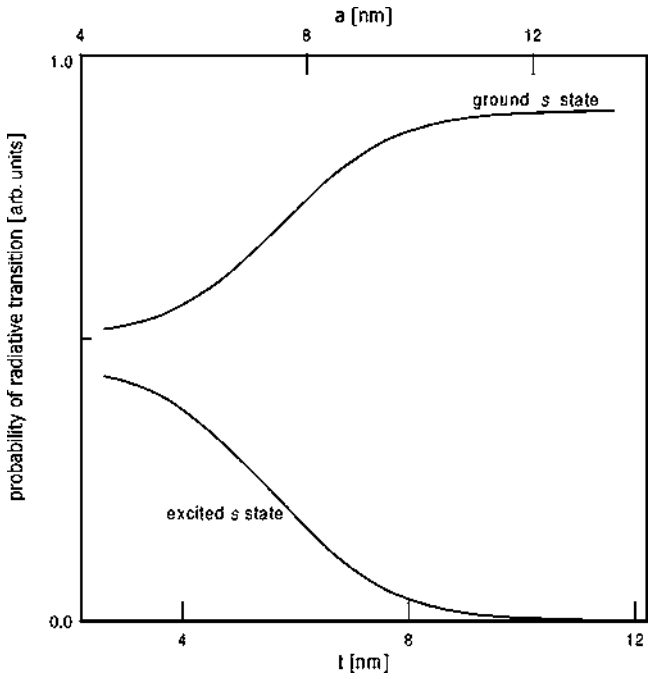

FIG. 8. Estimated probability of the radiative transitions from the even-parity ground and excited state of the exciton with $m=0$ confined in the coupled QD's as a function of barrier thickness t (distance between the dot centers a). The transition probability is expressed in arbitrary units.

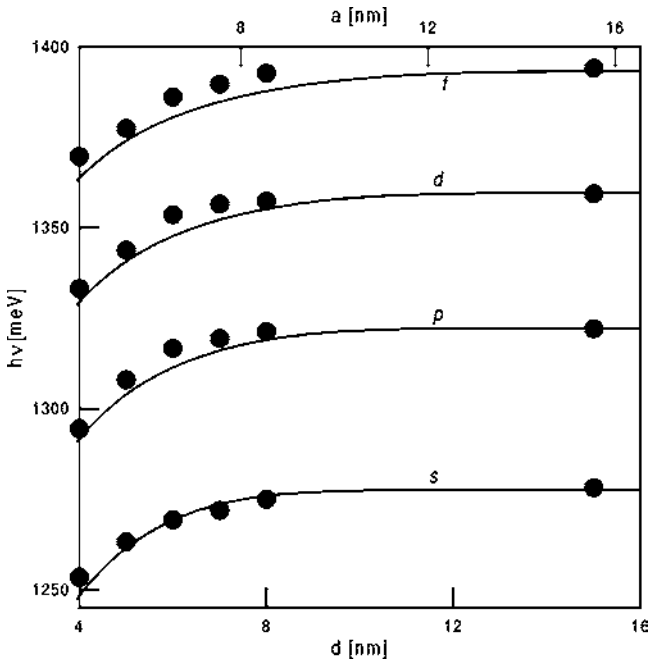

FIG. 9. Energy $h\nu$ of radiative transitions from the even-parity exciton states with one-particle angular-momentum quantum numbers $m=0$ (s),1 (p),2 (d), and 3 (f) as a function of spacer thickness d (a is the interdot-center distance, whereas $d=a-T_{WL}$). Solid curves show the results of the present calculations and full circles show results of the experimental data [Ref. 21].

terdot distances—the broken-parity self-consistent solutions possess a lower total energy.[28]

The parity of the exciton state strongly affects the probability of radiative transitions, i.e., the electron-hole recombination. In Fig. 8, we have plotted the radiative-transition probability calculated according to formula (6) for the optically active exciton states with $m=0$ (s states) and even total parity. The probabilities of the radiative transitions from the ground s state take on fairly large values for all the distances between the QD's. In the ground state, the probability for the electron and the hole to be localized in different QD's increases with the decreasing interdot distance [cf. Figs. 5 (a), 6(a), and 7(a)], which leads to the decreasing probability of the electron-hole recombination. The behavior of the probability of the recombination from the excited even-parity s state is just opposite. In this state, the charge carriers are spatially separated for large interdot distances [cf. Fig. 5(d)]. Therefore, the exciton wave function under integral (6) is equal to zero, which causes the probability of the radiative transition from the excited state to vanish. When the distance between the dots decreases, the charge carriers can be localized in the same QD and the excited-state recombination probability takes on nonzero and increasing values (Fig. 8). However, the probability of the radiative transition from the excited state always remains smaller than that from the ground state.

We have performed similar calculations for the exciton states with higher angular momentum quantum number m. The results (not presented here) show that the properties of the energy levels and relative recombination probabilities for the states of higher m are qualitatively the same those for the s states. This means that the vertical interdot coupling is only weakly affected by the in-plane motion.

As we have shown the radiative transitions are forbidden for the odd-parity initial states and are less probable for the excited even-parity states (cf. Fig. 8). This leads to the conclusion that the dominant contribution to the photoluminescence spectrum of the coupled dots originates from the lowest-energy even-parity exciton states for given m. The interdot coupling shifts the energies of these states towards the lower values (cf. Fig. 4).

Based on these results, we can now compare the predictions of the present model with the experiment.[21] In Fig. 9, we have plotted the energies calculated for the allowed radiative transitions. The experimental data,[43] marked by the full circles, have been extracted from Ref. 21. Figure 9 shows that the calculated transition energies agree very well with the measured positions of the photoluminescence lines.[21] The exciton recombination lines exhibit the pronounced redshift with the decreasing interdot distance. The following physical interpretation of this redshift can be given: the decrease of the interband transition energy means that the exciton binding energy increases with the decreasing interdot separation. This effect mainly results from the lowering of the one-particle energies (cf. Fig. 3), i.e., the stronger quantum confinement of the electron and the hole in the double quantum well with the growing effective range.

In the experimental spectra,[21] taken for the QD's with

height $h \simeq 2$ nm, no additional photoluminescence lines were observed. The appearance of additional photoluminescence lines was reported[21] for the coupled QD's of the larger height ($h = 3$ nm). Unfortunately, the evolution of these additional lines with the varying interdot distance was not presented, probably because of a strong overlap of the luminescence maxima. The authors suggested[21] that the *s* exciton line does not split and that the splitting becomes considerably larger for the highly excited exciton states. Based on the results of the present calculations, we argue that these suggestions are not correct. The calculated spacings between the energy levels of the even-parity *s* and *p* states are comparable (cf. Fig. 4) and the dependence of the relative recombination probability on the barrier thickness is similar for both the states. Therefore, if the higher-energy *p* state is observed, the higher-energy *s* state should also be observed.

Let us discuss a possibility of an experimental observation of the energy-level splitting for the exciton in the coupled QD's. As we have shown above (cf. Fig. 4), in the limit of large interdot distances, for given *m* the two pairs of energy levels are twofold degenerate. These levels are associated with the twofold parity-degenerate ground and excited states. In each pair, only one state (of even total parity) is optically active and can be detected experimentally. This feature is independent of the interdot distance. Therefore, a possible removal of the degeneracy of the two exciton states with the different total parity cannot be observed experimentally.

The higher-energy exciton states of even total parity can be observed under certain conditions. The even-parity states corresponding to the same angular momentum are *always*, i.e., for all interdot distances, energetically separated (cf. Fig. 4). In the limit of large interdot distances, the higher-energy exciton states cannot be detected, since the electron and the hole occupy different dots (cf. Fig. 5) and the transition probability vanishes (cf. Fig. 8). The recombination from the excited states can be observed only for small interdot distances (Fig. 8). If the additional photoluminescence lines connected with the higher-energy states of even parity appear in the spectrum, they are already blueshifted by at least 15 meV with respect to the lines corresponding to the lowest-energy states for given *m* (cf. Fig. 4). The new peaks (with increasing transition energies) can occur in the photoluminescence spectrum if the distance between QD's is sufficiently small. According to our results, one of the new peaks with the lowest energy should correspond to the excited *s* state of the even total parity.

V. SUMMARY

In the present paper, we have introduced a theoretical model of a single QD based on the assumption of the Gaussian distribution of indium concentration. We have generalized this model in order to describe the coupling between the vertically stacked self-assembled QD's. The eigenvalue problem for the exciton in the coupled QD's has been solved with the use of the many-element variational basis, which partially takes into account the two-particle correlation effects. A good agreement has been obtained between the calculated and measured positions of photoluminescence peaks for different interdot distances. This agreement supports our hypothesis of the negligible influence of the inter-exciton interaction on the photoluminescence spectra in the self-assembled quantum dots. The present results show that the proposed Gaussian concentration distribution with the parameters fixed for the single QD is a universal function, which implicitly includes the most important effects in real QD's and properly describes the electronic properties of both the isolated single QD and coupled double QD's. For the coupled QD's we have studied the symmetry with respect to the parity of the exciton states. The present results show that—in a general case—the exciton wave functions do not possess a definite one-particle parity and only the total two-particle parity is conserved. For very small interdot distances the ground-state exciton wave functions exhibit the one-particle parity, but in an approximate manner only. We have also suggested that the recent assignment of the additional photoluminescence lines observed for the small interdot distances should be revised.

ACKNOWLEDGMENTS

This work has been partially supported by the Polish State Scientific Research Committee (KBN) under Grant No. 5 P03B 049 20. One of us (BS) gratefully acknowledges the support of the Foundation for Polish Science (FNP).

*Email address: bszafran@agh.edu.pl

[1] For review articles, see T. Chakraborty, Comments Condens. Matter Phys. **16**, 35 (1992); M.A. Kastner, Phys. Today **46**(1), 24 (1993); M.A. Kastner, Comments Condens. Matter Phys. **17**, 349 (1996).

[2] P.A. Maksym and T. Chakraborty Phys. Rev. Lett. **65**, 108 (1990).

[3] S. Bednarek, B. Szafran, and J. Adamowski, Phys. Rev. B **59**, 13 036 (1999).

[4] B.T. Miller, W. Hansen, S. Manus, R.J. Luyken, A. Lorke, J.P. Kotthaus, S. Huant, G. Medeiros-Ribeiro, and P.M. Petroff, Phys. Rev. B **56**, 6764 (1997).

[5] A. Wójs, P. Hawrylak, S. Fafard, and L. Jacak, Phys. Rev. B **54**, 5604 (1996).

[6] R.J. Warburton, C.S. Dürr, K. Karrai, J.P. Kotthaus, G. Medeiros-Ribeiro, and P.M. Petroff, Phys. Rev. Lett. **79**, 5282 (1997).

[7] M. Grundmann, O. Stier, and D. Bimberg, Phys. Rev. B **52**, 11 969 (1995).

[8] B. Szafran, J. Adamowski, and S. Bednarek, Phys. Rev. B **61**, 1971 (2000).

[9] M. Bayer, O. Stern, P. Hawrylak, S. Fafard, and A. Forchel, Nature (London) **405**, 923 (2000).

[10] P. Hawrylak, G.A. Narvaez, M. Bayer, and A. Forchel, Phys. Rev. Lett. **85**, 389 (2000).

[11] A. Wójs and P. Hawrylak, Phys. Rev. B **53**, 10 841 (1996).

[12] R.J. Warburton, B.T. Miller, C.S. Dürr, C. Bödefeld, K. Karrai, J.P. Kotthaus, G. Medeiros-Ribeiro, P.M. Petroff, and S. Huant, Phys. Rev. B **58**, 16 221 (1998).

[13] G. Park, O.B. Shchechin, D.L. Huffaher, and D.G. Deppe, Appl. Phys. Lett. **73**, 3351 (2000).
[14] R.H. Blick, D. Pfannkuche, R.J. Haug, K. von Klitzing, and K. Eberl, Phys. Rev. Lett. **80**, 4032 (1998).
[15] D.G. Austing, T. Honda, K. Muraki, Y. Tokura, and S. Tarucha, Physica B **249**, 206 (1998).
[16] B. Kochman, T.B. Norris, B. Kochman, J. Singh, and P. Bhattacharya, Appl. Phys. Lett. **76**, 2394 (2000).
[17] J.J. Palacios and P. Hawrylak, Phys. Rev. B **51**, 1769 (1995).
[18] C.Y. Fong, B.M. Klein, L.A. Hemstreet, L.H. Yang, and J.S. Nelson, J. Phys.: Condens. Matter **10**, 4335 (1998).
[19] Y. Tokura, D.G. Austing, and S. Tarucha, J. Phys.: Condens. Matter **11**, 6023 (1999).
[20] B. Partoens and F.M. Peeters, Phys. Rev. Lett. **84**, 4433 (2000).
[21] S. Fafard, M. Spanner, J.P. McCaffrey, and Z.R. Wasilewski, Appl. Phys. Lett. **76**, 2268 (2000).
[22] S. Raymond, X. Guo, J.L. Merz, and S. Fafard, Phys. Rev. B **59**, 7624 (1999).
[23] M. Eto, Jpn. J. Appl. Phys., Part 1 **36**, 3924 (1997).
[24] U. Merkt, J. Huser, and M. Wagner, Phys. Rev. B **43**, 7320 (1991).
[25] D. Pfannkuche, V. Gudmundsson, and P.A. Maksym, Phys. Rev. B **47**, 2244 (1993).
[26] J.-L. Zhu, Z.-Q. Li, J.-Z. Yu, K. Ohno, and Y. Kawazoe, Phys. Rev. B **55**, 15 819 (1997).
[27] R.M.G. Garcia-Castelan, W.S. Choe, and Y.C. Lee, Phys. Rev. B **57**, 9792 (1998).
[28] S.M. Reimann, M. Koskinen, M. Manninen, and B.R. Mottelson, Phys. Rev. Lett. **83**, 3270 (1999).
[29] A.J. Williamson, L.W. Wang, and A. Zunger, Phys. Rev. B **62**, 12 963 (2000).
[30] A. Franceschetti, H. Fu, L.W. Wang, and A. Zunger, Phys. Rev. B **60**, 1819 (1999).
[31] L. Quiroga and N.F. Johnson, Phys. Rev. Lett. **83**, 2270 (1999).
[32] P.D. Siverns, S. Malik, G. McPherson, D. Childs, C. Roberts, R. Murray, B.A. Joyce, and H. Davock, Phys. Rev. B **58**, R10 127 (1998).
[33] R. Colombelli, V. Piazza, A. Badolato, M. Lazzarino, F. Beltram, W. Schoenfeld, and P. Petroff, Appl. Phys. Lett. **76**, 1146 (2000).
[34] S.B. Nam, D.C. Reynolds, C.W. Litton, R.J. Almassy, T.C. Collins, and C.M. Wolfe, Phys. Rev. B **13**, 761 (1976).
[35] M. Cardona, Phys. Rev. **154**, 696 (1967); Phys. Rev. B **13**, 761 (1976).
[36] J. Adamowski, M. Sobkowicz, B. Szafran, and S. Bednarek, Phys. Rev. B **62**, 4234 (2000).
[37] C.W. Litton, R.B. Dennis, and S.D. Smith, J. Phys. C **2**, 2146 (1969).
[38] A.L. Mears and R.A. Stradling, J. Phys. C **4**, L22 (1971).
[39] F. Matossi and F. Stern, Phys. Rev. **111**, 472 (1958).
[40] A.K. Walton and W.K. Mishira, J. Phys. C **1**, 533 (1968).
[41] D.J. BenDaniel and C.B. Duke, Phys. Rev. **152**, 683 (1966).
[42] A. Wójs and P. Hawrylak, Phys. Rev. B **51**, 10 880 (1995).
[43] The experimental points have been taken from Fig. 2 in Ref. 21 as the positions of the photoluminescence peaks.

Exciton and negative trion dissociation by an external electric field in vertically coupled quantum dots

B. Szafran,[1,2] T. Chwiej,[1,2] F. M. Peeters,[1] S. Bednarek,[2] J. Adamowski,[2] and B. Partoens[1]
[1]*Departement Fysica, Universiteit Antwerpen (Campus Drie Eiken), Universiteitsplein 1, B-2610 Antwerpen, Belgium*
[2]*Faculty of Physics and Applied Computer Science, AGH University of Science and Technology, al. Mickiewicza 30, 30-059 Kraków, Poland*

(Received 27 July 2004; revised manuscript received 15 November 2004; published 26 May 2005)

We study the Stark effect for an exciton confined in a pair of vertically coupled quantum dots. A single-band approximation for the hole and a parabolic lateral confinement potential are adopted which allows for the separation of the lateral center-of-mass motion and consequently for an exact numerical solution of the Schrödinger equation. We show that for intermediate tunnel coupling the external electric field leads to the dissociation of the exciton via an avoided crossing of bright and dark exciton energy levels which results in an atypical form of the Stark shift. The electric-field-induced dissociation of the negative trion is studied using the approximation of frozen lateral degrees of freedom. It is shown that in a symmetric system of coupled dots the trion is more stable against dissociation than the exciton. For an asymmetric system of coupled dots the trion dissociation is accompanied by a positive curvature of the recombination energy line as a function of the electric field.

DOI: 10.1103/PhysRevB.71.205316 PACS number(s): 73.21.La, 71.35.Pq, 73.21.Fg

I. INTRODUCTION

Strained self-assembled InAs/GaAs quantum dots grown on subsequent layers stack spontaneously one above the other[1,2] forming artificial molecules with spatially extended states due to the tunnel interdot coupling. The photoluminescence (PL) spectrum of the coupled dots consists of a number of lines which are blue or redshifted by the coupling[2,3] depending on the way the single-particle electron and hole wave functions contribute to the exciton states in question.[4] Application of an electric field oriented along the growth direction offers the possibility of external control of the strength of the tunnel coupling. Recent experimental results[5] on the Stark effect for vertically coupled pairs of nonidentical dots showed the effect of tunnel coupling through the appearance of avoided crossings between states localized in different dots. Previously, tunnel-coupling related Stark shift of the electroabsorption spectra has been observed in vertical stacks of several quantum dots.[6]

Stark effect on the exciton states in vertically coupled self-assembled quantum dots has previously been studied in Refs. 7 and 8. An anomaly in the ground-state Stark shift was found[7] by the $\mathbf{k}\cdot\mathbf{p}$ method accounting for the strain effects and realistic shapes of the dots. This anomaly consists in deviation of the ground-state energy line from the usual quadratic dependence[9] on the external field

$$E(F) = E(F_0) - p(F - F_0) - \beta(F - F_0)^2, \qquad (1)$$

where F_0 is the electric field for which the overlap of the electron and the hole wave functions is the largest and for which the recombination energy is maximal, p is the dipole moment and $\beta > 0$—the polarizability. The shift calculated[7] for coupled dots can only be approximated with two parabolas: one for $F < F_0$ and the other for $F > F_0$, amounting in a cusp at F_0. Although this deviation was attributed[7] to the strain distribution it was shown that such a behavior can also be obtained in a single band model of coupled quantum disks neglecting the strain.[8] Actually, as we discuss below analyzing the Stark shift of the first excited state, this deviation is due to a near degeneracy of the ground-state around F_0 resulting from the weakness of the hole tunnel coupling. In the present paper we report on another deviation of the Stark shift from quadratic form related to the exciton dissociation via a ground-state anticrossing of a bright state with both carriers in the same dot and a dark state with separated carriers.

Quantitative modeling[10–19] of single quantum dots requires taking into account the valence band mixing, the gradient in the indium distribution, strain effects, and confinement geometry which are very different for quantum dots fabricated at various laboratories. In this paper we present a qualitative study of the effects of the external electric field on the *interdot* tunnel coupling visible in the Stark shifts of the bright energy levels, which should be universal for various types of coupled dots. In particular we focus on the effect of the electron-hole interaction which was neglected[7] or treated in an approximate manner[8] in previous work. For a single quantum dot the Coulomb interaction may have a small effect on the Stark shift since the interaction energy only weakly changes with the small displacement of the electron and hole wave functions inside a single dot. On the other hand, the role of the interaction for the Stark effect in coupled dots is essential since the effect of the external field on the exciton consists in breaking the electron-hole binding and segregation of carriers into different dots.

In the present work we use a simple model potential[25] with a square quantum well for the vertical confinement and parabolic lateral confinement adopting the single band approximation for the hole. Due to the applied idealizations the model is exactly solvable. Our results fully account for the interparticle correlations due to the Coulomb interaction and cover also the excited states.

A recent experiment[5] on the Stark effect in a vertically coupled system of quantum dots was performed on a charge tunable structure, similar to the one used in studies of negatively charged excitons.[20] A spectacular change in the spectrum was observed,[5] when an electron was trapped in the dot closer to the electron reservoir. Namely, a sudden drop of the recombination energy and an unexplained positive curvature of the recombination line as a function of the electric field was observed.[5] This observation motivated us to look at the Stark effect for the negatively charged trion. For the negative trion we apply the approximation that the lateral degrees of freedom are frozen. The validity of this approximation is first verified for the Stark shift of the exciton energy levels. In nanostructures the trion binding energies with respect to the dissociation into an exciton and a free electron are considerably increased.[21] However, the trion binding energy is usually substantially smaller than the exciton binding energy. We report here that for a symmetric system of vertically coupled quantum dots the trion is *more* stable for dissociation by the external electric field than the exciton. The study of the dissociation mechanism shows, that for the pair of identical dots the trion is dissociated into a pair of electrons confined in one dot and a hole in the other. Only for the asymmetric system of coupled dots a dissociation into an exciton and a free electron is obtained as an intermediate step before the final separation of the hole from the two electrons. In this case, the trion is more easily dissociated than the exciton. The positive curvature of the recombination energy as a function of the electric field is obtained for the trion ionization process into an exciton and a free electron.

Previously, trions in vertically coupled dots were studied in the absence of the external field[22] and neglecting tunnel coupling between the dots.[23]

This papers is organized as follows, the next section contains the description of the theoretical approach, the results are given in Sec. III, their discussion is presented in Sec. IV. Section V is devoted to the summary and conclusions.

II. THEORY

We assume a parabolic lateral confinement potential with equal electron and hole confinement energy ($\hbar\omega$). Vertical confinement for the electron $[V_e(z_e)]$ and the hole $[V_h(z_h)]$ is taken as double well potentials of depth V_e^0 for the electron and V_h^0 for the hole and of width $w=6$ nm separated by a barrier of thickness b. Isolated quantum dots may possess a built-in strain-induced electric field pushing the hole to the top of the dot as found in the photocurrent measurements of the Stark effect on buried quantum dots.[24] However, in coupled quantum dots the built-in electric field has the opposite orientation.[5] Therefore, this intrinsic electric field is neglected in the present calculations (in fact, such a build in electric field can also be interpreted as a shift of our applied field). For self-assembled quantum dots the assumption of harmonic lateral confinement is not valid, however, it should not essentially modify the susceptibility of the carriers to the electric field oriented vertically.

In the present model the Hamiltonian of the system can be written as

$$H = -\frac{\hbar^2}{2m_e}\nabla_e^2 - \frac{\hbar^2}{2m_h}\nabla_h^2 + \frac{m_e\omega^2}{2}\rho_e^2 + \frac{m_h\omega^2}{2}\rho_h^2 + V_e(z_e) + V_h(z_h) - \frac{e^2}{4\pi\epsilon\epsilon_0 r_{eh}} + e\Phi(z_e) - e\Phi(z_h), \tag{2}$$

where $\rho_e^2=x_e^2+y_e^2$, (x_e,y_e,z_e) and (x_h,y_h,z_h) are the position vectors of electron and the hole, respectively. r_{eh} is the electron hole distance, m_e (m_h) is the electron (hole) effective band mass, ϵ is the dielectric constant, and $\Phi(z)$ is the potential of the external electric field taken as

$$\Phi(z) = \begin{cases} Fz_{max} & \text{for} \quad z_{max} \leqslant z \\ Fz & \text{for} \quad z_{min} < z < z_{max} \\ Fz_{min} & \text{for} \quad z \leqslant z_{min} \end{cases}, \tag{3}$$

where F is the value of the electric field assumed to be uniform between z_{min} and z_{max} (which can be identified as the positions of the electrodes). In the calculations we leave a space of 10 nm between the dots and the points z_{min} and z_{max} beyond which the electric field is assumed to be zero.

The model of the coupled quantum dots used in this paper was previously applied[25] to describe the exciton coupling between dots in the absence of an external electric field. The authors[25] used the configuration interaction scheme to account for the lateral correlations between the electron and the hole. The configuration interaction approach for the electron-hole systems is computationally much more challenging than for the electron systems due to its slow convergence.[26] Therefore, in this paper we will make explicit use of the lateral separability of the center of mass. After introduction of the lateral relative $\boldsymbol{\rho}_{eh}=(x_e-x_h,y_e-y_h)$ and lateral center-of-mass $\boldsymbol{\rho}_{cm}=(m_e x_e+m_h x_h, m_e y_e+m_h y_h)/M$ coordinates, the Hamiltonian can be expresses as a sum of the lateral center-of-mass Hamiltonian (H_{cm}) and the Hamiltonian for the relative lateral—and the single-particle vertical—motion (H_{rv}), which are given by

$$H_{cm} = -\frac{\hbar^2}{2M}\nabla_{\rho_{cm}}^2 + \frac{M\omega^2}{2}\rho_{cm}^2 \tag{4}$$

and

$$H_{rv} = -\frac{\hbar^2}{2\mu}\nabla_{\rho_{eh}}^2 - \frac{\hbar^2}{2m_e}\frac{\partial^2}{\partial z_e^2} - \frac{\hbar^2}{2m_h}\frac{\partial^2}{\partial z_h^2} + \frac{\mu\omega^2}{2}\rho_{eh}^2 + V_e(z_e) + V_h(z_h) - \frac{e^2}{4\pi\epsilon\epsilon_0 r_{eh}} + e\Phi(z_e) - e\Phi(z_h), \tag{5}$$

with $M=m_e+m_h$, $\mu=m_e m_h/(m_e+m_h)$, ∇_ρ^2 stands for the Laplacian in the x-y plane. The exciton wave function can be written as

$$\Psi(\mathbf{r_e},\mathbf{r_h}) = \chi(\boldsymbol{\rho}_{eh},z_e,z_h)\psi_{cm}(\boldsymbol{\rho}_{cm}), \tag{6}$$

where χ and ψ_{cm} are the eigenfunctions of the H_{rv} and the H_{cm} Hamiltonians, respectively. Functions ψ_{cm} are simply the eigenfunctions of a two-dimensional harmonic oscillator.

The eigenstates of Hamiltonian (5) have definite z component of total angular momentum and for $F=0$ also have definite parity with respect to a change of sign of the z coordinates.[4] The absorption/recombination probability for state μ is proportional to the integral

$$p_\mu = \left| \int d^6\mathbf{r}\Psi_\mu(\mathbf{r_e},\mathbf{r_h})\delta^3(\mathbf{r_e}-\mathbf{r_h}) \right|^2 = \left| \int dx_e dy_e \psi_{cm}(x_e,y_e) \int dz_e \chi_\mu(0,z_e,z_e) \right|^2. \quad (7)$$

In the present paper, we consider only states whose symmetry does not prevent them to be bright, i.e., states in which *both* the relative χ and the center of mass ψ_{cm} eigenstates possess zero angular momentum. In the following we show and discuss only results for states in which the center of mass is in the ground state. The spectrum with s-symmetry center-of-mass excitations is simply a replica of the spectrum corresponding to the ground state of the center of mass shifted by the energy $2\hbar\omega$. The recombination probabilities for the states corresponding to zero angular momentum center-of-mass excitations are *exactly* equal to the corresponding states with the ground-state center of mass, since integrals of all the s type wave functions of a two-dimensional harmonic oscillator are equal, which is due to a property of Laguerre polynomials. For potentials, in which the parity is a good quantum number, i.e., for identical quantum dots without an external field, we consider only states of even parity, the odd parity states being dark.

The eigenfunctions χ of Hamiltonian (5) are calculated on a three-dimensional finite-difference mesh with the imaginary time technique.[27] We use the material parameters for an $In_xGa_{1-x}As$ quantum dot embedded in a GaAs matrix with a uniform concentration of indium in the quantum dot $x=0.66$.[4] We take the following parameters for the alloyed quantum dot material $\epsilon=12.5$, $m_e=0.037m_0$, $m_h=0.45m_0$, where m_0 is the free electron mass, $V_e^0=-0.508$ eV, $V_h^0=-0.218$ eV, and we take for the lateral confinement $\hbar\omega=20$ meV. We note, that in the limit of $\hbar\omega=0$ the present problem reduces to the Stark effect for an exciton in coupled quantum wells.[28]

For a particle of mass m confined in a harmonic oscillator potential of energy $\hbar\omega_0$ the localization radius defined as the square root of the expectation value of x^2+y^2 is equal to $\sqrt{\hbar/m\omega_0}$. For the assumed center-of-mass separation the hole is therefore more strongly localized than the electron by a factor of $\sqrt{m_h/m_e}$. In InAs/GaAs quantum dots the hole confinement is stronger than the electron confinement which is due to the finite quantum well effect[29] and the electron-hole interaction which localizes the heavy hole much more strongly than the light electron. In Fig. 7 we show that a change in the strength of the hole and electron lateral confinement does not influence the qualitative features of the spectra in an external electric field. It merely leads to shifts of the energy levels along the energy axis.

For the negative trion in quantum dots with a rectangular-well confinement the effect of a stronger hole localization leads to a larger electron-hole interaction energy than the electron-electron interaction energy.[30] This produces a redshift of the negative trion recombination line which increases with decreasing size of the dot and consequently leads to a decrease of the redshift due to the tunnel effect in coupled quantum dots.[22] In two-dimensional quantum wells the experimentally observed[31] positive and trion recombination energies for zero-magnetic field are nearly equal, although in strictly[21] two-dimensional confinement significantly lower recombination energy for the positive trion was predicted. This effect is explained[31–33] by stronger hole localization. Therefore, the adopted confinement potential takes into account the electron-hole interaction enhancement[22,30–33] with respect to the electron-electron interaction.

III. EXCITON IN VERTICALLY COUPLED DOTS

A. Stark effect

For $F>0$ the electric field pushes the electron to the left and the hole to the right dot. The dependence of the energy spectrum on the external electric field for $b=2$ nm is plotted in Fig. 1(a). At zero electric field the first excited state is of odd parity and corresponds to the excitation of the hole [see the inset to Fig. 1(a)—excitation energy is just 0.25 meV]. The electric field breaks the parity symmetry of the system and the excited state becomes optically active [cf. the inset to Fig. 1(a)]. The dependence of the wave functions on the electric field is displayed in Fig. 2(a). In order to explain the field dependence of the spectrum we have plotted in Fig. 2(b) the probability densities integrated over the lateral degrees of freedom, which gives more accurate information about the localization of particles than the wave function on the axis [whose integral over z_e and z_h gives the recombination probability, cf. Eq. (7)]. In the ground state the hole becomes entirely localized in the right quantum dot for a relatively weak electric field [see the plots for $F=30$ kV/cm in Figs. 2(a) and 2(b)]. The ground-state localization of the electron in the left dot appears at a much higher electric field, leading eventually to the extinction of the recombination intensity. In the excited part of the spectrum one observes two bright energy levels which tend to degeneracy at high electric field [cf. levels labeled by b_l and b_r in Figs. 1(a), 2(a), and 2(b)]. In these two energy levels the electron and the hole occupy the same quantum dot [it is more clearly visible in Fig. 2(b), for the wave function plots presented in Fig. 2(a) this tendency is apparent only at high electric field, cf. the plots for the third and fourth excited states for $F=90$ kV/cm]. In the bright energy levels marked by b_l the carriers become localized in the left quantum dot which is favorable for the electrostatic energy of the electron and unfavorable for the electrostatic energy of the hole. In the higher bright energy level marked by b_r the electron and the hole are localized in the right quantum dot, favorable for the hole and unfavorable for the electron. The b_l level increases when the electric field is switched on. On the other hand the b_r energy level decreases with field. This behavior is due to a reaction of the electron on the field which is delayed with respect to the reaction of the hole being more easily localized in one of the dots by the field [cf. Fig. 2(b)].

Figure 1(a) shows that the two bright energy levels exhibit avoided crossings and anticrossings with the dark energy lev-

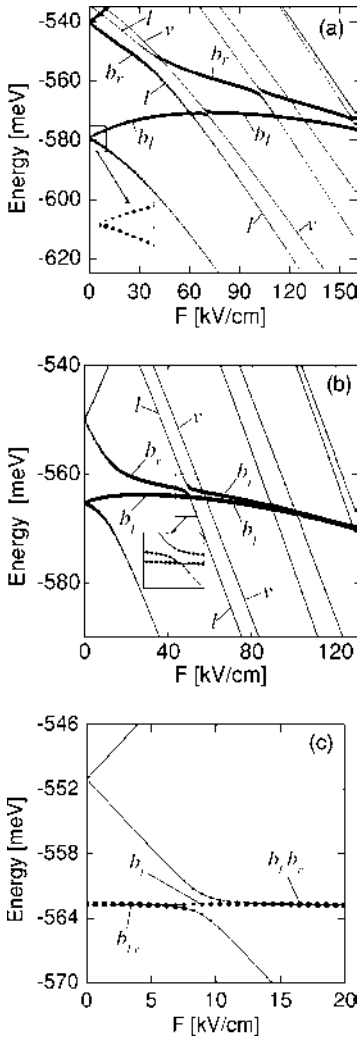

FIG. 1. Exciton energy spectrum as a function of external electric field F for barrier thickness $b=2$ nm (a), $b=4$ nm (b), $b=7$ nm (c). The area of the dots is proportional to the recombination probability. The insets in (a) and (b) show zooms of regions marked by rectangles.

els for which the carriers are separated by the electric field in the same way as in the ground state. The lowest excited dark energy level [marked by l in Figs. 1(a), 2(a), and 2(b)] corresponds to a lateral excitation. In the second excited dark energy level [marked by v in Figs. 1(a), 2(a), and 2(b)] the hole in the right quantum dot is in a state excited in the vertical direction. For $b=2$ nm the first anticrossing in the low-energy spectrum appears between the bright b_r and the dark l energy levels around $F=40$ kV/cm at about -555 meV. This anticrossing is wide and is due to the electron tunnel coupling of the left and right dots (the hole is entirely localized in the right quantum dot in both states). The dark energy level l goes below the lower bright energy level b_l via a crossing. A crossing instead of anticrossing is observed here because in the b_l energy level the hole is in the other (left) dot. The dark state v with a hole excitation crosses the b_r level and goes below the b_l level in a very narrow anticrossing.

For weaker tunnel coupling, i.e., for $b=4$ nm [cf. Fig. 1(b)] the two bright energy levels become degenerate already at about $F=90$ kV/cm. All the avoided crossings become narrower with respect to the stronger tunnel coupling case of Fig. 1(a). The most pronounced anticrossing is the one between the b_r and l energy levels, like for $b=2$ nm [cf. Fig. 1(a)]. The curvature of the degenerate bright energy levels at high electric fields results from the electric-field-induced deformation of the electron and hole wave functions within each of the quantum dots.

The most interesting spectrum is obtained for larger barrier thickness. Figure 1(c) displays the electric-field dependence of the exciton energy spectrum for $b=7$ nm. For $F=0$ the twofold degenerate ground state corresponds to both carriers in the same quantum dot [cf. Fig. 2(b)], while in the nearly degenerate excited state the carriers occupy different quantum dots. The degenerate ground state energy is not affected by the electric field, since the electrostatic energy gained by the electron is lost by the hole and *vice versa*. The electric-field dependence of both the split excited energy levels, which correspond to spatially separated charge carriers, is strictly linear. This energy level anticrosses the b_r bright energy level around $F=9$ kV/cm. After the avoided crossing the state with carriers separated by the external electric field becomes the ground state. The bright state b_l is not involved in the anticrossing and its energy is independent of F. For larger b the discussed anticrossing becomes narrow and barely visible.

Figure 2(c) for $F=5$ kV/cm shows that in the ground-state the charge of the hole is considerably shifted to the right dot and that a part of the electron charge is also transferred to the right dot. In order to present the movement of the carriers between the dots in more detail we plotted in Fig. 3 the charge accumulated in the left dot as a function of the electric field for different barrier thicknesses. We see that the dependence of the hole charge on the external field is monotonous. On the other hand the electron initially follows the movement of the hole to the right dot. For $b=10$ nm the electron charge transferred to the right dot is exactly equal to the hole charge for F smaller than 6 kV/cm. Up to this field both quantum dots remain neutral and the dipole moment (see inset to Fig. 3) is zero. When both particles become completely localized in different dots the dipole moment reaches $e(b+w)$.

B. Nonidentical quantum dots

The confinement potential of vertically stacked dots usually exhibits asymmetry, which even for identical dots can be induced by the strain effects.[7] Let us consider the effect of the asymmetry of the confinement potential on the exciton spectrum. It was established[7] that for stacked strained truncated pyramids the ground state of the hole is completely localized in one of the dots, while the electron (noninteracting[7] with the hole) still forms bonding and antibonding states.

Here, we simulate this type of localization assuming unequal depths of the quantum wells for the hole. The effect of the electric field on the spectrum of asymmetric coupled dots for $b=6$ nm is presented in Fig. 4(a) for the right dot deeper by 3 meV for the hole. Two bright energy levels around

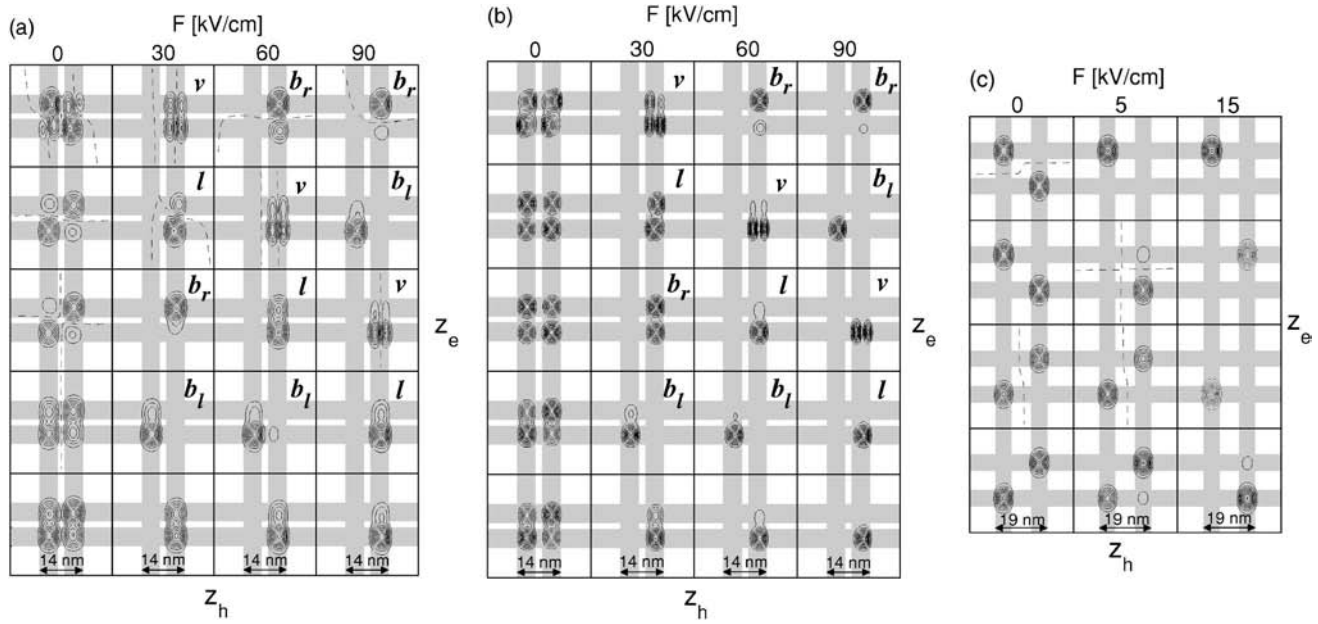

FIG. 2. (a), (c) contour plots of wave functions at the axis $\rho=0$ of the system and (b) probability density integrated over the lateral degrees of freedom $\int_0^\infty d\rho\rho|\chi(\rho,z_e,z_h)|^2$ for different values of the electric field for barrier thickness $b=2$ nm (a), (b) and $b=7$ nm (c). Lower plots correspond to lower energies. Shaded area show the quantum wells for the electron and for the hole. Dashed line shows the nodal surface of the wave function.

−563 and −560 meV are obtained. In the lower (upper) of energy levels both the carriers are localized in the deeper (shallower) of the dots. The lowest dark energy level decreasing linearly in energy with F has the hole localized in the right dot [cf. Fig. 5(a)] so it crosses the higher bright energy level with both the carriers in the left dot. The interchange of the energy order of this dark state with the lower bright energy level appears via an avoided crossing, since in both these states the hole is localized in the right (deeper) dot [cf. Fig. 5(a)]. For $F<0$ the hole in the lowest energy dark state is localized in the shallower of the dots. For this reason the corresponding energy level anticrosses the higher bright energy level and crosses the lower one.

Let us now suppose that the left dot is shallower for the electron (by 3 meV) and that the hole confinement is symmetric. Figure 4(b) shows the spectrum for this case. Surprisingly the spectrum for the electron confinement asymmetry

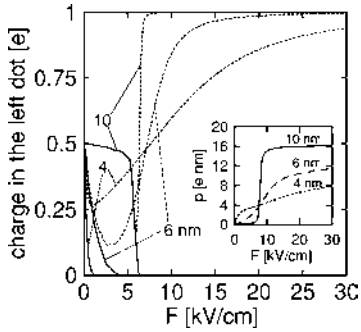

FIG. 3. Electron (dotted line) and hole (solid line) charge accumulated in the left quantum dot as function of the electric field for different barrier thicknesses. Inset shows the dipole moment as function of the field.

is just shifted by +2.5 kV/cm with respect to the spectrum for the hole confinement asymmetry [cf. Fig. 4(a)]. In the lower (upper) of the bright energy levels the electron stays in the deeper (shallower) of the dots and the Coulomb interaction binds the hole in the same dot [cf. Fig. 5(b)]. The crossing/anticrossing mechanism is the same as for the hole confinement asymmetry.

For smaller barrier thickness the anticrossings of the dark and bright energy levels become wider and as a consequence the region near $F=0$ in which the two lowest energy levels are nearly independent of F is narrower. The spectra for the hole asymmetry for $b=4.5$ and 3 nm are displayed in Figs. 6(a) and 6(b), respectively. The two parallel energy levels near $F=0$ observed for weak tunnel coupling in Fig. 4 are now (see Fig. 6) converted into a crossing at a small negative F. This feature results in the cusp of the ground-state energy reported previously[7] for a thin (1.8 nm) interdot barrier. For the electron asymmetry the spectra are still shifted to higher values of the field by about 2.5 kV/cm with respect to the hole asymmetry, like in the weak coupling case of Fig. 4. The crossing of the bright energy levels still appears at $F<0$. The reason of this similarity is that in the ground state at $F=0$ the dipole moment induced by the electron and hole asymmetry is the same in sign and not very different in size. For small b the electron charge is smeared over *both* dots. If the right dot is deeper for the electron it binds a *larger* part of its charge. Consequently, the *entire* charge of the hole is pulled to the right dot. On the other hand, for the hole confinement asymmetry the dot which is deeper for the hole localizes its charge completely even for small b since the hole tunnel coupling is negligible. The localization of the hole in the right dot results in a larger localization of the electron in the right dot. In this way the asymmetry of the confinement for one particle is translated into an asymmetry

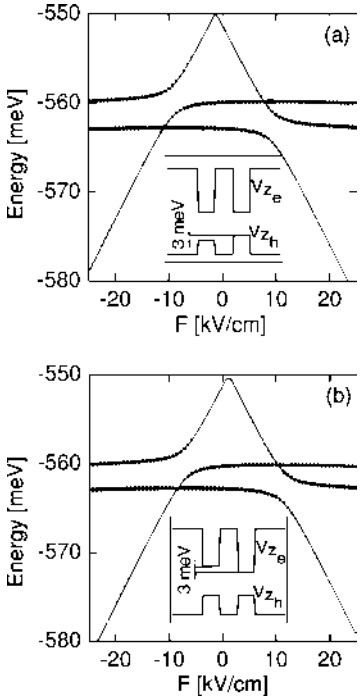

FIG. 4. Stark effect for the asymmetric system of quantum dots at $b=6$ nm. In (a) the electron confinement is symmetric and the left dot for the hole is shallower by 3 meV. In (b) the hole confinement is symmetric and the left dot for the electron is shallower by 3 meV. The insets in (a) and (b) show a schematic drawing of the vertical confinement for $F=0$.

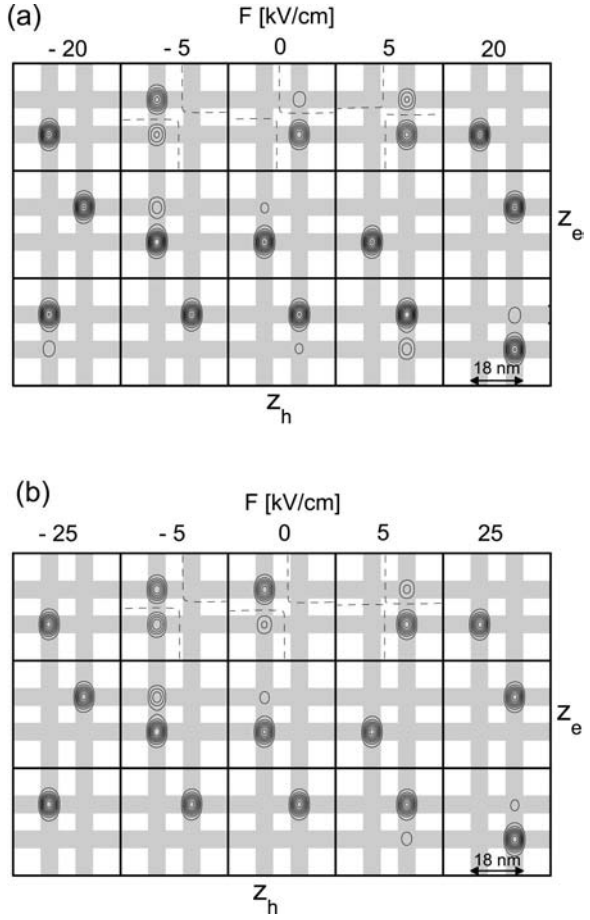

FIG. 5. (a) Contour plots of the wave functions at the axis $\rho=0$ corresponding to the energy levels shown in Fig. 4(a). (b) similar as for Fig. 4(b). Higher plots correspond to higher energies.

of the potential felt by the other particle via the Coulomb interaction. Although it is possible experimentally to determine which of the dots is deeper by looking at the electric-field dependence of the bright energy levels one cannot deduce from the F dependence of the exciton energy levels alone which of the carriers is responsible for the asymmetry.

C. Frozen lateral degrees of freedom

The exact separability of the center of mass used in the previous calculations was possible because of the assumption of identical lateral confinement energies for the electron and the hole. When the center of mass is not separable[26] the exact calculations become much more complex. However, as long as the interest of calculations relies in a qualitative description of the influence of the electric field applied in the growth direction the actual form of the lateral confinement is not essential. In this case one may try to integrate out the lateral degrees of freedom.[34,35] Such an adiabatic approximation is valid for strong lateral confinement, as in the case of self-assembled quantum dots. Thus we assume that the electron and hole lateral wave functions can be identified with the ground-state of the harmonic oscillator. This assumption allows us to integrate[35] over the lateral degrees of freedom and arrive at the effective Hamiltonian for the vertical motion

$$H_{\mathrm{eff}} = -\frac{\hbar^2}{2m_e}\frac{\partial^2}{\partial z_e^2} - \frac{\hbar^2}{2m_h}\frac{\partial^2}{\partial z_h^2} + V_e(z_e) + V_h(z_h) - V_{\mathrm{eff}}(|z_e - z_h|) + e\Phi(z_e) - e\Phi(z_h) + 2\hbar\omega, \qquad (8)$$

with $V_{\mathrm{eff}}(z)$ the effective potential[35] of one-dimensional interaction given by

$$V_{\mathrm{eff}}(z) = \frac{e^2}{4\pi^{1/2}\epsilon\epsilon_0 l}\mathrm{erfcx}(|z|/l), \qquad (9)$$

with $l=\sqrt{\hbar(1/m_e+1/m_h)/\omega}$. The solution to the eigenequation of the effective Hamiltonian (8) describes the effects appearing in the growth direction at the expense of a simplified picture of the lateral motion.

Figure 4 shows the comparison of the exact results (solid lines) obtained with the separated center-of-mass and approximate results calculated for frozen lateral degrees of freedom (dashed lines) for identical quantum dots separated by a barrier of thickness $b=4$ nm, as considered above in Fig. 4(b). The approximate method reproduces the correct qualitative shape of the energy lines. Also the recombination probability dependence on the electric field does not significantly differ. However, the approximation of the frozen lateral state eliminates the lateral excitations. The avoided

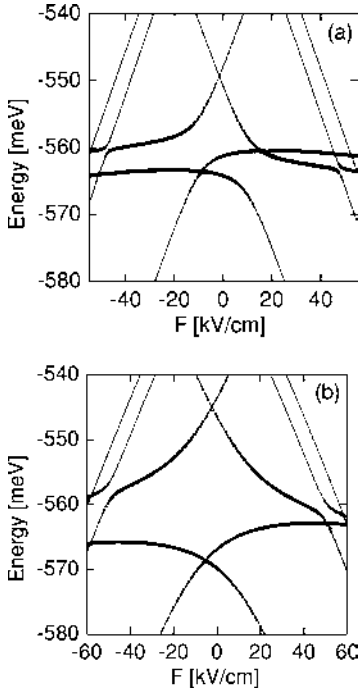

FIG. 6. Stark effect for the asymmetric hole confinement of Fig. 4(a) for $b=4.5$ nm (a) and $b=3$ nm (b). The area of the dots shows the recombination probability.

crossings of the bright energy levels with the dark energy levels with lateral excitations are therefore overlooked in the present approximation [cf. avoided crossing at $F=50$ kV/cm missing for lines marked with dashed lines]. The accuracy of the approximate method is better for dark states with separated charge carriers than for the bright energy levels for which the electrons and hole wave function overlap.[35] The discussed approximation can be applied to evaluate the qualitative dependence of the bright energy levels on the external field when lateral excitations are absent. In the following section we will use this approach to study the effect of the external field on the negatively charged trion in coupled dots.

The dotted lines in Fig. 7 show the results of frozen-degree-of-freedom calculations performed for the electron confinement unchanged but weakened hole confinement for which the lateral confinement radii of the electron and the hole are equal. For weakened hole confinement the electron-hole interaction energy is smaller, which leads to a blueshift of the energy levels for $F=0$ with respect to the equal confinement energies case (dashed lines in Fig. 7). The interaction energy of the dissociated electron-hole pair is less strongly affected by the change of the hole localization strengths. Figure 7 shows that the electric-field dependence on the electric field is essentially not altered by the strength of the hole localization, which justifies *a posteriori* the assumption of the adopted center-of-mass separability.

IV. STARK EFFECT FOR NEGATIVE TRION

We consider the effect of the electric field on the ground state of a negatively charged trion in which the electron sub-

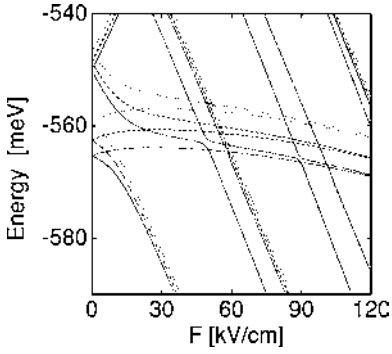

FIG. 7. The exact results solid lines and the results with the frozen degree of freedom for equal hole and electron confinement energies (dashed lines) and with equal hole and electron confinement lengths (dotted line) for the parameters of Fig. 4(b).

system is in the singlet state. The approximation of the frozen lateral wave functions will be used with the quasione-dimensional[35] electron-electron (V_{eff}^{ee}) and electron-hole interaction potential [Eq. (9)]. Electron-electron V_{eff}^{ee} potential is obtained for m_h replaced by m_e in formula (9). The Hamiltonian for the trion reads

$$H_{\mathrm{eff}}^{X^-} = -\frac{\hbar^2}{2m_e}\left(\frac{\partial^2}{\partial z_{e1}^2}+\frac{\partial^2}{\partial z_{e2}^2}\right)-\frac{\hbar^2}{2m_h}\frac{\partial^2}{\partial z_h^2}+V_e(z_{e1})+V_e(z_{e2}) + V_h(z_h)-V_{\mathrm{eff}}(|z_{e1}-z_h|)-V_{\mathrm{eff}}(|z_{e2}-z_h|) + V_{\mathrm{eff}}^{ee}(|z_{e2}-z_{e1}|)+e\Phi(z_{e1})+e\Phi(z_{e2})-e\Phi(z_h)+3\hbar\omega, \tag{10}$$

where z_{e1} and z_{e2} are coordinates of the first and second electron, respectively.

Figure 8(a) shows the difference of the trion ground state energy and the ground state energy of a single electron as function of the electric field for different values of the barrier thickness and identical pair of quantum dots of width 6 nm. The energy difference presented in Fig. 8(a) can be identified[22] with the energy of the photon released when the hole recombines with one of the electrons (calculated with respect to the GaAs energy gap similarly as for the exciton). For comparison the exciton ground state energy calculated with the same approximation of the frozen lateral states is also shown by the dashed lines. In the absence of the electric field the recombination line of the negative trion has a lower energy than the exciton recombination energy [cf. the inset to Fig. 8(a)]. We found that the redshift of the trion line is smaller for smaller barrier thickness. This behavior as obtained by neglecting the lateral correlations is in perfect qualitative agreement with extensive variational calculations accounting for both vertical and lateral correlations in a nearly exact way.[22] Inset to Fig. 8(a) shows that for high F the energy difference of the trion and exiton energy lines is an increasing function of b. This is due to the fact that the interaction energy between the electrons confined in the same dot is larger than the Coulomb interaction between the hole and electron separated by the barrier.

For larger barrier thickness [cf. plots for $b=6$ and 8 nm in Fig. 8(a)] the recombination line of the trion is independent

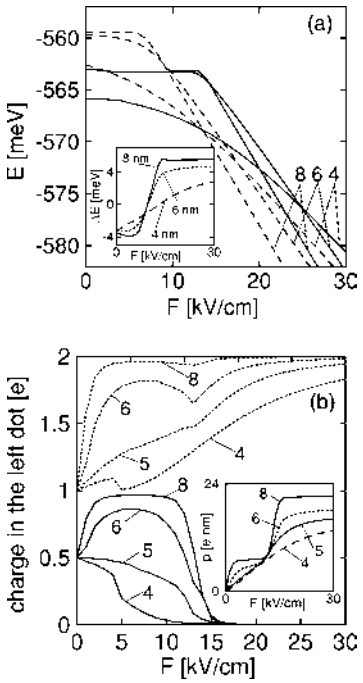

FIG. 8. (a) Difference of the ground-state trion energy and the electron ground state (trion recombination energy with respect to GaAs energy gap—solid lines) and the exciton ground-state energy (exciton recombination energy—dashed lines). The curves are labeled by the barrier thickness b in nanometers. Inset shows the difference of the exciton and trion energy lines. (b) Electron (dotted lines) and hole (solid lines) charge on the left side of the origin as function of the electric field. Inset shows the dipole moment.

of the electric field for F lower than about 13 kV/cm. The flat part of the plots corresponds to both the electrons and the hole staying in the same quantum dot (as discussed above for exciton). We can see that the ground state of the trion is more resistant to the dissociation by the electric field than the exciton ground state. The exciton energy decreases faster than the trion recombination line, which results in the reversal of the order of the lines at $F=14$ kV/cm for $b=4$ nm and $F=10$ kV/cm for $b=6$ and 8 nm. For large values of F for which the hole and the electron charges in both the exciton and the trion ground states are completely separated, the trion and exciton energy lines for each b run parallel to each other.

To explain the large stability of the trion ground state in the symmetric coupled dots against dissociation by the electric field we plotted in Fig. 8(b) the hole and the electron charge accumulated in the left dot as a function of the electric field for different barrier thicknesses. For large b the distribution of the electron and the hole charges between the dots before the dissociation of the trion is qualitatively different than in the exciton case (cf. Fig. 3). For $F=0$ the hole (electron) charge in the right dot is 0.5 (1) due to the symmetry of the system. For large barrier thickness ($b=8$ nm) the electrons become localized in the left dot already under the influence of a weak electric field. The hole initially follows the electrons into the left dot (cf. the local maximum of the solid line for $b=8$ nm). We remind the reader that for the exciton an opposite behavior was observed (cf. Fig. 3): the

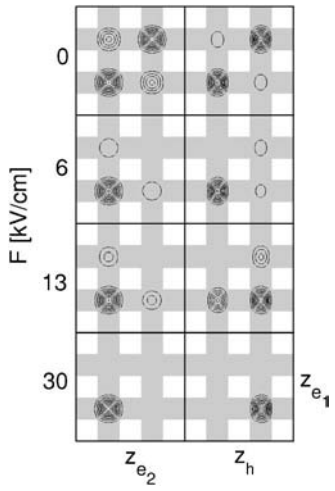

FIG. 9. Probability density integrated over the vertical coordinate of one of the electrons (right panel) and the vertical coordinate of the hole (left panel) for $b=6$ nm and different values of the electric field F. The shaded areas show the positions of the quantum dots.

electron initially followed the hole for weak electric fields. The trion becomes dissociated around 13 kV/cm, when the field moves the hole from the left to the right dot. The reaction of the carriers on the electric field is the most complex for $b=6$ nm [cf. Fig. 8(b)]. We have illustrated this in Fig. 9 by additional plots of the probability densities integrated over the vertical coordinate of one the three particles. For zero electric field there is a nonzero probability of finding the electrons in different dots (cf. the left plot for $F=0$ in Fig. 9), and the probability of finding an electron in a different quantum dot than the hole (cf. the right plot for $F=0$ in Fig. 9) is much smaller. For $b>8$ nm all the three particles are found in the same dot. The leakage of particles to the other dot seen in Fig. 9 is a result of the electron tunnel coupling which is already nonzero for $b=6$ nm. In contrast to the case of $b=8$ nm, for $b=6$ nm a part of the electron charge stays in the right dot when the field is switched on (cf. the left plot for $F=6$ kV/cm in Fig. 9). When the hole is transferred to the right dot (cf. the plots for $F=13$ kV/cm, part of the electron charge follows it, which results in a local minimum of the electron charge accumulated in the left dot for F around 13 kV/cm [cf. Fig. 8(b) for $b=6$ nm]. For larger F the particles become separated. For stronger tunnel coupling between the dots, i.e., for $b=5$ and 4 nm the hole charge accumulated in the left dot depends on the external field monotonically [cf. Fig. 8(b)], and a part of the electron charge attempts to follow the hole when it leaves the left dot. Therefore, for small b the mechanism of the trion resistance to dissociation becomes similar to the one observed for the exciton (cf. Fig. 3). The present results show that for symmetric quantum dots the trion becomes dissociated into a pair of electrons in one dot and the hole in the other without the intermediate step consisting of an exciton confined in the right dot and an electron in the left dot. This mechanism is more clearly pronounced for larger b. The Coulomb interaction of the electrons with the hole stabilizing the complex against field-induced dissociation without the intermediate step is two times larger than for exciton.

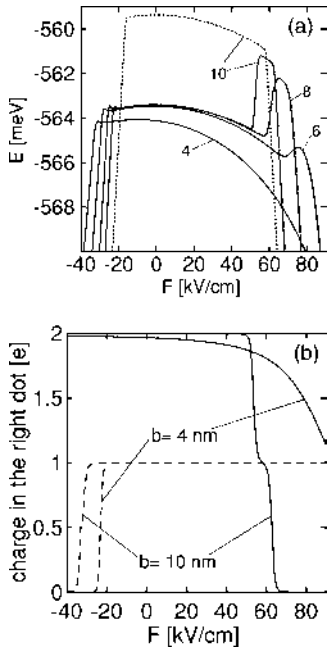

FIG. 10. (a) The trion recombination energies as functions of the electric field (solid lines) for a pair of coupled quantum dots. The curves are labeled by the barrier thickness in nanometers. Right dot has a width of 6 nm and the width of the left dot is 4 nm. Dotted line shows the exciton recombination energy for $b=10$ nm. (b) The electron (solid lines) and the hole (dashed lines) charge accumulated in the right dot for $b=4$ and 10 nm

Note that for the trion [cf. Fig. 8(b)] the barrier thickness has the opposite effect on the sensitivity of the electrons and the hole to the electric-field induced localization. For smaller b the electric field is less effective in localizing the electrons in the left dot but more effective in localizing the hole in the right dot. The effect for the electrons is obviously due to the strong electron tunnel coupling. For smaller b a smaller F localizes the hole in the right dot because the energy of its interaction with electrons changes less drastically after the dissociation and the hole tunnel coupling is negligible.

The inset to Fig. 8(b) shows the electric dipole moment for the trion as a function of the electric field. For high F, when the particles are separated into different dots the dipole moment takes the value $3e(w+b)/2$.[36] Note, that for a thick barrier the dipole moment develops a plateau for the region of fields in which the hole accompanies the electrons to the right dot. For a thick barrier the recombination energy [cf. inset of Fig. 8(a)] starts to change only when the second plateau of the dipole moment is reached.

We found a qualitatively different dissociation mechanism of the trion in an asymmetric system of coupled dots. Suppose that the right quantum dot has a thickness of 6 nm (as anywhere else in the present paper) and that the left dot has a thickness of only 4 nm. Figure 10(a) shows the trion recombination energies for different barrier thicknesses. The charge accumulated in the right (wider) dot is plotted in Fig. 10(b). For $F=0$ the three carriers stay in the right dot. For strongly coupled dots ($b=4$ nm) the electrons resist strongly to being removed to the thinnest dot. For $F=90$ kV/cm less than one elementary charge is localized in the left dot. On the other hand the negative electric field removes abruptly the hole to the thinnest dot at $F<-25$ kV/cm. For thicker interdot barrier the trion recombination energy develops a local maximum for positive electric fields [see the plots for $b=6$, 8, and 10 nm in Fig. 10(a)]. Let us analyze the origin of these maxima for the case of $b=10$ nm. For positive electric field up to 50 kV/cm both the electrons are confined in the right dot [cf. Fig. 10(b)]. Then between $F=50$ kV/cm and $F=55$ kV/cm one of the electrons is transferred to the right dot. In this electric field range the trion is dissociated into an exciton confined in the right dot and a spectator electron in the left quantum dot. The final state after the trion recombination, i.e., the ground state of a single electron, is localized in the left quantum dot for $F>50$ kV/cm, i.e., for the same value of the electric field which induces the transition of the first electron from the trion state to the left quantum dot.[37] After the trion dissociation the recombination energy almost reaches the recombination energy of the exciton [cf. dotted line in Fig. 10(a)]. The slight redshift of the dissociated trion line with respect to the exciton in this electric field range is due to the Coulomb perturbation of the exciton remaining in the right quantum dot by the spectator electron in the left quantum dot. The second electron is removed from the right dot between 60 and 65 kV/cm.

Note, that the observed mechanism of dissociation of the trion into an exciton and an electron does not occur in the system of symmetric quantum dots (cf. Fig. 8). For asymmetric quantum dots the stronger confinement energy in the thinner of the dots prevents the second electron from entering it simultaneously with the first one. In the asymmetric system the exciton becomes dissociated into an electron and a hole for *larger* electric fields than the one inducing dissociation of the trion into an exciton and a free electron [cf. Fig. 10(b)]. On the other hand the exciton created in the right quantum dot after the trion dissociation is more resistant to the electric field induced dissociation than the exciton. The electron remaining in the right dot is less willing to pass to the left quantum dot if it is already occupied by an electron.

The recombination energy lines of the trion in the asymmetric system of coupled dots present a positive second derivative with respect to the electric field for a certain range of F. Namely, for $b=6$ nm the second derivative is positive for the electric field range $F\in(61,71)$, $F\in(57,60)$, and $F\in(50,52)$ kV/cm for $b=6$, 8, and 10 nm, respectively.

For symmetric dots the mechanism behind the trion dissociation into an electron pair confined in one dot and the hole in the other, without an intermediate step consisting of an exciton in one dot, and the electron occupying the other quantum dot, is easily explained when considering large b using a simple reasoning in which the tunnel effect and the interdot Coulomb interactions are neglected. In this model the dependence of the energy of the trion on the external field can be written as $E_{X^-}=-2E_{eh}+E_{ee}-Fbe/2$, where E_{eh} (E_{ee}) is the absolute value of the electron-hole interaction for the particles localized in the same dot. The trion is localized in the dot in which the electron localization is favored by the field. The lowest energy level corresponding to the exciton confined in one dot and the electron in the other is $E_X=-E_{eh}-Fbe/2$, and the energy level corresponding to a completely dissociated system is $E_d=E_{ee}-3Fbe/2$. For

$E_{eh} < E_{ee}$ the trion is bound at $F=0$ and at nonzero field the ground state energy equals either E_{X^-} or E_d. The energy splitting of E_{X^-} and E_X is not affected by the field which explains the absence of an exciton as an intermediate step of trion ionization. A similar simple reasoning can be used for coupled asymmetric dots where the intermediate step of trion dissociation is now found.

V. DISCUSSION

As mentioned in the introduction previous ground-state calculations[7,8] for the Stark effect in vertically coupled dots detected a deviation of the energy dependence on the electric field from the expected quadratic form obtained within the second order perturbation theory.[9] The inset to Fig. 1(a) shows that for identical quantum dots this deviation, i.e., a cusp of the recombination energy in function of the electric field, is due to a narrow avoided crossing of two lowest energy levels. In the absence of the electric field these two energy levels are nearly degenerate. This near degeneracy results from the smallness of the hole tunnel coupling between the dots. For the case presented in Fig. 1(a) these two energy levels correspond to opposite parity of the hole [cf. Fig. 2(a) for $F=0$]. The electric field easily mixes the two energy levels localizing the hole in the right dot (in the ground state) and in the left quantum dot (in the first excited state). When the confinement potential is asymmetric the discussed anticrossing of the two lowest energy levels are replaced by a crossing (cf. Fig. 6). This is due to a nearly complete localization of the hole in left or right quantum dot in the two states. The cusp of the ground-state is produced by *two* energy levels crossing or nearly crossing. It is therefore clear that second order perturbation theory for a single *nondegenerate* energy level given[9] for a *single* quantum dot is not applicable to the ground state in coupled quantum dots. There is therefore no reason for which the ground state should follow the quadratic formula and the deviation from parabolicity does not really deserve to be called an anomaly.

In the present paper we have found another deviation from the common quadratic Stark shift, also involving two energy levels. This deviation appears for an intermediate barrier thickness and is due to an avoided crossings of a bright energy level with both carriers in the same dot and a dark energy with separated charge carriers. This unusual Stark effect, shown in Fig. 2(c) for a symmetric dot, should be visible in low-excitation PL spectroscopy.[3] The observation of the excited exciton states should be facilitated by a relatively weak tunnel coupling between the quantum dots. In the corresponding PL spectrum, one of the lines should be independent of the electric field in both energy and intensity. The additional structure below and above the constant-energy line should be observed in the form of an anticrossing. The intensity of the constant-energy line should be reduced in the region, in which the anticrossing appears.

Real InAs/GaAs quantum dots exhibit a strain-induced intrinsic dipole moment at $F=0$.[24] The intrinsic dipole moment has been neglected in the present calculations. However, the unusual Stark shift for the coupled dots is predicted for quite small electric fields (lower than 15 kV/cm), for which the effect of the intrinsic dipole moment is negligible. For comparison in the experiment the intrinsic dipole moment leads to a shift of the transition energy by about 5 meV for $F=100$ kV/cm.[24] Therefore, the intrinsic dipole moment should not modify the qualitative features of the effect predicted in the present paper. The second order effect of the polarizability related to the electric-field induced deformation of the electron and hole wave function for the discussed low electric field range should be even smaller. Similar mechanism of the exciton dissociation via an avoided crossing has been found for asymmetric dots [cf. Figs. 5(a) and 5(b)]. The difference between the ideally symmetric system and the more realistic asymmetric one is that the bright state which does not participate in the avoided crossing is shifted to a different energy, lower or higher depending on the direction of the electric field. The mechanism of the exciton dissociation via an avoided crossing of a dark and a bright energy level described here has been recently confirmed experimentally[38] after the present paper has been submitted.

Second-order perturbation theory for a single nondegenerate energy level[9] predicts a nonpositive curvature of the energy level as a function of the electric field. Although the curvature is indeed nonpositive in the ground state, a positive curvature is obtained for the excited bright energy levels in the presence of the avoided crossings with lower energy levels [see Figs. 4(a)–4(c), 9, and 10]. A nondegenerate perturbation theory for a single level[9] obviously does not apply for the the energy level interaction.

In view of the present results the pronounced drop of the recombination energy for a bias voltage for which an electron is trapped in the quantum dot[5] closer to the electron reservoir can be understood provided that the recombination signal in the observed range of wavelengths comes from this dot. Otherwise, the charge of the electron trapped in the dot closer to the reservoir would have a negligible influence on the energy of exciton recombination in the other dot separated by a barrier of 12 nm [cf. the small energy spacing between the exciton recombination lines with and without a spectator electron in the other dot for $b=10$ nm in Fig. 10(a)]. The drop would result from the electrostatics of the negative trion in which the energy of the electron-hole attraction is larger than the electron-electron repulsion due to a difference of the strength of lateral localization of the carriers (see the discussion given in Ref. 22). The observed growth of the recombination energy for the smaller absolute value of the bias voltage could be related to a passage of one of the electrons to the upper dot. The presented calculations for the trion were limited to the ground state. However, the PL line observed in the experiment which we here attribute to the trion recombination in the *lower* of the dots does not correspond to the ground state since the quantum dot in the upper layer are *larger*. Therefore, in the experiment the dissociation of the trion localized in the lower dot could be associated with an avoided crossings with lower energy states, which as obtained for the exciton, can produce a positive curvature of the recombination line over a wide range of electric field values.

VI. SUMMARY AND CONCLUSIONS

We have studied the exciton and negative trion states in a simple but exactly solvable model of vertically coupled

quantum dots allowing for a description of the effects related to the modification of the electron-hole interaction by an electric field applied in the growth direction. The effect of the tunnel coupling between the dots and the confinement potential asymmetry was considered. The mechanism of the electric-field induced exciton and trion dissociation was described.

We have shown that the previously[7,8] found deviations from the quadratic Stark effect are due to energy levels crossings (or very narrow avoided crossings). For weaker tunnel coupling we have found another nonquadratic feature due to an avoided crossing of bright and dark energy levels. This feature appears also in the presence of the asymmetry of the coupled dots and is due to the Coulomb interaction. Positive curvature of the bright excited exciton energy levels is obtained in the range of electric fields corresponding to avoided crossings with lower levels.

Although in the presence of asymmetry of the coupled dots the trion is dissociated into an exciton and an electron by the electric field, for symmetric dots the dissociation mechanism is different, i.e., the trion is directly separated into an electron pair in one dot and the hole in the other. The trion is more stable against this mechanism of dissociation than the exciton. The process of trion dissociation into an exciton and a free electron that we obtain for the case of asymmetric coupling leads to a positive curvature of the PL line as a function of the electric field which has never been observed for the exciton ground state.

ACKNOWLEDGMENTS

This paper was supported by the Polish Ministry of Scientific Research and Information Technology in the framework of the solicited Grant No. PBZ-MIN-008/P03/2003, the Flemish Science Foundation (FWO-Vl), the Belgian Science Policy, the University of Antwerpen (VIS and GOA) and the European Commission GROWTH programme NANOMAT project, Contract No. G5RD-CT-2001-00545, and the EU-NoE SANDiE. T.C. is partly supported by the Marie Curie Training Site Programme of the European Union. B.S. is supported by the Foundation for Polish Science (FNP) and by the EC Marie Curie IEF Project No. MEIF-CT-2004-500157. We are thankful for Dr. Ruth Oulton for helpful discussions and for making the experimental data accessible prior to publication.

[1] G. S. Solomon, J. A. Trezza, A. F. Marshall, and J. S. Harris, Phys. Rev. Lett. **76**, 952 (1995).
[2] S. Fafard, M. Spanner, J. P. McCaffrey, and Z. Wasilewski, Appl. Phys. Lett. **76**, 2707 (2000).
[3] M. Bayer, P. Hawrylak, K. Hinzer, S. Fafard, M. Korkusinski, Z. Wasilewski, O. Stern, and A. Forchel, Science **291**, 451 (2001).
[4] B. Szafran, S. Bednarek, and J. Adamowski, Phys. Rev. B **64**, 125301 (2001).
[5] R. Oulton, A. I. Tartakovskii, A. Ebbens, J. J. Finley, D. J. Mowbray, M. S. Skolnick, and M. Hopkinson, cond-mat/0407072 (unpublished).
[6] J. H. Ser, Y. H. Lee, J. W. Kim, and J. E. Oh, Jpn. J. Appl. Phys., Part 1 **39**, 518 (2000).
[7] W. Sheng and J.-P. Leburton, Phys. Rev. Lett. **88**, 167401 (2002).
[8] K. L. Janssens, B. Partoens, and F. M. Peeters, Phys. Rev. B **65**, 233301 (2002).
[9] J. A. Barker and E. P. O'Reilly, Phys. Rev. B **61**, 13 840 (2000).
[10] M. Grundmann, O. Stier, and D. Bimberg, Phys. Rev. B **52**, 11 969 (1995).
[11] M. A. Cusack, P. R. Briddon, and M. Jaros, Phys. Rev. B **54**, R2300 (1996).
[12] C. Pryor, Phys. Rev. B **57**, 7190 (1998); **60**, 2869 (1999).
[13] O. Stier, M. Grundmann, and D. Bimberg, Phys. Rev. B **59**, 5688 (1999).
[14] L. Landin, M. E. Pistol, C. Pryor, M. Persson, L. Samuelson, and M. Miller, Phys. Rev. B **60**, 16 640 (1999).
[15] R. Heitz, O. Stier, I. Mukhametzhanov, A. Madhukar, and D. Bimberg, Phys. Rev. B **62**, 11 017 (2000).
[16] A. J. Williamson and A. Zunger, Phys. Rev. B **61**, 1978 (2000).
[17] W. Sheng and J.-P. Leburton, Phys. Rev. B **63**, 161301(R) (2001).
[18] F. Guffarth, R. Heitz, A. Schliwa, O. Stier, N. N. Ledentsov, A. R. Kovsh, V. M. Ustinov, and D. Bimberg, Phys. Rev. B **64**, 085305 (2001).
[19] F. Guffarth, R. Heitz, A. Schliwa, O. Stier, M. Geller, C. M. A. Kapteyn, R. Sellin, and D. Bimberg, Phys. Rev. B **67**, 235304 (2003).
[20] B. Urbaszek, R. J. Warburton, K. Karrai, B. D. Gerardot, P. M. Petroff, and J. M. Garcia, Phys. Rev. Lett. **90**, 247403 (2003).
[21] B. Stébé and A. Ainane, Superlattices Microstruct. **5**, 545 (1989); C. Riva, F. M. Peeters, and K. Varga, Phys. Rev. B **61**, 13873 (2000).
[22] B. Szafran, B. Stébé, J. Adamowski, and S. Bednarek, Phys. Rev. B **66**, 165331 (2002).
[23] E. Anisimovas and F. M. Peeters, Phys. Rev. B **68**, 115310 (2003).
[24] P. W. Fry, I. E. Itskevich, D. J. Mowbray, M. S. Skolnick, J. J. Finley, J. A. Barker, E. P. O'Reilly, L. R. Wilson, I. A. Larkin, P. A. Maksym, M. Hopkinson, M. Al-Khafaji, J. P. R. David, A. G. Cullis, G. Hill, and J. C. Clark, Phys. Rev. Lett. **84**, 733 (2000).
[25] F. Troiani, U. Hohenester, and E. Molinari, Phys. Rev. B **65**, 161301(R) (2002).
[26] V. Halonen, T. Chakraborty, and P. Pietiläinen, Phys. Rev. B **45**, 5980 (1992).
[27] K. T. Davies, H. Flocard, S. Kreger, and M. S. Weiss, Nucl. Phys. A **342**, 112 (1980).
[28] F. M. Peeters and J. E. Golub, Phys. Rev. B **43**, 5159 (1991).
[29] A. Wójs, P. Hawrylak, S. Fafard, and L. Jacak, Phys. Rev. B **54**, 5604 (1996).
[30] B. Szafran, B. Stébé, J. Adamowski, and S. Bednarej, J. Phys.: Condens. Matter **12**, 2453 (2000).
[31] S. Glasberg, G. Finkelstein, H. Shtrikman, and I. Bar-Joseph, Phys. Rev. B **59**, R10 425 (1999).
[32] A. V. Filinov, C. Riva, F. M. Peeters, Yu. E. Lozovik, and M.

Bonitz, Phys. Rev. B **70**, 035323 (2004).
[33] B. Stébé and A. Moradi, Phys. Rev. B **61**, 2888 (2000).
[34] A. Esser, R. Zimmermann, and E. Runge, Phys. Status Solidi B **227**, 317 (2001).
[35] S. Bednarek, B. Szafran, T. Chwiej, and J. Adamowski, Phys. Rev. B **68**, 045328 (2003).
[36] For the trion, unlike for the exciton, the value of the dipole moment depends on the choice of the origin. The values displayed in the inset of Fig. 8(b) are calculated for the origin set in the middle of the barrier.
[37] If the ground state of a single electron was localized in the left dot for higher value of the electric field, the recombination energy, calculated as the difference of the ground state of the trion and electron, would have a doubtful physical interpretation since it would additionally assume that the recombination of the electron-hole pair is accompanied by the passage of the electron from the right to the left dot.
[38] H. J. Krenner, M. Sabathil, E. C. Clark, A. F. Kress, D. Schuh, M. Bichler, G. Abstreiter, and J. J. Finley, Phys. Rev. Lett. **94**, 057402 (2005).

J. Phys.: Condens. Matter **12** (2000) 2453–2459. Printed in the UK PII: S0953-8984(00)10156-0

Recombination energy for excitonic trions in quantum dots

B Szafran†‡, B Stébé‡, J Adamowski† and S Bednarek†

† Faculty of Physics and Nuclear Techniques, University of Mining and Metallurgy (AGH), Kraków, Poland

‡ Université de Metz, Institut de Physique et d'Electronique, Metz, France

Received 7 December 1999

Abstract. A theoretical study of excitonic trions, X^- and X_2^+, in semiconductor quantum dots is presented. The model of a spherical quantum well of finite depth is applied to determine the influence of the three-dimensional quantum confinement on the recombination energies of the excitonic trions. A new type of variational wave function, expanded in a Gaussian basis, has been proposed. It is shown that the blue-shift of the recombination induced by the quantum confinement is much stronger for the positive trion X_2^+ than for the negative trion X^-.

Excitonic trions (charged excitons) are electronic excited states of semiconductors, which are created when an additional electron or a hole is bound to a pre-existing exciton. The existence of negatively (X^-) and positively (X_2^+) charged excitons in bulk semiconductors was predicted theoretically [1–5] and observed experimentally in Ge [6], Si [7], and CuCl [8, 9] bulk crystals. In the bulk crystals, the recombination energies of neutral and charged excitons are very close. Moreover, the binding energies of charged excitons are small compared to the thermal excitation energies. Therefore, the identification of the excitonic trions in the bulk materials is rather difficult. In quasi-two-dimensional quantum wells (QWs), a strong increase of both the binding energy of the charged excitons and the energy separation between the neutral- and charged-exciton recombination lines has been theoretically shown by Stébé *et al* [10]. The charged excitons have been experimentally observed in CdTe/CdZnTe [11] and in GaAs/GaAlAs [12–14] semiconductor QWs. The negatively charged excitons have been observed [15] in InAs self-assembled quantum dots (QDs). The binding energies of charged excitons in pyramidal QDs have been calculated by Lelong and Bastard [18]. Wójs and Hawrylak [19] have studied the X^- confined in a two-dimensional harmonic potential in an external magnetic field. It is well known that the quantum confinement results in a blue-shift of the exciton-related photoluminescence lines [20, 21].

In the present paper, we study the influence of the three-dimensional quantum confinement on the recombination energy of excitonic trions X^- and X_2^+ in QDs. We take into account the fully three-dimensional character of the Coulomb interaction, which has been recently shown to be important even for quasi-two-dimensional QDs [22].

The effective-mass Hamiltonian for the confined negatively charged exciton (X^-) can be written as follows:

$$H = -\frac{\hbar^2}{2m_e^*}(\nabla_1^2 + \nabla_2^2) - \frac{\hbar^2}{2m_h^*}\nabla_h^2 + V_e(\boldsymbol{r}_1) + V_e(\boldsymbol{r}_2) + V_h(\boldsymbol{r}_h) + \frac{e^2}{\varepsilon}\left(\frac{1}{r_{12}} - \frac{1}{r_{1h}} - \frac{1}{r_{2h}}\right) \quad (1)$$

where m_e^* (m_h^*) is the effective electron (hole) band mass, ε is the effective dielectric constant, V_e (V_h) is the confinement potential for the electrons (holes), $\boldsymbol{r}_1$, $\boldsymbol{r}_2$, and $\boldsymbol{r}_h$ are the position

0953-8984/00/112453+07$30.00

vectors of the two electrons and the hole with respect to the dot centre, r_{12}, r_{1h}, and r_{2h} are the electron–electron and electron–hole distances. The energy of the electrons (holes) is measured from the conduction band minimum (valence band maximum) of the QD material. We assume that the effective masses as well as the dielectric constants are the same in the well and barrier materials. The Hamiltonian for the positively charged exciton X_2^+ can be obtained from (1) by interchanging the electron and hole masses and the confinement potentials.

The confinement potentials result from the conduction and valence band offsets at the QD/barrier interface. Therefore, we have approximated them by spherically symmetric quantum wells of radius R. The barrier height is equal to V_0^e for the electrons and V_0^h for the holes. The present model is fully three-dimensional and applies to confinement potentials of finite range and depth, i.e., it is adequate for QD nanocrystals embedded in an insulating medium, e.g., GaAs [23] and InAs [24]. Contrary to the usually applied harmonic oscillator model potential [19,25], the quantum-well potential does not commute with the kinetic energy operator of the centre-of-mass motion. Therefore, Hamiltonian (1) cannot be separated into the centre-of-mass and relative-motion Hamiltonians. Hence, the ground-state wave function for the trion confined in the spherical quantum well has to be dependent on the six distances appearing in Hamiltonian (1). In the present paper, we propose the following variational trial wave function for the singlet ground state of the X^- trion:

$$\Psi(\boldsymbol{r}_1, \boldsymbol{r}_2, \boldsymbol{r}_h) = \psi_1(\boldsymbol{r}_1, \boldsymbol{r}_2, \boldsymbol{r}_h) + \psi_2(\boldsymbol{r}_1, \boldsymbol{r}_2, \boldsymbol{r}_h) \tag{2}$$

where ψ_1 and ψ_2 are expanded in the following two Gaussian bases with N_1 and N_2 elements, respectively:

$$\psi_1(\boldsymbol{r}_1, \boldsymbol{r}_2, \boldsymbol{r}_h) = \exp(-br_{1h}^2 - br_{2h}^2)(1 + P_{12}) \sum_{i_1 i_2 i_3}^{N_1} c_{i_1 i_2 i_3} \exp(-\alpha_{i_1}^e r_1^2 - \alpha_{i_2}^e r_2^2 - \alpha_{i_3}^h r_h^2) \tag{3}$$

and

$$\psi_2(\boldsymbol{r}_1, \boldsymbol{r}_2, \boldsymbol{r}_h) = \exp(-a^e r_1^2 - a^e r_2^2 - a^h r_h^2)(1 + P_{12}) \times \sum_{j_1 j_2 j_3}^{N_2} d_{j_1 j_2 j_3} \exp(-\gamma_{j_1} r_{12}^2 - \beta_{j_2} r_{1h}^2 - \beta_{j_3} r_{2h}^2). \tag{4}$$

In equations (3) and (4), P_{12} is the permutation operator interchanging the electron indices $1 \leftrightarrow 2$; $c_{i_1 i_2 i_3}$, $d_{j_1 j_2 j_3}$, α_i^e, α_i^h, β_j, γ_j, a^e, a^h, and b are the variational parameters. The trial wave function for the positively charged exciton X_2^+ has been chosen in a similar way.

Trial wave function ψ_1 describes the trions in a strong-confinement regime [26], for which the interparticle correlations are weak. In the weak-confinement regime (bulk limit) [26], the correlations between the three particles are of crucial importance. They are described by trial wave function ψ_2. The choice of the double basis in formula (2) enables us to obtain reliable energy estimates in both the limiting cases, i.e., in the strong- and weak-confinement regimes. The applicability of the Gaussian basis to the few-particle problem for the spherically symmetric quantum dot of finite depth has been discussed in detail by Bednarek *et al* [27]. The Gaussian basis was proved to be useful in the variational calculations of bulk and confined exciton complexes [28, 29]. Moreover, we have performed test calculations with the use of variational wave function (2) and obtained a ground-state energy equal to -0.2611 (in double atomic rydbergs: 2 Ryd $=$ 27.2116 eV) for X^- in a bulk material with $m_e^* = m_h^*$. For comparison, the 'exact' value obtained by Frost *et al* [30] is equal to -0.2620.

The three-dimensional nanocrystals of nearly spherical shape were fabricated from GaAs in organic solvents [23] and other three-dimensional GaAs/GaAlAs nanostructures were experimentally studied by Ugajin *et al* [31]. In the present paper, we consider the excitonic

trions in the spherical GaAs quantum dot embedded in the $Ga_{0.8}Al_{0.2}As$ matrix. We apply the GaAs effective masses and dielectric constant for the confined charged excitons and neglect the discontinuities of both the parameters at the QD boundary. In our previous paper [32], we have shown that the influence of effective-mass discontinuity on the ground-state energies of electrons and neutral donor impurities is negligibly small for the spherical GaAs/$Ga_{0.8}Al_{0.2}As$ QDs. The neglect of the dielectric constant discontinuity is justified by the similarity of the dielectric properties of the GaAs and $Ga_{0.8}Al_{0.2}As$ materials. Throughout the present paper, we use the following values of the barrier heights [33]: $V_0^e = 140.1$ meV for the electron and $V_0^h = 105.7$ meV for the hole; and the effective masses [34]: $m_e^*/m_0 = 0.0665$ for the electron and $m_h^*/m_0 = 0.34$ for the hole, where m_0 is the electron rest mass, and the dielectric constant [35] $\varepsilon = 12.5$.

We have performed systematic test calculations with an increasing number of basis elements in expansions (3) and (4). The results of table 1 show that convergence is nearly reached for N_1 and $N_2 \simeq 100$. In the following calculations, we have used the trial wave function with $N_1 = 75$ and $N_2 = 84$ terms, which provides quite reliable estimates.

Table 1. Test of the convergence of the variational basis (equations (2)–(4)) with N_1 and N_2 terms in ψ_1 and ψ_2, respectively. The results are given for the GaAs/$Ga_{0.8}Al_{0.2}As$ quantum dot with $R = 2\ a_D$. The calculated ground-state energy of the X^- (X_2^+) trion is quoted in the third (fourth) column and the corresponding recombination-energy shifts are listed in the fifth and sixth columns. In this quantum dot, the electron, hole, and exciton confinement energies are equal to 1.021 77, 0.218 92, and 0.256 70, respectively. The energy is expressed in double donor rydbergs ($2R_D = 11.4$ meV) and the length in donor Bohr radii ($a_D = 99.47$ Å).

N_1	N_2	$E(X^-)$	$E(X_2^+)$	$\Delta E(X^-)$	$\Delta E(X_2^+)$
40	42	1.12290	0.37539	0.15556	0.10023
75	84	1.10928	0.36788	0.16918	0.10773
126	144	1.10230	0.36284	0.17616	0.11278
196	225	1.09914	0.35663	0.17932	0.11899

The energy estimates obtained with the use of only ψ_1 or ψ_2 are quoted in table 2. These results enable us to give a physical interpretation of both the trial wave functions. Wave function ψ_1 yields the dominant contribution to the ground-state energy in the strong-confinement regime, while ψ_2 yields that in the weak-confinement regime. In the intermediate-confinement regime, the contributions originating from the two wave functions are comparable. Table 2 also provides the test of the reliability of the present results for the intermediate-confinement regime.

Table 2. Ground-state energy of the X^- complex confined in the GaAs/$Ga_{0.8}Al_{0.2}As$ quantum dot as a function of quantum-dot radius R calculated with the use of trial wave functions ψ_1, ψ_2, and Ψ. The units are the same as for table 1.

R/a_D	ψ_1	ψ_2	Ψ
20	−0.3087	−0.4220	−0.4308
10	−0.2937	−0.3676	−0.4054
5	−0.1615	−0.0907	−0.2609
2	1.2114	1.3021	1.0928
1	5.8065	8.2818	5.7016

We have determined the amount of energy released in an electron–hole recombination process for the positive (X_2^+) and negative (X^-) trions confined in a QD. The recombination energy is the difference between the energies of the initial and final states. The ground state of

the trion is the initial state. The final state, after the electron–hole recombination, corresponds to the confined hole (electron). Thus, the recombination energies are given by

$$h\nu_{X_2^+} = \epsilon_g + E_{X_2^+} - E_h \tag{5}$$

$$h\nu_{X^-} = \epsilon_g + E_{X^-} - E_e \tag{6}$$

for the positive and negative trions, respectively, where ϵ_g is the energy gap of the QD, $E_{X_2^+}$ and E_{X^-} are the ground-state energies of the confined charged excitons, E_e and E_h are the energies of the confined electron and hole. The recombination energy of the neutral exciton $h\nu_X = \epsilon_g + E_X$, where E_X is the ground-state energy of the exciton confined in the QD. We define the recombination-energy shifts

$$\Delta E_{X_2^+} = h\nu_X - h\nu_{X_2^+} \tag{7}$$

$$\Delta E_{X^-} = h\nu_X - h\nu_{X^-}. \tag{8}$$

The calculated energy shifts are shown in figure 1 as functions of the inverse square of the dot radius R for the weak-confinement regime of the GaAs/GaAlAs QDs. In the bulk crystal, i.e., for $R \to \infty$, the recombination-energy shift for the X_2^+ is larger than that for the X^-, which agrees with the results of the previous studies [3–5]. This results from the fact that the binding energy of X_2^+ is larger than that of X^- for $m_e^*/m_h^* < 1$. However, figure 1 shows that the quantum confinement changes the order of the recombination-energy shifts for the dot radius $R \sim 12\,a_D$, which—for small QDs—leads to the recombination-energy shift for the X^- being up to ∼50% larger than that for the X_2^+. In figure 2, we have plotted the energy shifts for a wider range of QD radii, which includes the strong-confinement regime. The energy shift ΔE_{X^-} for the negative trion increases with the decreasing QD radius. The behaviour of the energy shift for the positive X_2^+ trion is more complex. In the weak-confinement regime,

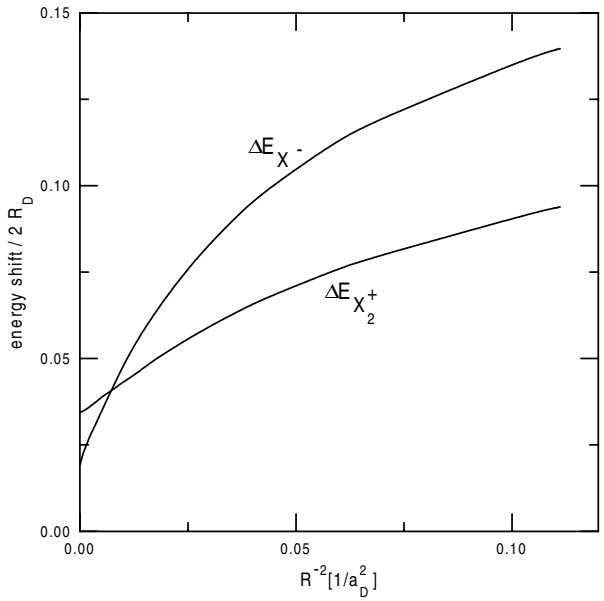

Figure 1. Calculated recombination-energy shifts for the trions X^- and X_2^+ confined in a $GaAs/Ga_{0.8}Al_{0.2}As$ quantum dot as functions of the inverse square of the dot radius R in the weak-confinement regime. The unit of energy is twice the donor rydberg ($2R_D$), the unit of length is the donor Bohr radius (a_D) for GaAs.

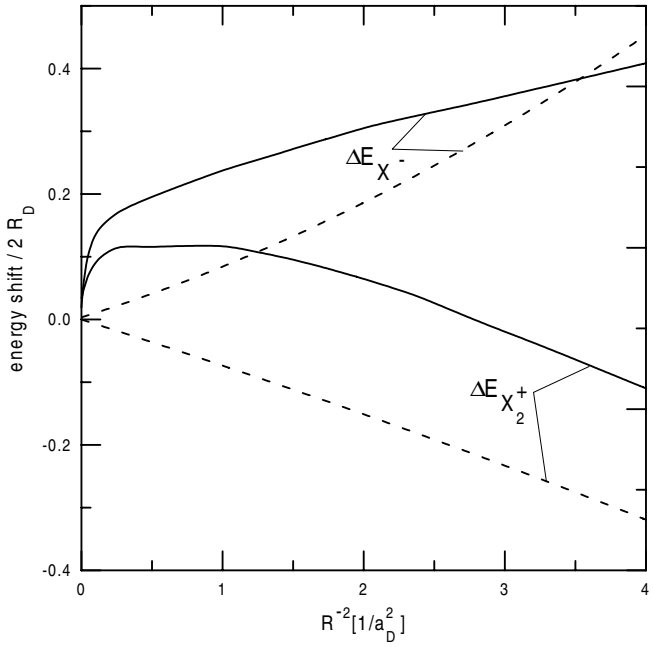

Figure 2. Recombination-energy shifts for the trions X^- and X_2^+ confined in a GaAs/$Ga_{0.8}Al_{0.2}As$ quantum dot as functions of the inverse square of the dot radius R in the intermediate- and strong-confinement regimes. The units are the same as for figure 1. Solid (dashed) curves show the variational (perturbation theory) results.

the energy shift $\Delta E_{X_2^+}$ increases if the QD radius decreases. In the intermediate-confinement regime ($a_D \leqslant R \leqslant 2\ a_D$), this shift is almost independent of the dot size. In the strong-confinement regime, i.e., for $R < a_D$, $\Delta E_{X_2^+}$ decreases, which leads to the blue-shift of the X_2^+ line with respect to the neutral-exciton line.

In order to get physical insight into this surprising behaviour of the confinement-induced shift of the X_2^+ recombination line, we have used the first-order perturbation theory. In the strong-confinement limit, the Coulomb interactions between the charge carriers can be treated as a perturbation when determining the qualitative properties of the confined electron–hole systems [26]. According to the first-order perturbation approach, energy shifts (7) and (8) result from the Coulomb interactions only and can be expressed as follows:

$$\Delta E_{X_2^+} = V_{eh} - V_{hh} \tag{9}$$

$$\Delta E_{X^-} = V_{eh} - V_{ee} \tag{10}$$

where V_{eh}, V_{hh}, and V_{ee} are the Coulomb integrals

$$V_{eh} = \langle \varphi_e(r_1)\varphi_h(r_2)|\frac{1}{r_{12}}|\varphi_e(r_1)\varphi_h(r_2)\rangle \tag{11}$$

$$V_{hh} = \langle \varphi_h(r_1)\varphi_h(r_2)|\frac{1}{r_{12}}|\varphi_h(r_1)\varphi_h(r_2)\rangle \tag{12}$$

and

$$V_{ee} = \langle \varphi_e(r_1)\varphi_e(r_2)|\frac{1}{r_{12}}|\varphi_e(r_1)\varphi_e(r_2)\rangle. \tag{13}$$

Here, φ_e and φ_h are the exact wave functions of the electron and the hole confined in spherical potential wells of depths V_0^e and V_0^h, respectively. Integrals (11)–(13) can be evaluated in a semi-analytical way. The localization of the hole in the quantum well is—due to the larger effective mass—much stronger than the localization of the electron. This leads to the following inequalities:

$$V_{ee} < V_{eh} < V_{hh} \tag{14}$$

and

$$\Delta E_{X_2^+} < 0 < \Delta E_{X^-}. \tag{15}$$

Finally, we obtain the following blue-shift:

$$h\nu_{X^-} < h\nu_X < h\nu_{X_2^+}. \tag{16}$$

The energy shifts calculated with the help of the first-order perturbation theory have been plotted in figure 2 as dashed curves. We see that—in the strong-confinement regime—the qualitative predictions of the perturbational and variational methods agree with each other. We can therefore conclude that the predicted blue-shift of the X_2^+ recombination line with respect to the lines for the neutral exciton and negatively charged exciton is caused by the strong localization of holes in the QD.

Recently, evidence for both the X^- and X_2^+ trions in CuCl QDs has been claimed by Kawazoe and Masumoto [16, 17]. Due to the use of the donor units of energy and length, the present results (figures 1 and 2) can also be applied to these QDs (although in a rather qualitative sense because of the ionic character of these structures). The authors of [16, 17] have argued that they observed the confined excitonic trions in CuCl quantum cubes embedded in a NaCl crystal in a luminescence hole-burning experiment. The interpretation in [16, 17] is based on the application of energy-conservation formulae [16] to the measured recombination-energy shifts [16]. Unfortunately, in the formulae used by the authors of [16], the energies of the confined electron and hole have been omitted in the final states. If we include these energies, which are necessary for the energy conservation, we obtain dramatic changes of the slopes of the Stokes shift versus burning-energy dependence (cf. figure 4 in reference [16]). The accurate slopes are 3.88 and 26.5 times greater than those calculated in reference [16] for lines *A* and *B*, respectively. The correct application of the energy-conservation law leads to a complete disagreement with the experimental data in [16] and to the change of order of the lines attributed to the X_2^+ and X^- trions. In view of the above arguments, the lines in [16, 17] cannot be interpreted as resulting from the excitonic trions, but could be tentatively attributed to the excited-state recombination of neutral excitons or neutral-exciton complexes [36]. Therefore, experimental evidence for trions in these QDs awaits further research.

Finally, we briefly discuss the influence of different material parameters on the present results. The change of the electron and hole confinement potentials fundamentally changes the recombination energies. However, the recombination-energy shifts, calculated as energy differences (7) and (8), change only slightly. The recombination energies of X, X^-, and X_2^+ tend to the same value if dielectric constant ε increases. For equal electron and hole band masses, i.e., for $m_e^* = m_h^*$, the X^- and X_2^+ recombination energies are equal to each other.

In summary, we have calculated for the first time the ground-state and recombination energies for X^- and X_2^+ excitonic trions confined in spherical quantum dots. We have predicted a confinement-induced change of order of the X^- and X_2^+ recombination lines and a strong blue-shift of the X_2^+ recombination line.

Acknowledgments

This work was performed in the framework of the French–Polish scientific cooperation programme POLONIUM and was partially supported by the French Government during the stay of one of us (BS) at the University of Metz.

References

[1] Lampert M A 1958 *Phys. Rev. Lett.* **1** 450
[2] Gerlach B 1974 *Phys. Status Solidi* b **63** 459
[3] Munschy G and Stébé B 1974 *Phys. Status Solidi* b **64** 213
[4] Munschy G and Stébé B 1975 *Phys. Status Solidi* b **72** 135
[5] Stébé B and Munschy G 1975 *Solid State Commun.* **17** 1051
[6] Thomas G A and Rice T M 1977 *Solid State Commun.* **23** 359
[7] Kawabata T, Muro K and Narita S 1977 *Solid State Commun.* **23** 267
[8] Stébé B, Sauder T, Certier M and Comte C 1978 *Solid State Commun.* **26** 637
[9] Ishii T, Taniguchi M, Kakizaki A, Naito K, Sugawara H and Nagakura I 1986 *Phys. Rev.* B **33** 5664
[10] Stébé B, Munschy G, Stauffer L, Dujardin F and Murat J 1997 *Phys. Rev.* B **56** 12 454
[11] Kheng K, Cox R T, Merle d'Aubigné Y, Bassani F, Saminadayar K and Tatarenko S 1993 *Phys. Rev. Lett.* **71** 1752
[12] Buhmann H, Mansouri L, Wang J, Beton P H, Mori N, Eaves L and Henini M 1995 *Phys. Rev.* B **51** 7969
[13] Finkelstein G, Shtrikman H and Bar-Joseph I 1996 *Phys. Rev.* B **53** 12 593
[14] Shields A J, Osborne J L, Whittaker D M, Simmons M Y, Pepper M and Ritchie D A 1997 *Phys. Rev.* B **55** 1318
[15] Warburton R J, Dürr C S, Karrai K, Kotthaus J P, Medeiros-Ribeiro G and Petroff P M 1997 *Phys. Rev. Lett.* **79** 5282
[16] Kawazoe T and Masumoto Y 1996 *Phys. Rev. Lett.* **77** 4942
[17] Kawazoe T and Masumoto Y 1997 *J. Lumin.* **72–74** 862
[18] Lelong P and Bastard G 1996 *Solid State Commun.* **98** 819
[19] Wójs A and Hawrylak P 1995 *Phys. Rev.* B **51** 10 880
[20] Yoffe A D 1993 *Adv. Phys.* **42** 173
[21] Kayanuma Y 1988 *Phys. Rev.* B **38** 9797
[22] Rontani M, Rossi F, Manghi F and Molinari E 1999 *Phys. Rev.* B **59** 10 165
[23] Olshavsky M A, Goldstein A N and Alivisatos A P 1990 *J. Am. Chem. Soc.* **112** 9438
[24] Guzelian A A, Banin U, Kadavanich A V, Peng X and Alivisatos A P 1996 *Appl. Phys. Lett.* **69** 1432
[25] Xie W-F and Chen C-Y 1998 *Solid State Commun.* **107** 439
[26] Banyai L and Koch S W 1993 *Semiconductor Quantum Dots* (Singapore: World Scientific)
[27] Bednarek S, Szafran B and Adamowski J 1999 *Phys. Rev.* B **59** 13 036
[28] Usukura J, Suzuki Y and Varga K 1999 *Phys. Rev.* B **59** 5652
[29] Riva C, Varga K, Schweigert V A and Peeters F M 1998 *Phys. Status Solidi* b **210** 689
[30] Frost A A, Inoukuti M and Lowe J P 1964 *J. Chem. Phys.* **41** 482
[31] Ugajin R, Ishibashi A and Mori Y 1994 *J. Vac. Sci. Technol.* B **12** 3160
[32] Szafran B, Adamowski J and Stébé B 1998 *J. Phys.: Condens. Matter* **10** 7575
[33] Lee H J, Juravel L Y, Wolley J C, and Springthorpe A J 1980 *Phys. Rev.* B **21** 659
[34] Miller R C, Kleinmann D A and Gossard A C 1984 *Phys. Rev.* B **29** 7085
[35] Greene R I, Bajaj K K and Phelps D E 1984 *Phys. Rev.* B **29** 1807
[36] Sakura N and Masumoto Y 1997 *Phys. Rev.* B **56** 4051

Excitonic trions in single and double quantum dots

B. Szafran,[1,2,*] B. Stébé,[1] J. Adamowski,[2] and S. Bednarek[2]
[1]*Université de Metz, Institut de Physique et d'Electronique, 1 Boulevard Arago, 57070 Metz Cedex 6, France*
[2]*Faculty of Physics and Nuclear Techniques, University of Mining and Metallurgy (AGH), Kraków, Poland*
(Received 5 June 2002; revised manuscript received 30 August 2002; published 31 October 2002)

Excitonic trions in quantum dots with Gaussian confinement potential are studied by the variational method. We show that the photoluminescence line associated with the negative trion is always shifted towards lower energies with respect to the exciton line, and that this shift is larger for smaller dots. The qualitative behavior of the photoluminescence line of the positive trion is the same only in dots which resemble quantum wells or quantum wires. In other dots the size dependence of the positive-trion shift is more complex. In particular, we show that the order of the positive-trion line and the exciton line can be changed. The present approach has been generalized to the trion states in vertically coupled dots. We discuss the trion energy-level splitting induced by the coupling between the dots, as well as the relation between the photoluminescence-line shift with the binding energy of the trion in the double quantum dots.

DOI: 10.1103/PhysRevB.66.165331 PACS number(s): 78.67.Hc

I. INTRODUCTION

The excitonic trions are charged exciton complexes composed of either two holes and one electron (positive trion X_2^+) or two electrons and one hole (negative trion X^-). These complexes have been a subject of an extensive theoretical[1–17] and experimental study.[18–24] In bulk semiconductors the excitonic trions are stable against dissociation into an exciton and a free carrier. However, their binding energies in bulk materials are very small. The confinement of the trions in two-dimensional quantum wells increases these binding energies by an order of magnitude.[2] The enhancement of the trion binding energy in quantum wells allows for experimental observation[18] of this complex. The excitonic trions confined in quantum dots (QD's) are observed in charge-tunable nanostructures.[23,24]

The first observations of QD-confined charged excitons were performed on ensembles of QD's.[23] The results of these experiments were perturbed by the inhomogenous broadening caused by the variation of the sizes of the dots. Recently, measurements of the photoluminescence (PL) spectra of charged excitons from a single self-assembled QD were reported.[24] This technique, which allows for selection of a single dot as a signal source, may be used in order to determine the dependence of the trion PL lines on the size and geometry of the dots. A theoretical study of this dependence will be useful in the interpretation of the experimental data. The aim of the present paper is to furnish this study. The present work is also motivated by the measurements of the exciton spectra in coupled self-assembled QD's.[25] The present results for the splitting of the trion-energy levels induced by the coupling between the dots should be useful for identification of the trion-related lines in the PL spectra of coupled dots. The present paper is a continuation of our previous research on neutral[26] and charged[15] excitons. In Ref. 15 we studied the exciton trions in spherical quantum dots with square-well confinement potential. Here, we generalize this study to more realistic cylindrical symmetry. In Ref. 26 we studied the neutral-exciton spectra in vertically coupled QD's. The present paper extends the previous work[26] to the problem of charged excitons.

The exciton PL peak, as well as peaks corresponding to exciton complexes are blueshifted (i.e., shifted towards higher energies) by the confinement in quantum wells, wires, and dots.[27] Here, we present a theoretical study of the excitonic trions confined in single and double QD's. In particular, we are interested in the confinement-induced shift of the excitonic trion PL line with respect to the exciton line. This shift is a basic quantity of experimental interest for the excitonic trions. The excitonic trion PL line is shifted with respect to the exciton PL line by[15]

$$S_{X_2^+} = h\nu_X - h\nu_{X_2^+} = E_X + E_h - E_{X_2^+} \tag{1}$$

for the positive trion and by

$$S_{X^-} = h\nu_X - h\nu_{X^-} = E_X + E_e - E_{X^-} \tag{2}$$

for the negative trion. If $S>0$, the energy of the trion PL line is smaller than the energy of the exciton line. Then, we speak about the redshift of the trion PL line with respect to the exciton line. If the energy difference is negative ($S<0$), the trion line is blueshifted with respect to the exciton line. We will shortly refer to energy differences (1) and (2) as the positive-trion energy shift $S_{X_2^+}$ and the negative-trion energy shift S_{X^-}. In bulk materials, quantum wells and quantum wires, energy shifts (1) and (2) can be identified with the binding energy of the trions. However, it is not the case for QD's[15] (cf. a discussion of the binding energy of D^- center in the QD[28]).

This paper is organized as follows. In Sec. II we present the model of the single QD, introduce the variational wave functions for the exciton and excitonic trions, and discuss the influence of the shape and geometry of the QD on the trion PL line shifts. In Sec. III we generalize the approach of Sec. II to the trions in double QD's. Section IV contains conclusions and the summary.

II. EXCITONIC TRIONS IN A SINGLE QUANTUM DOT

A. Confinement potential and variational wave functions

In the present paper we adopt the Gaussian model of the confinement potential,[29] which was successfully applied[26] to a quantitative interpretation of the exciton spectra[25] in $In_xGa_{1-x}As$ self-assembled QD's. The confinement potential in $In_xGa_{1-x}As$ QD's embedded in the GaAs matrix can be derived from spatial distribution of indium concentration within the QD's.[30] We assume that this distribution can be described by a cylindrically symmetric Gaussian function[26]

$$X(\rho,z;R,Z)=X_0\exp(-\rho^2/R^2-z^2/Z^2), \tag{3}$$

where $\rho^2=x^2+y^2$, R is the radius of the QD, Z is half of its height, and X_0 is the concentration of indium at the center of the QD. In accordance with Eq. (3), we take the confinement potential for electrons

$$V_e(\rho,z;R,Z)=-0.7\Delta E_g X(\rho,z;R,Z) \tag{4}$$

and for holes

$$V_h(\rho,z;R,Z)=-0.3\Delta E_g X(\rho,z;R,Z), \tag{5}$$

where ΔE_g is the energy-gap difference between GaAs and InAs. We assume that the band offset ratio is 70/30.[31] Throughout the paper, we take the conduction-band minimum of the barrier material as the reference energy level for the electrons and the barrier valence-band maximum as the reference energy level for the holes. The calculations have been performed for $\Delta E_g=1.11$ eV[26] and the material parameters of GaAs, i.e., the static dielectric constant $\varepsilon=12.5$, the band mass of the electron $m_e=0.0667$, and the band mass of the hole $m_h=0.5$.

In order to determine the trion-energy shifts we need to know the trion ground-state energy, as well as the ground-state energies of the exciton, electron, and hole confined in the QD. For this purpose we use the confinement potentials (4) and (5) and assume the effective-mass approximation for electrons and holes. The ground-state energy of a single electron and a single hole confined in a QD with radius R and height $2Z$ is determined by the variational method with a Gaussian trial-wave-function

$$\phi_{e(h)}(\mathbf{r}_{e(h)};R,Z)=\sum_{i=1}^{N_{e(h)}}\sum_{j=1}^{M_{e(h)}} c_{ij}\exp(-\alpha_i^{e(h)}\rho^2-\beta_j^{e(h)}z^2), \tag{6}$$

where c_{ij} are the linear variational parameters, $\alpha_i^{e(h)}$ and $\beta_j^{e(h)}$ are the nonlinear variational parameters, which describe the localization of the particles radial and vertical directions, respectively. In this paper, we take $M_h=1$, $N_h=2$, $M_e=2$, and $N_e=4$, which ensures that the one-particle energies are determined with a precision of 0.1 meV.

The Hamiltonian of the exciton confined in the QD has the form

TABLE I. Ground-state energy E_X (in meV) of the exciton confined in the single QD calculated with wave function (8) with $M_e=2$, $N_e=4$, and $N_h=2$ quoted for several numbers of exponents describing the relative electron-hole position in x-y plane M_{eh} and in z direction N_{eh}. The parameters of the QD are $X_0=0.67$, $R=24.9$ nm, and $Z=0.92$ nm. The total number of basis elements ($N=M_e\times N_e\times N_h\times M_{eh}\times N_{eh}$) is listed in the third column.

M_{eh}	N_{eh}	N	E_X
1	1	16	−261.47
2	1	32	−262.19
2	2	64	−262.20
3	2	98	−262.23
3	3	144	−262.25

$$H_X=-\frac{\hbar^2}{2m_e}\nabla_e^2-\frac{\hbar^2}{2m_h}\nabla_h^2-\frac{1}{4\pi\varepsilon_0\varepsilon r_{eh}}+V_e(\rho_e,z_e;R,Z)+V_h(\rho_h,z_h;R,Z), \tag{7}$$

where $r_{eh}=|\mathbf{r}_e-\mathbf{r}_h|$. The ground-state energy of the exciton confined in the QD can be determined with the following variational wave function

$$\Psi_X^{(1)}(\mathbf{r}_e,\mathbf{r}_h)=\sum_{i_e=1}^{M_e}\sum_{j_e=1}^{N_e}\sum_{j_h=1}^{N_h}\sum_{i_{eh}=1}^{M_{eh}}\sum_{j_{eh}=1}^{N_{eh}} c_{i_e j_e j_h i_{eh} j_{eh}}\times\exp(-\alpha_{i_e}^e\rho_e^2-\beta_{j_e}^e z_e^2-\alpha^h\rho_h^2-\beta_{j_h}^h z_h^2-\alpha_{i_{eh}}^{eh}\rho_{eh}^2-\beta_{j_{eh}}^{eh}z_{eh}^2), \tag{8}$$

where $\rho_{eh}^2=(x_e-x_h)^2+(y_e-y_h)^2$, $z_{eh}=z_e-z_h$, $\alpha_{i_{eh}}^{eh}$ and $\beta_{j_{eh}}^{eh}$ are the variational parameters, which describe the relative position of the electron and the hole in x-y plane and z direction, respectively. The other variational parameters in Eq. (8) play the same role as in wave function (6). The convergence of variational basis (8) with respect to the number of the Gaussians applied was verified for the values[26] of parameters corresponding to $In_xGa_{1-x}As$ self-assembled QD's,[25] i.e., $X_0=0.67$, $R=24.9$ nm, $Z=0.92$ nm. The variational estimates of the exciton ground-state energy obtained with various numbers of terms in Eq. (8) are listed in Table I. We note, that the convergence of these estimates is very fast. The results are not significantly improved if one introduces a second β^{eh} exponent or a third α^{eh} parameter. The electron and hole wave functions are stiffened in z direction due to the strong confinement and react only weakly to the mutual Coulomb interaction. The change of the one-particle wave functions under the influence of the interaction is more pronounced in x-y plane, where the confinement is weaker. In this paper we consider not only the QD's in form of flat disks, but also QD's of different shape and size. Therefore, we have taken $M_{eh}=N_{eh}=3$ in the following calculations.

The results of Table I show, that variational wave function (8) is an effective tool in the calculations for the confined exciton ground state. However, this wave function is not suitable for a direct generalization to the problem of trions, since the number of basis elements grows very fast with the num-

TABLE II. Ground-state energy E_X (in meV) of the exciton confined in the single QD calculated with trial function (9). The parameters of the QD are the same as in Table I. In the first two columns, the number of elements taken in sum (9) is listed. In the third column, the energy E_X' calculated with the fixed variational parameters $R_{e(h)}=R$ and $Z_{e(h)}=Z$ is quoted. The number of basis elements is equal to $M_{eh}\times N_{eh}$. The results in the fourth column are obtained with optimized parameters $R_{e(h)}$ and $Z_{e(h)}$.

M_{eh}	N_{eh}	E_X'	E_X
1	1	−261.17	−261.34
1	2	−261.17	−261.36
2	1	−261.93	−262.19
3	1	−262.03	−262.22

ber of particles. Therefore, we have elaborated another approach to the problem of the QD-confined trions, which we will first demonstrate on the example of the confined electron-hole pair. The dependence of the wave function on the relative interparticle positions will be referred to as the ''correlation between the particles.'' In wave function (8), this correlation is directly described by the exponents with α^{eh} and β^{eh}. However, even if the parameters α^{eh} and β^{eh} are set equal to zero, wave function (8) cannot be separated into a product of one-particle functions. Therefore, even without α^{eh} and β^{eh} exponents, a part of correlation is indirectly included in wave function (8). Now, we introduce another trial wave function for the QD-confined exciton, which takes into account the correlation between the particles in the direct way only,

$$\Psi_X^{(2)}(\mathbf{r}_e,\mathbf{r}_h)=\phi_e(\mathbf{r}_e;R_e,Z_e)\,\phi_h(\mathbf{r}_h;R_h,Z_h)\times\sum_{i_{eh}=1}^{M_{eh}}\sum_{j_{eh}=1}^{N_{eh}} c_{i_{eh}j_{eh}}\exp(-\alpha_{i_{eh}}^{eh}\rho_{eh}^2-\beta_{j_{eh}}^{eh}z_{eh}^2). \tag{9}$$

Trial wave function (9) is applied to the exciton confined in the QD with radius R and height $2Z$. It is composed of the ground-state wave functions of the electron (ϕ_e) confined in potential (4) with effective parameters R_e and Z_e and the hole (ϕ_h) confined in potential (5) with effective parameters R_h and Z_h. The double sum in Eq. (9) describes the electron-hole correlation. The parameters R_e, Z_e, R_h, and Z_h are treated as variational parameters. In this way, the one-particle wave functions ϕ_e and ϕ_h are allowed to change their spatial extension under influence of the Coulomb interaction between the particles.

The results obtained with wave function (9) are listed in Table II, which shows that the energy estimates obtained with the values of the variational parameters $R_{e(h)}$, $Z_{e(h)}$ fixed at the physical values of the QD size $R_{e(h)}=R$ and $Z_{e(h)}=Z$ converge to a value, which is larger by 0.2 meV than the energy obtained with basis (8) (cf. Table I). However, if we perform the optimization with respect to $R_{e(h)}$ and $Z_{e(h)}$, we obtain results equivalent to those obtained with wave function (8). Although wave function (9) does not require less numerical effort than function (8), the number of basis elements is much smaller and less memory consuming, so, it can be easily generalized to the problem of excitonic trions.

The Hamiltonian for the negatively charged trion X^- confined in a QD has the form

$$H_{X^-}=-\frac{\hbar^2}{2m_e}\nabla_1^2-\frac{\hbar^2}{2m_e}\nabla_2^2-\frac{\hbar^2}{2m_h}\nabla_h^2+\frac{1}{4\pi\varepsilon_0\varepsilon}\left(-\frac{1}{r_{1h}}-\frac{1}{r_{2h}}+\frac{1}{r_{12}}\right)+V_e(\mathbf{r}_1;R,Z)+V_e(\mathbf{r}_2;R,Z)+V_h(\mathbf{r}_h;R,Z), \tag{10}$$

where $\mathbf{r}_1$ and $\mathbf{r}_2$ are the position vectors of the electrons, $\mathbf{r}_h$ determines the position of the hole, $r_{12}=|\mathbf{r}_1-\mathbf{r}_2|$, $r_{1h}=|\mathbf{r}_1-\mathbf{r}_h|$, and $r_{2h}=|\mathbf{r}_2-\mathbf{r}_h|$. The Hamiltonian for the positive trion X_2^+ can be obtained from Eq. (10) by interchanging the indices $e\leftrightarrow h$ and ascribing the indices 1 and 2 to the holes.

In the negative-(positive) trion ground state, the electron (hole) subsystem is a spin singlet. This means that the ground-state spatial wave function of the negative (positive) trion is symmetric with respect to the interchange of the position vectors of the electrons (holes). Therefore, we apply the following trial wave function for the negative trion

$$\Psi_{X^-}(\mathbf{r}_1,\mathbf{r}_2,\mathbf{r}_h)=\phi_e(\mathbf{r}_1;R_e,Z_e)\,\phi_e(\mathbf{r}_2;R_e,Z_e)\,\phi_h(\mathbf{r}_h;R_h,Z_h)\times\sum_{i_1i_2i_{12}}\sum_{j_1j_2j_{12}} c_{i_1i_2i_{12}j_1j_2j_{12}}(1+P_{12})\times\exp(-\alpha_{i_1}^{eh}\rho_{1h}^2-\alpha_{i_2}^{eh}\rho_{2h}^2-\alpha_{i_{12}}^{ee}\rho_{12}^2)\times\exp(-\beta_{j_1}^{eh}z_{1h}^2-\beta_{j_2}^{eh}z_{2h}^2-\beta_{j_{12}}^{ee}z_{12}^2). \tag{11}$$

The presence of the sum in wave function (11) introduces the correlation for the three particles. In Eq. (11), the summations start from 1 and run to M_{eh} over indices i_{1h} and i_{2h}, to N_{eh} over j_{1h} and j_{2h}, and to M_{12} and N_{12} over i_{12} and j_{12}. P_{12} is the operator which exchanges the coordinates of the two electrons. The factor $(1+P_{12})$ ensures, that the electron subsystem is in the symmetric spatial state and enables us to reduce the number of the basis elements. Namely all the basis elements, for which $j_1=j_2$ and $i_2>i_1$ are omitted in the summation (11). R_e, Z_e, R_h, and Z_h are treated as variational parameters like in wave function (9) for the exciton. For the positive trion we apply an analogous trial wave function. Similarly as in the case of the exciton confined in the flat QD, a single Gaussian is sufficient for the description of the correlations in z direction. The convergence of the variational results with the increasing number of Gaussians describing the in-plane correlation is displayed in Table III. In the following section we discuss the influence of the size and shape of the dot on the relative shifts of trion PL peaks. This discussion goes beyond the flat QD geometry, so the correlation in z direction should be described with the same precision as the in-plane correlation. The results presented in the following section have been obtained with 90-element basis

TABLE III. Ground-state energy E_{X^-} (in meV) of the negative excitonic trion calculated with trial wave function (11). The first column shows the number of Gaussians taken for the description of the electron-hole correlation in x-y plane. The number of Gaussians describing the electron-electron in-plane correlation is listed in the second column. In these calculations, a single Gaussian describing the correlation in z direction was applied. The third column shows the total number of basis elements. The parameters of the QD are the same as in Table I.

M_{eh}	M_{12}	N	E_X^-
1	1	1	−396.45
2	1	3	−397.91
2	2	6	−398.48
2	3	9	−398.59
3	3	12	−398.70
4	4	40	−398.71

generated by $M_{eh}=N_{eh}=2$ and $M_{12}=N_{12}=3$. We estimate that the trion ground-state energies are determined with precision of 0.2–0.3 meV.

B. Results

Figure 1 displays the energy shifts of the PL lines for the trions confined in a spherically symmetric ($R=Z$) QD with respect to the line of confined exciton. In bulk GaAs, the trion PL peaks are only slightly shifted with respect to the exciton PL line ($S_{X_2^+}\approx 0.4$ meV and $S_{X^-}\approx 0.25$ meV[4,15]). In large QD's (with radius R larger than ~ 100 nm), the shift of the positive-trion line is not significantly changed with respect to the bulk-limit value. If the radius of the dot decreases below 80 nm, X_2^+ PL line approaches the exciton line, i.e., $S_{X_2^+}$ decreases to 0. For $R\simeq 40$ nm the recombination of the electron-hole pair in the positive trion releases the same amount of energy as the exciton recombination. For $R<40$ nm $S_{X_2^+}$ takes on negative values; so, the order of the exciton and X_2^+ PL lines changes. The behavior of the negative-trion line is just opposite. The quantum confinement shifts X^- line deep below the exciton line on the energy scale. The opposite behavior of the positive- and negative-trion energy shifts was reported in our previous paper[15] on spherical quantum dots with the square-well confinement potential. In the strong confinement limit this effect can be explained in the framework of the perturbation theory. In this approach,[15] the trion-energy shifts are expressed in terms of the energies of the Coulomb interaction between the particles forming the trion complexes, as follows: $S_{X_2^+}=V_{eh}-V_{hh}$, and $S_{X^-}=V_{eh}-V_{ee}$, where V_{eh}, V_{ee}, and V_{hh} are the electron-hole, electron-electron, and hole-hole interaction energies, respectively. The quantum confinement in the QD's leads to the localization of the charge carriers, which is much stronger for the holes. Therefore, the absolute value of the Coulomb interaction energy between the holes increases more than the electron-hole and electron-electron interaction energies, i.e., $V_{hh}>V_{eh}>V_{ee}$, which explains the qualitative difference in the confinement-induced changes of X^- and X_2^+ energy lines in spherical QD's ($S_{X_2^+}<0<S_{X^-}$). The results of the present calculations show, that the same effect occurs also for spherical quantum dots with the Gaussian potential profile.

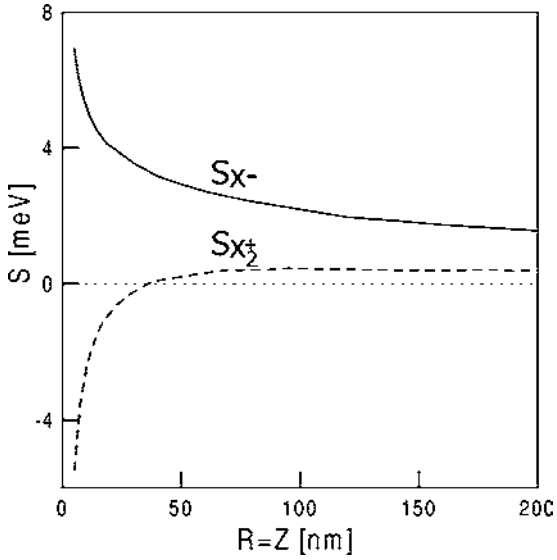

FIG. 1. Energy shifts S of the trion PL line with respect to the exciton PL line calculated for the spherical QD as a function of radius $R=Z$ for $X_0=0.67$. The solid (dashed) curve corresponds to the negative-(positive-) trion-energy shift ($S_{X^-}=E_X+E_e-E_{X^-}$ and $S_{X_2^+}=E_X+E_h-E_{X_2^+}$).

The problem is more complex if the QD is anisotropic. Then, the strength and range of the confinement potential in x-y plane and the growth direction are different. We have performed the calculations of the trion-energy shifts for different values of R and Z. Figure 2 shows the calculated trion-energy shifts as functions of Z (half of the QD height) for several values of the QD radius R. We have considered QD's with very different height-to-radius ratios. The left (right) end of horizontal axis of Fig. 2 corresponds to the QD in a form of a flat disk (elongated cylinder). Each of the curves in Fig. 2 passes through the point, for which the QD has spherical symmetry. These points are marked by circles. The curves for the negative-trion exhibit the following simple regularity: the smaller is the QD, the stronger is the redshift of X^- PL line with respect to the exciton line. The dependence of the positive-trion energy shift is more complex. In QD's of large height, the movement of the confined charge carriers in z direction is nearly free. We can say that these QD's resemble the quantum wires. We note, that the PL peaks of both the negative and the positive trions are redshifted with respect to the exciton PL line if the radius of the ''wire-like'' dot decreases. For $R=100$ nm, the positive-trion line is monotonously redshifted with the decreasing height of the QD. This dependence on the height is qualitatively the same as in the case of the two-dimensional quantum wells, in which both the positive- and negative-trion PL peaks are redshifted with respect to the exciton peak, if the width of the quantum well decreases.[16] In contrast to $S_{X_2^+}$ shift for $R=100$ nm, the curve for $R=50$ nm is nonmonotonous. When Z decreases below 120 nm the X_2^+ PL line ap-

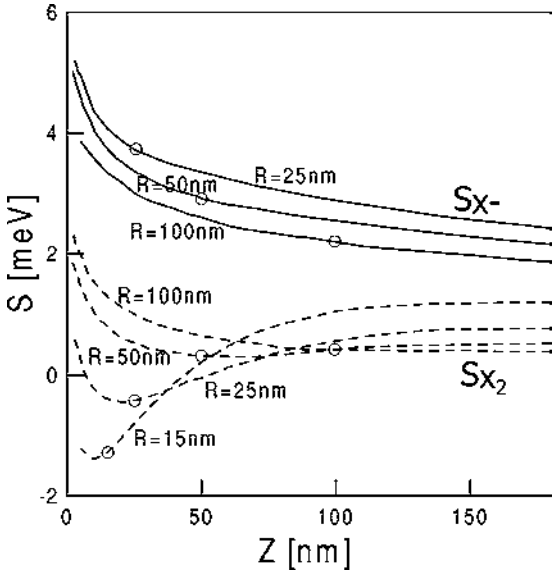

FIG. 2. Trion-energy shifts S with respect to the exciton PL line calculated as a function of Z (half of the QD height) for several values of the QD radius R. The solid curves show the results for the negative trion, and the dashed curves show the results for the positive trion. Open circles correspond to spherical symmetry of QD's.

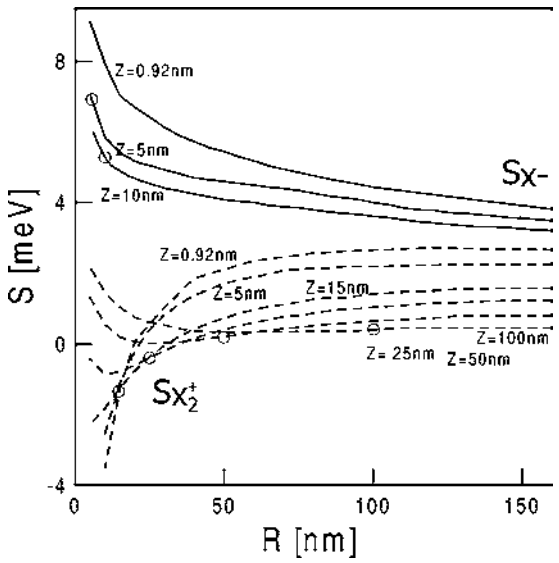

FIG. 3. Trion-energy shifts S calculated with respect to the exciton PL line as a function of radius R of the QD for several values of Z (half of the QD height). The solid (dashed) curves correspond to the negative (positive) trion. Open circles correspond to spherical QD's.

proaches the exciton PL peak. The curve for $R=50$ nm exhibits a flat minimum for Z between 50 and 80 nm. The minima of the curves for $R=25$ and 15 nm are distinctly more pronounced and appear at $Z=20$ and $Z=10$ nm, respectively. We note, that these minima correspond to quantum dots with nearly spherical shapes. The PL line of the positive-trion confined in the QD with radius $R=50$ nm has smaller energy than the exciton line regardless of Z. In other words, $S_{X_2^+}$ is always positive for $R=50$ nm. This is not the case of QD's with smaller radii, for which the value of the shift can be negative. The PL peak of the positive-trion confined in the dots with radius 25 or 10 nm can be blue shifted or redshifted with respect to the exciton line depending on the height of the QD.

Figure 3 shows the shifts of the trion PL lines with respect to the exciton line as functions of the radius of the dot for fixed values of its height. The points for which the QD potential is spherically symmetric are marked by circles. Again, the negative trion is redshifted more strongly for smaller QD's, while the dependence of the positive-trion shift is more complex. In Fig. 3, the QD with the radius $R \sim 150$ nm can be treated as a quasi-two-dimensional quantum well. In this QD, the redshift of the PL lines is largest for the lowest value of the height of the well. On the other hand, the QD with the largest value of the height ($Z=100$ nm) looks like a quantum wire and the redshift of the PL lines grows, when the radius of this ''wire-like'' QD decreases. The curve for $Z=50$ nm shows a flat minimum at $R=30$ nm. This minimum is more pronounced for QD's with smaller height. We note, that the minima of $S_{X_2^+}$ can correspond to negative values of the shift.

C. Conclusions

In this section, we have studied the dependence of the energy shifts of the trion PL peaks with respect to the exciton peak on the size and geometry of the QD's. The obtained results indicate, that the negative-trion PL peak is always redshifted with respect to the exciton line. The stronger is the confinement (the smaller is the QD) the larger is this redshift. The positive-trion line behaves qualitatively in the same manner only in the cases, where the QD geometry resembles a quantum well or a quantum wire. For the ''well-like'' QD's the redshift of X_2^+ PL line is larger for the small height of the quantum well, while for the ''wire-like'' QD's the redshift is more pronounced for the small radius of the ''wire.'' For the QD's with the diameter $2R$ comparable to the height $2Z$, the size dependence of the positive-trion energy shift is more complex. This energy shift plotted as a function of the radius or the height of the QD exhibits minima near $R/Z=1$, i.e., close to the QD's with the spherical symmetry. If the values of R or Z are of order of 25 nm or smaller, these minima correspond to negative values of the energy shift. Then, the order of exciton and positive-trion PL lines is opposite that in the bulk limit. The results presented in this section are in a qualitative agreement with the present knowledge on the trions in quantum wells,[4,16] and with the previous study of the trions in spherically symmetric QD's.[15] Moreover, based on the present results for the ''wire-like'' QD's, we can predict that the PL lines for both the negative and the positive trions in quantum wires should be redshifted with respect to the exciton line if the quantum-wire radius is decreased.

III. EXCITONIC TRIONS IN VERTICALLY COUPLED QUANTUM DOTS

A. Theory

The energy shifts S_{X^-} and $S_{X_2^+}$ for the trions confined in a single quantum dot cannot be identified with the trion binding energy.[15] However, if the QD is not single, i.e., if there is another identical QD at a distance large enough to exclude the coupling between the dots, the trion-energy shifts are exactly equal to the energy needed to transfer one electron (for X^-) or one hole (for X_2^+) from the QD occupied by the three charge carriers to the other empty QD. Let us assume, that the charge carriers have at their disposal two identical, remote QD's. Since in a single QD S_{X^-} is always positive, the ground state of a system composed of two electrons and one hole will always correspond to a state, in which all the particles are confined within the same QD (this is the confined-trion state). However, this is not the case for X_2^+ trion. For QD's in which the energy shift $S_{X_2^+}$ is negative, the ground-state corresponds to the electron-hole pair confined in one dot (confined exciton) and one hole confined in the other QD. If the QD's are closer, the coupling between them can essentially change the energies of the exciton complexes and the type of the localization of particles.[26] The coupling between vertically stacked $In_xGa_{1-x}As$ self-assembled QD's was observed in the PL spectroscopy[25] in the shifts of the PL peaks as functions of the thickness of the interdot barrier.

In this section we study the effect of the vertical coupling between the QD's on the trion states. We assume that the coupled dots have identical shapes and sizes, and possess a common axis of the rotational symmetry. We apply the following confinement potentials for the electrons and the holes:

$$V^c_{e(h)}(\rho_{e(h)},z_{e(h)}) = V_{e(h)}(\rho_{e(h)},z_{e(h)}-a/2;R,Z) + V_{e(h)}(\rho_{e(h)},z_{e(h)}+a/2;R,Z), \tag{12}$$

where V_e and V_h are the given by Eqs. (4) and (5), respectively, and a is the distance between the centers of the QD's. The thickness of the barrier between the QD's can be expressed in terms of the distance between the QD centers and the height of the QD as follows: $t=a-2Z$. We adopt the values of the QD parameters corresponding to $In_xGa_{1-x}As$ self-assembled QD's: $X_0=0.67$, $R=24.9$ nm, $Z=0.92$ nm (same as in the test calculations of Sec. II). The ground-state wave function of a single-particle confined in potential (12) possesses an even parity with respect to the change of sign of z coordinate. We calculate the one-particle ground-state energy using the wave function

$$\phi^c_{e(h)}(\rho_{e(h)},z_{e(h)}) = \phi_{e(h)}(\rho_{e(h)},z_{e(h)}-a/2;R,Z) + \phi_{e(h)}(\rho_{e(h)},z_{e(h)}+a/2;R,Z), \tag{13}$$

where $\phi_{e(h)}$ is wave function (6) of the ground state of the electron (hole) confined in the single isolated QD. Wave function (13) is a good approximation of the exact ground-state wave function for the studied range of the barrier thickness between the dots, i.e., for $t=a-2Z>2$ nm. The ground-state energy of the electron-hole pair in the coupled dots is determined variationally with the following trial wave function:

$$\Psi^c_X(\mathbf{r}_e,\mathbf{r}_h) = \sum_{k_e,k_h=0}^{1}\sum_{i_{eh}=1}^{M_{eh}} c_{i_{eh}k_ek_h}\phi_e [\rho_e,z_e+(-1)^{k_e}(a/2);R_e,Z_e]\phi_h [\rho_h,z_h+(-1)^{k_h}(a/2);R_h,Z_h] \times \exp(-\alpha^{eh}_{i_{eh}}\rho^2_{eh}-\beta^{eh}z^2_{eh}), \tag{14}$$

where $c_{i_{eh}k_ek_h}$ are the linear and $R_e,Z_e,R_h,Z_h,\alpha^{eh}_{i_{eh}},\beta^{eh}$ are the nonlinear variational parameters. This function is a direct generalization of trial wave function (9) for the exciton confined in an isolated QD with $N_{eh}=1$. In Eq. (14) the summations over k_e and k_h take into account all the possible distributions of the charge carriers over the two QD's. The z direction correlation between the particles confined in the same self-assembled QD is weak (cf. Tables I–II); so we neglect it almost totally in wave function (14). The interdot correlations are introduced via the two-center localization of the products of the one-particle functions $\phi_{e(h)}$.

We have calculated the lowest-energy levels of the negative-(positive) trion assuming that the electron (hole) subsystem is the spin singlet. For the negative trion we use the following wave function:

$$\Psi^c_{X^-}(\mathbf{r}_1,\mathbf{r}_2,\mathbf{r}_h) = \sum_{k_1k_2k_h}\sum_{i_1i_2i_{12}} c_{i_1i_2i_{12}k_1k_2k_h}(1+P_{12})\phi_h [\rho_h,z_h+(-1)^{k_h}(a/2);R_h,Z_h] \phi_e[\rho_1,z_1+(-1)^{k_1}(a/2);R_e,Z_e]\phi_e [\rho_2,z_2+(-1)^{k_2}(a/2);R_e,Z_e] \times \exp(-\alpha^{eh}_{i_1}\rho^2_{1h}-\alpha^{eh}_{i_2}\rho^2_{2h}) \times \exp(-\alpha^{ee}_{i_{12}}\rho^2_{12}-\beta^{eh}z^2_{1h}-\beta^{eh}z^2_{2h}), \tag{15}$$

where the summations over k_1 and k_h run from 0 to 1, over k_2 from 0 to k_1, over i_{12} from 1 to M_{ee}, and over i_1 and i_2 from 1 to M_{eh}. The terms with $k_1=k_2$ and $i_2>i_1$ are excluded from the sum, because of the symmetrization of the basis elements $(1+P_{12})$. Basis (15) takes into account all the possible distributions of the three particles between the two QD's. In the calculations, we take $M_{ee}=3$ and $M_{eh}=2$, like in the case of the trion in the single QD. In consequence, basis (15) consists of 60 elements. The trial wave function for the positive trion has been chosen in the same way.

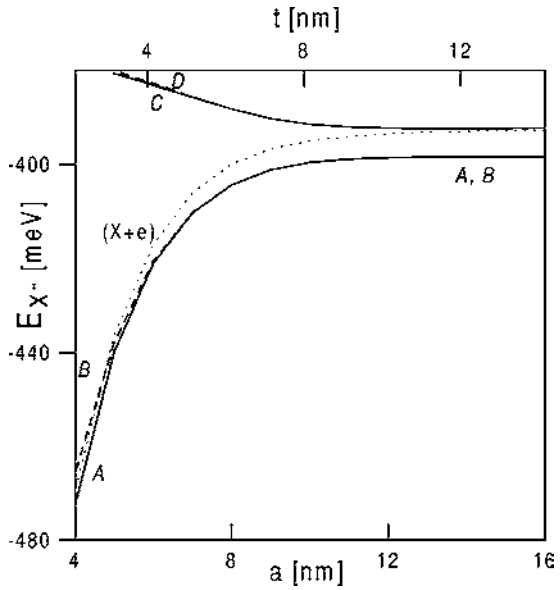

FIG. 4. Lowest-energy levels of the negative excitonic trion in the double QD as functions of the distance a between the centers of the QD's (thickness t of the barrier between the QD's). Solid (dashed) lines correspond to the energy levels of the even-(odd-) parity states. Thin dotted $(X+e)$ line shows the sum of the ground-state energies of the exciton and the single-electron confined in the double QD. The meaning of symbols $A,B,C,$ and D is explained in the text.

B. Results

Figure 4 shows the four lowest-energy levels for X^- states, in which the electron subsystem is the spin singlet. The corresponding barrier thickness t is marked on the upper horizontal axis. Since the confinement potential of the coupled QD's (12) is invariant with respect to the reflection through $z=0$ plane, the wave functions of the three-particle complex possess a definite (even- or odd-) parity symmetry with respect to the operation of a simultaneous change of signs of z coordinates for all the particles. The parity properties of considered states result from the symmetries of the calculated three-particle wave functions, cf. the detailed discussion of the parity symmetry for the electron-hole pair in vertically coupled self-assembled QD's given in Ref. 26. The wave functions associated with the energy levels A and C (solid lines) possess even parity, while the energy levels B and D (dashed lines) correspond to the wave functions with odd parity. For $a>$ 14 nm all the energy levels are independent of the interdot distance. Then, the QD's can be treated as separate (uncoupled). In this limit, the distribution of the charge carriers between the QD's is a definite property of all the eigenstates, i.e., in all the eigenstates, the charge carriers occupy with a 100% probability either the same QD or different QD's.[26] At large interdot distance, the degenerate states A and B correspond to the trion localized in one of the QD's. In these states all the charge carriers are confined within the same QD. The energy of these states is equal to the energy of the negative-trion confined in the single isolated QD (cf. Table III). The ground state is twofold degenerate, because the trion can be located in one of the two QD's.

For $a<14$ nm both the degenerate A and B energy levels start to decrease, which is a signature of the tunnel coupling between the QD's. The presence of the tunnel coupling means, that in states A and B there is a nonvanishing probability of finding one of the particles in the other QD than the remaining two charge carriers. However, the tendency of all the particles to occupy the same QD is still visible in these states.[26] The degeneracy of the energy levels A and B is lifted for $a<6$ nm. For $a=4$ nm ($t\approx 2$ nm) the QD's are strongly coupled. In the strong coupling limit the trion wave functions exhibit an approximate one-particle parity, i.e., parity with respect to the change of the sign of z coordinate of each of the particles separately.[26] Due to the difference of the electron and hole masses, the effective height of the barrier between the dots is much larger for the hole than for the electron. In consequence, the even-odd energy-level splitting for the electron is considerably larger than the splitting for the hole. Both A and B states correspond to an approximate even parity of both the electrons. Moreover in state A, the hole is in the even-parity state, whereas in state B, the hole is in the state with an approximate odd parity. In both the excited states C and D, one of the electrons is in the even-parity state and the other is in the odd-parity state. The corresponding C and D energy levels split for $a<6$ nm. Similarly as states A and B, states C and D differ by the parity of the hole, which is even in C state and odd in D state. In the limit of the separate QD's, C and D states have the same energy and correspond to the electron-hole pair confined in one of QD's, while the second electron is confined in the other QD.

The thin dotted line marked by $(X+e)$ in Fig. 4, shows the sum of the ground-state energies of the following two systems: the electron-hole pair and a single electron in the double QD structure. In the limit of large a, this sum coincides with the degenerate C and D energy levels. The difference between the sum of energies $(X+e)$ and the ground-state energy of the trion is equal to the shift of X^- PL peak with respect to the exciton line, i.e., to S_{X^-}. In the limit of separate QD's, the energy shift S_{X^-} becomes identical with the difference of the energies between the trion ground state (A,B energy levels) and the excited state (C,D energy levels). Then, this difference can be interpreted as the binding energy of the trion in the double QD structure, i.e., as the amount of energy needed to remove one of the electrons from the QD occupied by the trion and transfer it to the other QD. On the other hand, in the strong coupling limit, the double QD can be treated as a single QD with enlarged height (larger vertical extension). The trion energy shift S_{X^-} decreases with the decreasing distance between the QD's. This effect is consistent with the results of the preceding section, which show that the negative-trion energy shift is larger for smaller QD's.

The results for the lowest-energy states of X_2^+ trion are displayed in Fig. 5. We restrict our study to the singlet states of the hole subsystem. The energy levels corresponding to the states with even (odd) total parity are plotted by the solid (dashed) lines. In the limit of separate dots (large a), the ground state is twofold degenerate (cf. degenerate energy-levels marked by A and B). In the ground-state all the three particles occupy the same QD, while the other dot is empty.

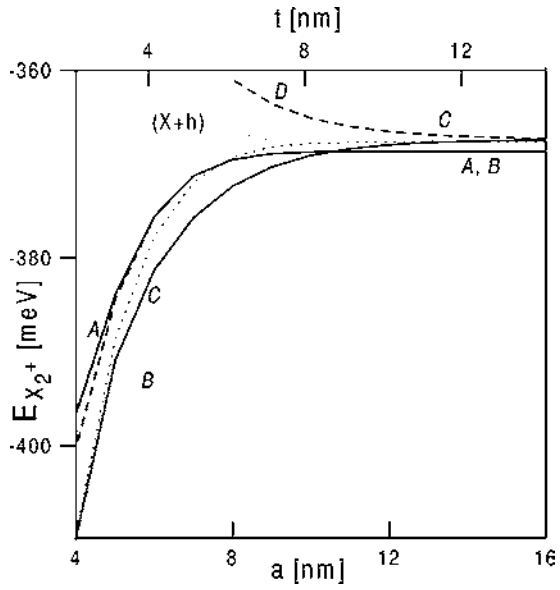

FIG. 5. Lowest-energy levels of the positive excitonic trion in the double QD as functions of the distance a between the centers of the QD's. Solid (dashed) lines present the energy levels of the states with the even (odd) parity. Thin dotted $(X+h)$ line shows the sum of the ground-state energies of the exciton and the single hole confined in the double QD. The meaning of symbols $A,B,C,$ and D is explained in the text.

In other words, for separate QD's the ground state corresponds to the positive trion X_2^+ localized in one of the QD's. In the limit of the separate QD's, the first-excited state energy level (C,D) is also degenerate. In the states C and D, an electron-hole pair is confined in one QD and the second hole is confined in the other QD. For comparison, the sum of the ground-state energies $(X+h)$ of the exciton and hole is plotted by the thin dotted line. For smaller values of the barrier thickness, the relative distribution of the charge carriers between the QD's is uncertain as a consequence of the coupling. Nevertheless, even for the coupled QD's, in A and B states, all the particles exhibit a tendency to occupy the same dot, while in the excited C and D states, the holes exhibit a tendency to occupy different QD's.

The degenerate excited-state energy level $(C,\ D)$ splits for larger values of the interdot distance than (A,B) level. The electron in A, B, and C states possesses an approximate even parity, therefore the corresponding energy levels decrease when the barrier thickness decreases. In D state the electron has an approximate odd parity, and in contrast to states A,B and C, its energy grows when the barrier thickness decreases. The state C corresponds to both the holes in even-parity states. In the state A (B) one hole (two holes) occupies the odd-parity state. The degeneracy of A,B energy levels is lifted for $a\simeq 6$ nm as the result of the splitting between the even- and odd-parity energy levels of the hole. The most interesting feature of the positive-trion spectrum is the fact, that the energy of C state passes below that of A and B states for $a<\sim 10$ nm. This change of order of energy levels can be understood in context of Fig. 2. In the single QD, the energy shift $S_{X_2^+}$ for $R=25$ nm and $Z=0.92$ nm is positive but decreases if the height of the QD increases. In particular, for $10\leqslant Z\leqslant 40$ nm the energy shift $S_{X_2^+}$ is negative (cf. Fig. 2). As we have noted before, the coupled QD's correspond to a single dot with a larger height. This explains why the state C, in which the holes tend to occupy different QD's, becomes the ground state of X_2^+ trion under influence of the interdot coupling. We note, that the change of order of A, B, and C energy-levels appears for the specific value of the height of the dot. In the limit of separate dots, C energy-level should correspond to the ground state for these values of the height for which the positive-trion shift $S_{X_2^+}$ is negative (cf. Fig. 2).

IV. CONCLUSIONS AND SUMMARY

We have presented the results of variational calculations for the excitonic trions confined in the single and vertically coupled QD's with the Gaussian confinement potential. We have proposed the trial wave function expanded in the Gaussian basis, which takes into account both the single-particle confinement effects and interparticle correlations. We have studied the influence of the shape and geometry of the confinement potential on the shifts of the trion PL lines with respect to the exciton line. We have considered all the geometries of the cylindrically symmetric QD from a very flat QD, which resembles the two-dimensional quantum well to an elongated wire-like QD. We have shown, that the negative-trion PL line is always redshifted with respect to the exciton line and that this shift is larger for smaller QD's. The positive-trion exhibits qualitatively the same behavior only in these QD's, which resemble quasi-one-dimensional quantum wire or quasi-two-dimensional quantum well. However, in the nanostructures with similar height and diameter, the positive-trion line can be blueshifted with respect to the exciton line, if the linear size of the QD is sufficiently small. The limit cases of the present results are in a qualitative agreement with the results of previous studies of the trion binding energy in quantum wells,[4,16] and also with the shifts of the trion PL lines found for the spherical QD's.[15] Based on these results we can also formulate predictions about the binding energy of the trions in quantum wires. Namely, the present results indicate that the binding energy of both the negative and the positive trions should increase when the radius of the quantum wire is decreased.

Moreover, we have extended our study to the excitonic trions in the vertically coupled $In_xGa_{1-x}As$ self-assembled QD's. We have considered the low-energy spectrum of the system of two electrons and one hole, as well as the system of two holes and one electron in a couple of vertically stacked QD's. We have shown, that the shifts of the trion PL lines with respect to the exciton line obtained for a single isolated QD can be identified with the binding energy of the trion complexes for a pair of identical remote QD's. We have studied the splitting of the trion-energy levels under influence of the coupling between the QD's. We have found, that the interdot coupling decreases the redshift of the negative-trion PL line with respect to the exciton line. Moreover, we

have shown that the coupling may induce a redistribution of the charge carriers between the dots in the positive-trion ground state. These effects have been explained on the basis of our studies for the single QD, since—in the strong-coupling limit—-the coupled QD's can be treated as a single QD with an enlarged extension in the vertical direction.

ACKNOWLEDGMENTS

This work has been performed in the framework of the French-Polish scientific cooperation program POLONIUM. One of us (B. Szafran) acknowledges the support of the Foundation for Polish Science (FNP).

*Email address: bszafran@agh.edu.pl

[1] M. A. Lampert, Phys. Rev. Lett. **1**, 450 (1958).
[2] B. Stébé and A. Ainane, Superlattices Microstruct. **5**, 545 (1989).
[3] B. Stébé, G. Munschy, L. Stauffer, F. Dujardin, and J. Murat, Phys. Rev. B **56**, 12 454 (1997).
[4] B. Stébé, A. Moradi, and F. Dujardin, Phys. Rev. B **61**, 7231 (2000).
[5] A. B. Dzyubenko and A. B. Sivachenko, Phys. Rev. Lett. **84**, 4429 (2000).
[6] C. Riva F. M. Peeters, and K. Varga, Phys. Rev. B **61**, 13 873 (2000).
[7] D. M. Whittaker and A. J. Shields, Phys. Rev. B **56**, 15 185 (1997).
[8] A. Wójs and P. Hawrylak, Phys. Rev. B **51**, 10 880 (1995).
[9] I. Szlufarska, A. Wójs, and J. J. Quinn, Phys. Rev. B **63**, 085305 (2001).
[10] W. Y. Ruan, K. S. Chan, H. P. Ho, R. Q. Zhang, and E. Y. B. Pun, Phys. Rev. B **60**, 5714 (1999).
[11] W. Y. Ruan, K. S. Chan, and E. Y. B. Pun, J. Phys.: Condens. Matter **12**, 7905 (2000).
[12] A. V. Chaplik, Phys. Low-Dimens. Semicond. Struct. **9-10**, 131 (1999).
[13] W. F. Xie, Phys. Status Solidi B **226**, 247 (2001).
[14] Y. P. Varshni, Phys. Status Solidi B **277**, 621 (2001).
[15] B. Szafran, B. Stébé, J. Adamowski, and S. Bednarek, J. Phys.: Condens. Matter **12**, 2453 (2000).
[16] L. C. O. Dacal and J. A. Brum, Phys. Rev. B **65**, 115324 (2002).
[17] L. C. O. Dacal, R. Ferreira, G. Bastard, and J. A. Brum, Phys. Rev. B **65**, 115325 (2002).
[18] K. Kheng, R. T. Cox, Y. Merle d'Aubigné, F. Bassani, K. Saminadayar, and S. Tatarenko, Phys. Rev. Lett. **71**, 1752 (1993).
[19] G. Finkelstein, V. Umansky, I. Bar-Joseph, V. Ciulin, S. Haacke, J.-D. Ganiere, and B. Deveaud, Phys. Rev. B **58**, 12 637 (1998).
[20] V. Ciulin, P. Kossacki, S. Haacke, J.-D. Ganiere, B. Deveaud, A. Esser, M. Kutrowski, and T. Wójtowicz, Phys. Rev. B **62**, R16 310 (2000).
[21] A. Esser, E. Runge, R. Zimmermann, and W. Langbein, Phys. Rev. B **62**, 8232 (2000).
[22] T. Vanhoucke, M. Hayne, M. Henini, and V. V. Moshchalkov, Phys. Rev. B **65**, 041307 (2002).
[23] R. J. Warburton, C. S. Durr, K. Karrai, J. P. Kotthaus, G. Medeiros-Ribeiro, and P. M. Petroff, Phys. Rev. Lett. **79**, 5282 (1997).
[24] R. J. Warburton, C. Schäflein, D. Haft, F. Bickel, A. Lorke, K. Karrai, J. M. Garcia, W. Schoenfeld, and P. M. Petroff, Nature (London) **405**, 926 (2000).
[25] S. Fafard, M. Spanner, J. P. McCaffrey, and Z. R. Wasilewski, Appl. Phys. Lett. **76**, 2268 (2000).
[26] B. Szafran, S. Bednarek, and J. Adamowski, Phys. Rev. B **64**, 125301 (2001).
[27] C. F. Klingshirn, *Semiconductor Optics* (Springer-Verlag, Berlin, 1997).
[28] B. Szafran, J. Adamowski, and B. Stébé, J. Phys.: Condens. Matter **10**, 7575 (1998).
[29] J. Adamowski, M. Sobkowicz, B. Szafran, and S. Bednarek, Phys. Rev. B **62**, 4234 (2000).
[30] P. D. Siverns, S. Malik, G. McPherson, D. Childs, C. Roberts, R. Murray, B. A. Joyce, and H. Davock, Phys. Rev. B **58**, R10 127 (1998).
[31] R. Colombelli, V. Piazza, A. Badalto, M. Lazzarino, F. Beltram, W. Schoenfeld, and P. Petroff, Appl. Phys. Lett. **76**, 1146 (2000).